Forschungszentrum Karlsruhe
in der Helmholtz-Gemeinschaft

Wissenschaftliche Berichte
FZKA 7444

Institute for Nuclear Waste Disposal

Annual Report 2007

H. Geckeis, R. Klenze (Eds.)

Institut für Nukleare Entsorgung

November 2008

Forschungszentrum Karlsruhe

in der Helmholtz-Gemeinschaft

Wissenschaftliche Berichte

FZKA 7444

Institute for Nuclear Waste Disposal

Annual Report 2007

H. Geckeis, R. Klenze (Eds.)

Institut für Nukleare Entsorgung

Forschungszentrum Karlsruhe GmbH, Karlsruhe

2008

Dieser Bericht ist in schwarz-weiss gedruckt.
Die Farbabbildungen finden Sie in der elektronischen Version:

http://bibliothek.fzk.de/zb/berichte/FZKA7444.pdf

Forschungszentrum Karlsruhe GmbH
Postfach 3640, 76021 Karlsruhe

Mitglied der Hermann von Helmholtz-Gemeinschaft
Deutscher Forschungszentren (HGF)

ISSN 0947-8620

urn:nbn:de:0005-074442

Table of contents

1. Introduction to the Institut für Nukleare Entsorgung

Activities at the Institut für Nukleare Entsorgung (INE) are integrated into the research programme NUKLEAR of the Forschungszentrum Karlsruhe within the Helmholtz-Gemeinschaft Deutscher Forschungszentren (HGF). INE contributes to the German R&D on long-term safety assessment for final disposal of nuclear waste. Further activities deal with the separation of minor actinides from high-level waste (partitioning) for subsequent transmutation and the immobilization of high-level liquid waste by vitrification.

Based on the presently scheduled operation times for nuclear power plants in Germany, about 17400 t spent fuel containing approximately 174 t plutonium, 14 t minor actinides (neptunium, americium and curium) and 700 t of fission products will be generated until 2021. About 7000 t were shipped to France and UK for reprocessing to recover plutonium and uranium. The safe disposal of high-level radioactive waste, i.e. spent fuel and heat producing waste arising from reprocessing, is the responsibility of the federal government.

There is an international consensus that emplacement in deep geological formations is the safest way to dispose of highly radioactive waste. It ensures the effective protection of the population and the biosphere against radiation exposure arising from the waste over very long periods of time. The isolation and immobilization of nuclear waste in a repository is accomplished by the appropriate combination of redundant barriers (multi-barrier system). INE research focuses on the geochemical aspects of nuclear waste disposal. Special emphasis is laid on actinides and long-lived fission products because of their significant contribution to the radiotoxicity for long periods of time.

Relevant scenarios for the geological long-term behaviour of nuclear waste disposal in general have to take possible radionuclide transport via the groundwater pathway into account. Thermomechanical studies are performed at INE in order to describe the evolution of the repository after closure. The possible groundwater access to emplacement caverns is assumed to cause waste form corrosion. Radionuclide mobility is then determined by the various geochemical reactions in the complex aquatic systems: dissolution of the nuclear waste form (high-level waste glass, spent fuel), radiolysis phenomena, redox reactions, complexation with inorganic and organic ligands, colloid formation, surface sorption reactions at mineral surfaces, precipitation of pure solid phases and solid solutions. Prediction and quantification of all these processes requires the availability of thermodynamic data and a comprehensive understanding at a molecular scale. Relevant radionuclide concentrations in natural groundwater lie in the nano-molar range, which is infinitesimally small in relation to the main groundwater components. Quantification of chemical reactions occurring in these systems calls for the application and development of new sophisticated methods and experimental approaches, which provide insight into the chemical speciation of radionuclides. Innovative laser and X-ray spectroscopic techniques are continuously developed and applied at INE. A theoretical group has been established at INE to perform quantum chemical calculations on actinide complexes as an additional tool to support experimental results.

The long term safety assessment of a repository for nuclear waste has to be demonstrated by application of modeling tools on real natural systems over geological time scales. The experimental research programme at INE aims to acquire fundamental knowledge on model subsystems and to derive model parameters. Geochemical models and thermodynamic databases are developed as a basis for the description of geochemical behaviour of radionuclides in complex natural aquatic systems. The prediction of radionuclide migration in the geosphere necessitates a coupled modelling of geochemistry and transport. Transferability and applicability of model predictions are examined by designing dedicated laboratory experiments, field studies in underground laboratories and by studying natural analogue systems. This strategy allows to identify and to analyse key uncertainties related to the accuracy and the relevance of the developed models.

The Partitioning & Transmutation (P&T) strategy is pursued in many international programmes, in order to achieve a significant reduction of nuclear waste radiotoxicity. The aim of R&D at INE is to separate and isolate long-lived minor actinides from high-level nuclear waste for subsequent transmutation into short-lived or stable fission products, thus reducing the time horizon for waste storage from more than 100000 to less than 1000 years. INE develops highly selective extracting

agents and performs extraction experiments to derive kinetic and thermodynamic data for the extraction reaction. R&D spans theoretical and experimental work dedicated to a mechanistic understanding of extraction ligand selectivity on a molecular scale, to the development of extraction processes.

Beside research for the long-term safety assessment of nuclear waste disposal and reduction of nuclear waste radiotoxicity by partitioning, INE contributes to the decommissioning of nuclear facilities. The core process technology for the Karlsruhe Vitrification Plant (VEK) at the Karlsruhe Reprocessing Plant (WAK) site located at the Forschungszentrum Karlsruhe has been developed at INE. This work comprises design of process components, including the glass melting furnace and the off-gas cleaning installation. The VEK facility has now finished the cold commissioning phase and hot operation is scheduled for 2009. INE has been involved in functional testing of major process systems, the preparation of qualification records and certification of product quality and in the performance of the recent cold test operation.

Teaching of students and promotion of young scientists is of fundamental importance to ensure a high level of competence and to maintain a leading international position in the field of nuclear- and radiochemistry. Therefore, close cooperation with universities is indispensable. In association with the new director of INE (Prof. Dr. Horst Geckeis), a radiochemistry chair was established at the Karlsruhe University. The start of term is in winter semester 2008/2009. In addition INE scientists are strongly involved in teaching at the Universities of Heidelberg, Mainz, Jena and Berlin. Radiochemistry lectures at the Universities of Karlsruhe and Heidelberg are supplemented by practical training courses at FZK and the INE hot laboratories.

Presently, FZK and the University of Karlsruhe are going to merge in the “Karlsruhe Institute of Technology (KIT)”, a unique model in the German research landscape. KIT will bundle the activities in research and teaching to hold a key position in the international natural scientific community.

Through this engagement, students are educated in the field of nuclear and actinide chemistry, which most universities can presently no longer offer. Hence, INE makes a vital contribution to the medium and long-term perspective of maintaining nuclear technology competence. On the European level, the Network of Excellence ACTINET has been established to educate young scientists in actinide sciences by opening the main facilities in Europe, where handling of transuranium elements is possible, to universities and other national institutions. INE/FZK is one of the core institutions of this network.

INE laboratories are equipped with all facilities necessary to perform radionuclide/actinide research. Alpha glove boxes, shielded boxes with remote control devices and controlled atmosphere boxes are available. Classical α, β, γ spectroscopy instruments exist for the sensitive detection and analysis of radionuclides. Trace element and isotope analysis is made by instrumental analytical techniques such as X-ray fluorescence spectrometry (XRF), atomic absorption spectrometry (AAS), ICP-atomic emission spectrometry (ICP-AES) and ICP-mass spectrometry (ICP-MS). Surface sensitive analysis and characterisation of solid samples is done by X-ray diffraction (XRD), photoelectron spectroscopy (XPS) and atomic force microscopy (AFM). Laser spectroscopic techniques are developed and applied for sensitive actinide speciation analysis such as laser time-resolved laser fluorescence spectroscopy (TRLFS), laser photoacoustic spectroscopy (LPAS), sum frequency infrared spectroscopy, laser-induced breakdown detection (LIBD) and Raman spectroscopy. Recently a tunable optical parametric oscillator (OPO) laser system with TRLFS-detection was installed for high resolution spectroscopy at liquid He temperature. Structural insight into actinide species is obtained by extended X-ray fine structure (EXAFS) spectroscopy at the INE-Beamline at the Karlsruhe synchrotron source ANKA. The INE-Beamline, in the direct vicinity of INE actinide laboratories and analytic methods, represents a world-wide unique experimental and analytic infrastructure, which both profits from and contributes to INE’s expertise in the field of chemistry and spectroscopy of the actinides.

Additional facilities at INE include a non-radioactive vitrification test facility (1:1 mock-up of the VEK plant) used to investigate and to simulate vitrification processes for hot plants. INE is furthermore equipped with CAD workstations enabling construction and planning of hardware components, process layout and flowsheets.

2. Highlights

Contributions collected in this report provide a representative overview of the scientific outcome of INE research activities in 2007. The structure of the report follows widely the organisation of the institute according to research topics: Basic research towards understanding geochemical reactions of radionuclides on a molecular scale, with a direct link to applied studies of 'real' repository conditions. In order to obtain detailed chemical information on radionuclide speciation and structures, INE consequently develops speciation methods and analytical techniques. Beside spectroscopic methods, quantum chemical calculations are increasingly implemented as an additional tool to gain insight into the molecular and electronic structure of radionuclide species. Speciation techniques are not only applied to geochemical studies but also used to elucidate mechanisms underlying the partitioning of minor actinides by solvent extraction using new types of extractants.

Research dedicated to the immobilisation of high-level radioactive liquid waste is much more technically oriented. In this field, the long time experience of INE engineers has led to the realization of a vitrification plant on the WAK site using INE technology.

A selection of milestones and highlights out of the research activities in 2007 are listed below.

Laser fluorescence spectroscopy has been applied for ultrasensitive speciation of Cm(III) complexes; however it provides no structural information on the ligand interaction with the actinide ion. Recently, **spectroscopy of the vibronic side bands** (VSB), which accompany the much stronger electronic transitions, have been probed for Cm(III). VSB supply infrared-like spectra of the ligands in the first and second coordination sphere of the Cm(III), discriminating them from ligands in the bulk solution. This allows to deduce the type of ligands, their denticity and the differentiation between outer- and innersphere complexation. Thus VSB spectroscopy complements the powerful "Horrocks-method", which allows deriving the number of innersphere water molecules from the fluorescence lifetime. Contrary to the lanthanides, where a broad application is hampered by poor sensitivity, Cm(III) concentrations in the sub-μmol range were found to be sufficient. Thus it is expected that VSB spectroscopy could be applied routinely in TRLFS speciation studies.

A crucial point for prediction of the geochemical behaviour of radionuclides in the near-field of a repository for high-level heat producing nuclear waste is the lack of **thermodynamic data at elevated temperatures**. Depending on the host rock and backfill material and the design concept, temperature up to 200 °C at the container surface have to be considered. Only very few thermodynamic data up to 100 °C are available, but no relevant data at higher temperatures. Due to drastic change of the properties of water (dielectric constant, ionic product), stability constants may vary by several orders of magnitude without any reliable method for an extrapolation or theoretical prediction. First studies have been performed at INE to monitor the speciation of Cm(III) by TRLFS as a function of temperature. Because pH-sensors are not available in the temperature range from 140 to 200 °C, ligands showing no pronounced protolytic properties in weakly acidic solution such as nitrate have been chosen. The results are very promising and will be extended to other ligands more relevant for a repository environment.

Whereas huge progress in understanding geochemical processes on a molecular scale was recently achieved, much less is known in the micro and sub-micrometer range. This is mainly due to coupling of geochemistry with transport processes and to the heterogeneity frequently found in geological media. To tackle this problem, **spatial resolved speciation of actinides** in relation to other elements and phases **by various X-ray techniques (μ-XRF, μ-XAFS and μ-XRD)** has been performed. These methods have been developed and tested at synchrotron beam lines at HASYLAB, the ESRF and ANKA, using various focussing optics, preferentially in confocal arrangement to obtain depth information. Test measurements were made on uranium-rich sediment from the natural analogue Ruprechtov site. The combination of various methods showed the strong heterogeneity of the distribution of mineral phases, elements and their oxidation states on a micrometer scale. Based on this detailed information, a process leading to the precipitation of U within this sediment sample was deduced. These results gained high recognition from the scientific community. This is reflected in the next International Congress on X-ray Optics and Microanalysis, to be held in 2009 in Karlsruhe and organized by INE. Based on the success of these recent studies, a micro-focus X-ray set-up is being installed at the INE-Beamline.

Additional 2007 results of high interest are a continuation of **last year's highlights.** For example, the **ESI-MS investigation on Th(IV)-hydroxo oligomers,** following a study of the homologous Zr(IV) from last year, shows at lowest concentration $[Th]_{tot}$ =6 μM only monomeric Th species. The dominant species at 200 μM is a pentamer. Tetra- and hexamer species postulated in the literature are not observed. The strong **effect of Ca on the solubility of An(III/IV)** under alkaline conditions reported last year was quantified by TRLFS for Cm(III). The Ca effect was also observed for Np(V). In addition two ternary solid phases of Ca-Np-hydroxides are formed. The corresponding ternary Na-Np phases are stable only at much higher NaOH concentrations. Presention of these results at MIGRATION´07 gained high recognition by the audience.

The **Karlsruhe Vitrification plant** (VEK) has finalized the cold commissioning phase by performance of a three months test operation. The vitrification operation was conducted under representative conditions (including application of remote handling steps) and by following the approved operation manuals. The cold test served for the final integral operational check of the plant and for proof of the production of qualified glass canisters by application of the QA control steps. After release of the expected license for hot operation, start-up of VEK production operation can take place in 2009. The **Vitrification Project China** (VPC) has progressed contract initiation between the German consortium and the Chinese side on December 11, 2007 in Beijing.

3. National and International cooperation

INE research involves a number of national and international cooperations and projects. These are described in the following.

“Fundamental processes of radionuclide migration” (**FUNMIG**) is an Integrated Project within the European Commission’s 6th Framework Program. It started January 2005, with a duration of four years. With respect to the number of partners and geographical distribution, it is the largest such project within the EURATOM program. FUNMIG has 51 contractors from 15 European countries and 20 associated groups from an additional three European countries, Korea and Canada. All types of stakeholders are well represented, i.e. research organizations, universities, SME’s, national waste management organizations and national regulatory bodies. The project is coordinated by INE, with Enviros S.L. as the coordination secretariat. The FUNMIG research program builds around six research and technological development components (RTDC’s). Two of these deal with well established and less established processes, applicable to all host-rock types. Three of them deal with processes specific to the three host-rock types under investigation in Europe, clay, crystalline and salt. Another RTDC deals with integration of the scientific progress into long-term safety assessment of a nuclear repository. An important part of the project is management and dissemination of knowledge, including training.

The European "Network of Excellence for actinide sciences” (**ACTINET**) is a consortium of more than twenty-five European research institutions. The consortium is supported by the European Commission under a four year contract established in March 2004. The objective of ACTINET is to take steps to bring both research infrastructures and human expertise in Europe to an enhanced performance level, thereby contributing to the development of European research in the fields of physics and chemistry of actinides. INE acts as one of the core members of the ACTINET consortium together with the coordinating institution Commissariat à l’Energie Atomique (CEA, France), the Institute for Transuranium Elements (ITU, European Joint Research Center), and the Studiecentrum voor Kernenergie - Centre d’Etude de l’Energie Nucléaire (SCK•CEN, Belgium). A top priority objective within ACTINET is to pool selected parts of the major facilities for actinide research of some large European institutes (CEA, ITU, INE, SCK-CEN, Forschungs-zentrum Dresden (FZD), and Paul Scherrer Institut (PSI)) and to operate this pool as a multi-site user facility. From the beginning, INE laboratories equipped with state-of-the-art analytical techniques for actinide speciation, including the INE-Beamline for actinide research at ANKA were used extensively by the scientific community. From 2004 – 2007, INE initiated and participated in 21 ACTINET research projects. Within these projects, guest scientists worked at INE for in a total of 140 person weeks in different fields of actinide sciences.

INE is partner in the Integrated Project **EUROPART**. The research within this project concerns the separation (partitioning) of minor actinides contained in nuclear wastes from reprocessing of nuclear spent fuels. After separation, the actinides will be either destroyed into short-lived or stable nuclides by nuclear means (Partitioning & Transmutation, P&T strategy) or conditioned into stable dedicated solid matrices (Partitioning & Conditioning, P&C strategy). INE’s R&D is focused on the selective extraction of actinides over lanthanides. This includes spectroscopic investigations to understand the high selectivity of extraction reagents for trivalent actinides, as well as kinetic studies of the extraction process.

Two international projects focus on the influence of colloids on radionuclide migration in crystalline host rock: the Colloid Formation and Migration (**CFM**) experiment, coordinated by NAGRA (National Cooperative for the Disposal of Radioactive Waste, Switzerland) at the Grimsel Test Site, and the **Colloid Project,** initiated by SKB (Swedish Nuclear Fuel and Waste Management Co., Sweden), which includes field experiments at the Äspö Hard Rock laboratory. INE plays a decisive role in the laboratory programmes of both projects and is also involved in the field activities.

INE is involved in various bi- and multilateral cooperations with national universities on different topics. Scientific cooperation with various German universities is partly supported by the German Ministry for Economy and Technology (BmWI). These research programs are dedicated to actinide geochemistry and, specifically, the impact of colloidal and natural organic matter.

The collaborative project THEREDA should be specifically mentioned here. INE generates a centrally managed and administered database of evaluated thermodynamic parameters in cooperation with Gesellschaft für Anlagen- und

Reaktorsicherheit (GRS) mbH, Braunschweig, Forschungszentrum Dresden-Rossendorf, Institut für Radiochemie (FZD-IRC), Technische Universität Bergakademie Freiberg, Institut für Anorganische Chemie (TU-BAF) and AF-Colenco AG, Baden (Schweiz). Thermodynamic data are required for environmental applications in general and radiochemical issues in particular. This database is to be developed to a national (reference) standard and will be the basis for performance assessment calculations for a national nuclear waste repository. The project is supported by the Bundesministerium für Bildung und Forschung (BMBF), the Bundesministerium für Wirtschaft und Technologie (BMWi) and the Bundesministe rium für Umwelt, Naturschutz und Reaktor sicherheit (BMU).

Among the 15 Helmholtz University Young Scientist Groups (**HHNG**) supported in 2006, INE was successful with its research project on "Elucidation of Geochemical Reaction Mechanisms at the Water/Mineral Phases Interface." Its partner is the Faculty of Chemistry and Geosciences of the University of Heidelberg. The project will run for five years with funds totaling 1.25 million Euro, including funding of the positions for the working group leader and for scientific or technical staff members, as well as non-personnel items. The leader of the working group also has teaching functions at the university.

The **Virtual Institute Functional Properties of Aquatic Interfaces** supported by the HGF was successfully terminated mid-2007. Significant progress was achieved in understanding the oxide mineral/aqueous solution interface and the nature of sorbed actinide ions and natural organic matter. For the first time a consistent picture could be established for the corundum/water interface by sum frequency spectroscopic studies and quantum chemical calculations. Confocal laser scanning and X-ray spectro-microscopy were successfully applied to unravel the heterogeneity of actinide reactions with natural organic matter. Further activities were dedicated to investigation of reactions of natural organic matter at the oxide/water interface with acoustic methods and establishment of an analytical near-field microscope based on the Fischer near field probe.

In the meantime INE was successful with a second proposal for a virtual institute focussing on **Advanced Solid-Aqueous Radio-Geochemistry,** and a Joint Research Proposal for a Helmholtz Russia Joint Research Group on **Actinide nano-particles: formation, stability, and properties relevant to the safety of nuclear waste disposal**. Both projects will start beginning 2008.

4. Fundamental Studies: Process understanding on a molecular scale

The studies reported in this section deal with the aquatic chemistry of actinides, their interaction with mineral interfaces and the formation of actinide containing solid solution phases. Investigations on the non-expected formation of Ca-An(III, IV)-OH species increasing the solubility of actinides under special alkaline conditions by orders of magnitude, reported last year, has been extended to Cm(III) and Np(V). Fluorescence and absorption spectroscopy was used to derive directly the species distribution under the given conditions. Whereas in the direct vicinity to high-level waste canisters temperatures up to 200 °C may occur, relevant thermodynamic data on actinides are mostly available only for 25 °C. To overcome this limitation we started recently a survey to derive selected complexation reactions of Cm(III) using TRLFS. Interface reaction of trivalent actinides have been studied at INE focusing recently on corundum α-Al_2O_3. Here we present results on the sorption of actinide ions onto alteration phases of corundum formed by contact with water, such as gibbsite. Another very active research field presents the study on formation of actinide solid-solutions, which may be formed as secondary phases in the near and far field of the repository. Sound thermodynamic data based on detailed knowledge of the incorporation mechanism are necessary to benefit from this kind of retention process in performance assessment calculations. Common to all mentioned studies is the approach of achieving a fundamental process understanding of relevant reactions by the application of sophisticated speciation tools combined with the derivation of sound thermodynamic data.

4.1 Chemistry and thermodynamics of actinides in aqueous solution

M. Altmaier, N.L. Banik, W. Hauser, R. Klenze, P. Lindqvist-Reis, Ch. Marquardt, V. Neck, P.J. Panak, Th. Rabung, J. Runke, A. Skerencak, Th. Fanghänel

Introduction

The objectives were to fill in the gaps of thermodynamic data on solubility and complexation reactions of actinides. Emphasis is on the spectroscopic speciation of Cm(III) and Np(V) in alkaline Ca rich solutions, the nitrate complexation of Cm(III) and Eu(III) at temperatures up to 200 °C, and finally on preliminary studies on reduced U, Np and Pu species, notably, the stabilisation of their trivalent oxidation state in aqueous solution.

Solubility of actinides in chloride solutions and the formation of Ca-An-OH complexes

The solubility and aqueous speciation of actinides in chloride solutions is of particular interest for the storage of cementitious nuclear waste packages in underground salt mines. Intruding water is supposed to form NaCl- or $MgCl_2$-dominated salt brines but the corrosion of cementitious waste forms in $MgCl_2$ solution can also lead to alkaline $CaCl_2$ brines. Recent studies [1, 2] have shown that the solubilities of $ZrO_2 \cdot xH_2O$(s) at pH_c = 10 - 12 in 0.1 - 2.0 M $CaCl_2$ and of $ThO_2 \cdot xH_2O$(s) at pH_c = 11 - 12 in 0.5 - 4.5 M $CaCl_2$ are raised to unexpectedly high values by the formation of ternary Ca-M(IV)-OH complexes which could be identified as $Ca_3[Zr(OH)_6]^{4+}$ and $Ca_4[Th(OH)_8]^{4+}$, respectively, and characterized by extended X-ray absorption fine structure spectroscopy (EXAFS) [1]. The results reported for trivalent lanthanides and actinides, Nd(III) and Cm(III), and for pentavalent Np(V) indicate that the stabilization of anionic hydroxide complexes by Ca^{2+} ions is a more general phenomenon.

Thermodynamic model for the solubility and hydrolysis of Nd(III), Cm(III) and Am(III)

The solubility of $Nd(OH)_3$(s) was determined in an Ar glove box (22 ± 2°C) in 0.1, 0.5, 2.5 and 5.0 M NaCl (pH_c = 7 - 14) and in 0.25, 1.0, 2.5 and 3.5 M $MgCl_2$ and $CaCl_2$ where the pH_c range is limited to values of 9 and 12, respectively, by the solubility of magnesium and calcium hydroxides or hydroxychlorides. The equilibrium constants for Nd(III) at zero ionic strength are close to the known values for $Am(OH)_3$(s) and the aqueous Am(III) or Cm(III) hydroxide complexes $An(OH)_3^{3-n}$ with n = 1 - 3 [3]. In alkaline NaCl solutions up to 5 M NaCl-NaOH, there is no indication for a solubility increase due to the formation of anionic hydroxide complexes and a solubility study with $Am(OH)_3$(s) in 0 - 10 M KOH [4] indicates that the formation of $Am(OH)_4^-$ requires OH^- concentrations > 3 M. However, in $CaCl_2$ solutions above 2 M the solubility clearly increases already in the pH_c range 11 - 12 (Fig. 1).

In order to clarify the speciation in alkaline $CaCl_2$ solutions, time-resolved laser fluorescence spectroscopy (TRLFS) was used to study Cm(III) solutions ($[Cm]_{tot} = 2 \cdot 10^{-7}$ M) in 0.1 - 3.5 M $CaCl_2$ at $pH_c \approx 11.7$ and in three sets of constant ionic strength (1.0, 2.5 and 3.5 M $CaCl_2$) with pH_c varying from 10.8 to 11.9 [5]

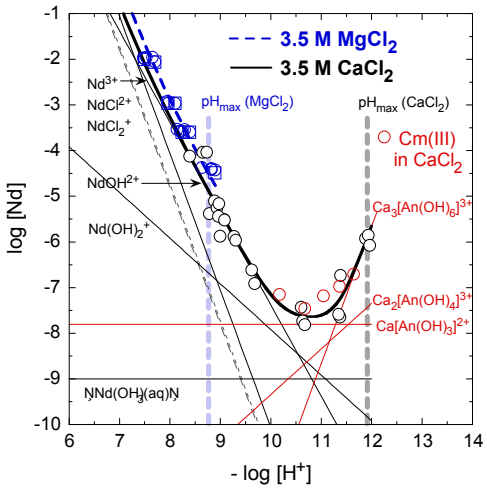

Fig. 1: *Solubility of $Nd(OH)_3$(s) in 3.5 M $MgCl_2$ and $CaCl_2$ (experimental data and Pitzer model calculation: fat fines represent the total Nd and Cm concentrations, thin line lines show the contributions of the different species)*

(Fig. 2a). The quantitative evaluation of the Cm(III) emission spectra (peak deconvolution and the pH dependence of the spectroscopic data) shows that hitherto unknown Cm(III) complexes with three, four and six OH^- ligands are formed. The emission bands of these complexes are regularly shifted to higher wavelength (λ_{max} = 607.5, 609.9 and 614.7 nm, respectively) compared to those of Cm^{3+}(aq),

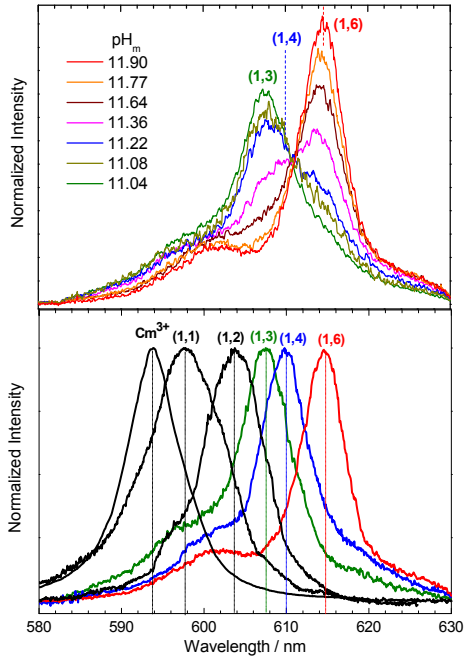

Fig. 2: ***a)*** *Normalized Cm(III) emission spectra in 3.5 M $CaCl_2$ at pH_c=11-12. The corresponding aqueous Cm(III) concentrations determined after ultrafiltration are shown as red circles in Fig. 1.* ***b)*** *Pure component TRLFS emission spectra of Cm^{3+}(aq) and the hydrolysis species (1,1) = $Cm(OH)^{2+}$, (1,2)= $Cm(OH)_2^+$, (1,3)= $Ca_x[Cm(OH)_3]^{2x}$, (1,4)= $Ca_y[Cm(OH)_4]^{2y-1}$ and (1,6)= $Ca_z[Cm(OH)_6]^{2z-3}$*

$Cm(OH)^{2+}$ and $Cm(OH)_2^+$ (Fig. 2b). Increasing the $CaCl_2$ concentration strongly enhances the intensity of the observed bands; the observed Cm(III) hydroxide complexes are stabilized by a strong interaction with Ca^{2+} ions. The Cm(III) concentration determined after 10 kD ultrafiltration, $[Cm(III)]_{aq}$ in equilibrium with colloidal $Cm(OH)_3$(am), increases accordingly [5]. In 5 M NaCl-NaOH solutions ($[OH^-]$ = 1 - 4 M) studied for comparison, TRLFS shows no distinct Cm(III) emission spectrum [5]. The dissolved curium is almost completely present as $Cm_m(OH)_{3m}$ polymers which show no fluorescence emission bands [6].

The extremely different hydrolysis behaviour of Cm(III) in alkaline $CaCl_2$ solutions compared to pure NaOH and KOH or NaCl-NaOH solutions cannot be explained by different ion interaction coefficients for $Cm(OH)_4^-$ and $Cm(OH)_6^{3-}$ with Ca^{2+} compared to those with Na^+ or K^+. A thermodynamic model valid for both Ca-free and Ca-containing solutions requires the formulation as ternary complexes $Ca_x[Cm(OH)_3]^{2x}$, $Ca_y[Cm(OH)_4]^{2y-1}$ and $Ca_z[Cm(OH)_6]^{2z-3}$. Unfortunately, the number of associated Ca^{2+} ions cannot be determined independently with the presently available methods. TRLFS is not sensitive to the second coordination sphere and the solution concentrations are not sufficient for EXAFS analysis. In analogy to the M(IV) complexes $Ca_3[Zr(OH)_6]^{4+}$ and $Ca_4[Th(OH)_8]^{4+}$, where the number of Ca^{2+} ions in the second shell and the coordination structure could be determined by EXAFS [1] (one Ca^{2+} ion bound to two OH^- ligands via edges of the $[M(OH)_n^{z-}]$ coordination polyhedra), we may assume the stoichiometries $Ca[Cm(OH)_3]^{2+}$, $Ca_2[Cm(OH)_4]^{3+}$ and $Ca_3[Cm(OH)_6]^{3+}$. Table 1 shows the standard state formation constants and ion interaction

Table 1: *Formation constants $log^*\beta^\circ_{p,1,n}$(I = 0, 25°C) and ion interaction (SIT) coefficients ε_{ik}(kg·mol^{-1}) for ternary Ca-M(III)-OH complexes $Ca_p[M(OH)_n]^{2p+3-n}$ (M = Cm, Nd)* [a].

Reaction	$log^*\beta^\circ_{p,1,n}$	$\varepsilon(Ca_p[M(OH)_n]^{2p+3-n}, Cl^-)$
$Ca^{2+} + M^{3+} + 3\ H_2O \Leftrightarrow Ca[M(OH)_3]^{2+} + 3\ H^+$	- 26.3 ± 0.5	0.05 ± 0.04
$2\ Ca^{2+} + M^{3+} + 4\ H_2O \Leftrightarrow Ca_2[M(OH)_4]^{3+} + 4\ H^+$	- 37.2 ± 0.6	0.29 ± 0.07
$3\ Ca^{2+} + M^{3+} + 6\ H_2O \Leftrightarrow Ca_3[M(OH)_6]^{3+} + 6\ H^+$	- 60.7 ± 0.5	0.00 ± 0.06

[a] *In combination with $log^*K^\circ_{s,0}$ = 17.2 ± 0.4 for both $Nd(OH)_3$(s) and colloidal $Cm(OH)_3$(am) and $\varepsilon(M^{3+}, Cl^-)$ = 0.23 ± 0.02, $\varepsilon(H^+, Cl^-)$ = 0.12 ± 0.01 and $\varepsilon(Ca^{2+}, Cl^-)$ = 0.14 ± 0.01 kg·mol^{-1} from NEA-TDB [3].*

(SIT) coefficients for the ternary Ca-M(III)-OH complexes included in the comprehensive set of equilibrium constants and ion interaction (SIT and Pitzer) parameters derived for modelling the solubility and hydrolysis in the system M(III)-Na^+-Mg^{2+}-Ca^{2+}-H^+-OH^--Cl^--H_2O at 25°C.

Solubility and hydrolysis of Np(V) in alkaline $CaCl_2$ solutions

The addition of small aliquots of a Np(V) stock solution to alkaline 0.25, 1.0 and 4.5 M $CaCl_2$ solutions led to the precipitation of ternary Ca-Np(V)-hydroxides, brownish precipitates which converted into a grey solid after aging for some weeks. Depending on the pH of the solution (in the range pH_c = 9 - 12) chemical analyses of the solids yielded Ca:Np ratios of about 1:2 and 1:1 suggesting solid phase compositions of $Ca_{0.5}NpO_2(OH)_2$(s,hyd) and $CaNpO_2(OH)_3$ (s,hyd). This observation is contrary to the behaviour in NaCl and $NaClO_4$ media where the solubility of Np(V) up to pH 14 is controlled by binary Np(V) hydroxide phases, grey-green, fresh NpO_2OH(am,hyd) or white NpO_2OH (aged) [3, 7, 8]; the formation of the pink coloured ternary hydroxides $NaNpO_2(OH)_2$ (s,hyd) and $Na_2NpO_2(OH)_3$(s,hyd) requires NaOH concentrations above 1 M [9]. The aqueous speciation of Np(V) in alkaline $CaCl_2$ solutions is also different from that in NaCl-NaOH and $NaClO_4$-NaOH solutions where, at pH_c = 11 - 14, only the complexes NpO_2OH(aq) and $NpO_2(OH)_2^-$ are formed [3, 7, 8]. With increasing $CaCl_2$ concentration, Np(V) forms tri-, tetra- und penta-hydroxide complexes at pH_c = 11 - 12 as indicated as well by the pH dependence of the solubility and by NIR absorption spectra. In 4.5 M $CaCl_2$ solutions the intense Np(V) absorption band with λ_{max} = 985 nm at pH_c = 2.5 is shifted to 1020 - 1050 nm at pH_c > 11. These preliminary results show that, similar as for trivalent and tetravalent actinides, the hydrolysis of Np(V) in alkaline $CaCl_2$ solutions is also affected by strong interaction with Ca^{2+} ions, i.e., by the formation of ternary Ca-Np(V)-OH complexes.

Complexation of Eu(III) and Cm(III) with nitrate in the temperature range from 5 to 200°C studied by TRLFS

Introduction

The long term safety assessment of a nuclear waste repository requires fundamental knowledge on the mechanisms and thermodynamics of chemical reactions of actinides under near field conditions. In the past few years considerable progress in establishing a thermodynamic database for lanthanides and actinides has been achieved [3]. However, most of the available data is restricted to ambient temperature. Depending on the disposed waste and the surrounding geological barrier, the temperature in the direct vicinity can reach up to 200°C. Therefore, it is necessary to investigate complexation reactions of actinides at elevated temperatures in order to gain a reliable model which describes the behaviour of radionuclides under near field conditions over a long time period.

As natural waters contain a variety of inorganic ligands such as OH^-, CO_3^{2-}, SO_4^{2-}, Cl^-, F^-, $H_2PO_4^-$, $H_3SiO_4^-$, HCO_3^-, and NO_3^-, the complexation of actinides with inorganic ligands is of particular interest for a better understanding of the migration behaviour of actinides under natural conditions. Focussing on near field conditions, complexation reactions of trivalent actinides are studied at elevated temperature to determine thermodynamic constants.

In this work investigations on the nitrate complexation of Eu(III) and Cm(III) are performed in a temperature range from 5 to 200 °C. Although the nitrate anion is a weak ligand, it forms exclusively inner sphere complexes with lanthanides and actinides [10, 11].

For speciation of nitrate complexes of Eu(III) and Cm(III), time resolved laser fluorescence spectroscopy (TRLFS) is applied. The high sensitivity of TRLFS enables the speciation of Eu(III) and Cm(III) compounds in the submicromolal concentration range, which is below the solubility limit of actinides in natural systems. The experiments are performed in a special high temperature and high pressure cell which was designed and built at the INE (Fig. 3) [12].

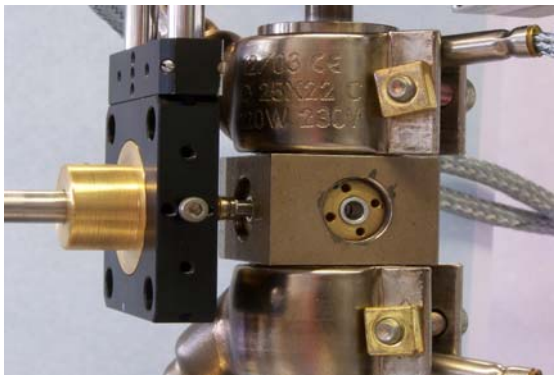

Fig. 3: *Custom-built high temperature and high pressure cell with a coupled optrode*

The nitrate concentration ranges from 0 to 4.61 m, adjusted by dissolving an adequate amount of $NaNO_3$ in MilliQ-Water. To avoid hydrolysis and significant changes in the pH of the samples with increasing temperature, the experiments are performed at pH 1. The concentration of Eu(III) and Cm(III) is kept constant at $1 \cdot 10^{-3}$ m and $1 \cdot 10^{-7}$ m, respectively.

Results and discussion

The first series of experiments, not shown here, is performed with inactive Eu(III). The strong intensity increase observed at elevated temperature for the hypersensitive $^5D_0 \rightarrow ^7F_2$ transition relative to that of the $^5D_0 \rightarrow ^7F_1$ indicates a strong increase of complexation with temperature. However, the spectral shape of both mentioned transitions is only marginally influenced by temperature preventing a peak deconvolution of the emission spectrum and a quantification of the Eu(III) species in solution. The results at room temperature are in good agreement with the literature [13,14, 15].

For this reason a further series of experiments is carried out with Cm(III), which is much more sensitive to changes in the first coordination shell than the lanthanide ions [16]. Fig. 4 displays the temperature dependent emission spectra of Cm(III) at two different nitrate concentrations (0.51 m and 4.61 m). The emission intensity of the recorded spectra decreases with increasing temperature. Therefore, the spectra are normalized to equal peak area for better comparison. The spectrum at 0.51 m [NO_3^-] and 25°C is a composition of the emission spectra of two different species: the Cm(III)-aquo ion at 593.8 nm and a second species at 596.6 nm which is attributed to the $CmNO_3^{2+}$-complex. As shown in Fig. 4, the

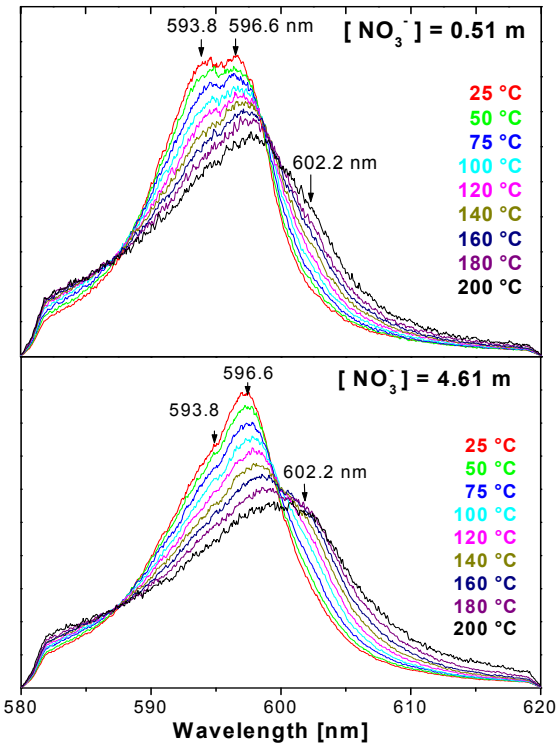

Fig. 4: *Normalized emission spectra of Cm(III) nitrate from 25 to 200°C at 0.51 m and 4.61 m nitrate concentration*

fraction of the $CmNO_3^{2+}$-complex increases with increasing nitrate concentration and increasing temperature. At higher temperatures around 160°C and high nitrate concentrateions a shoulder at 602.2 nm appears. This third band is more pronounced at higher nitrate concentrations and higher temperatures and can therefore be attributed to a $Cm(NO_3)_2^+$ species.

The species distribution at various nitrate concentrations and temperatures is directly derived by peak deconvolution of the emission spectra using reference spectra of the individual species at each temperature. Then the stability constants for the formation of the Cm-mono-nitrate and the –di-nitrate complexes are calculated at each temperature.

To obtain comparable data, we extrapolate the stability constants for zero ionic strength using linear SIT regression. The stability constants for the first and second complexation reaction are summarized in Table 2. The results show that both constants increase by almost one logarithmic unit with increasing temperature.

Table 2: *Logarithmic stability constants of $CmNO_3^{2+}$ and $Cm(NO_3)_2^+$ for zero ionic strength.*

Temp [°C]	log β_1^0	log β_2^0
25	1.29 ± 0.06	-0.36 ± 0.10
50	1.30 ± 0.03	-0.30 ± 0.10
75	1.38 ± 0.05	-0.08 ± 0.17
100	1.58 ± 0.18	-0.07 ± 0.12
120	1.71 ± 0.30	0.07 ± 0.12
140	1.94 ± 0.18	0.17 ± 0.12
160	1.99 ± 0.24	0.19 ± 0.16
180	2.03 ± 0.18	0.54 ± 0.21
200	2.08 ± 0.24	0.80 ± 0.27

The first approach to model the temperature dependence of the stability constants utilizes a linear Van't-Hoff regression, assuming a constant enthalpy and no change in the standard molal heat capacity. As shown in Fig. 5, between 25 and 75 °C the fit is in good agreement with our experimental data. However, at higher temperatures the data shows a distinct deviation from the linear plot.

Therefore, an extended fit equation is used to model the data over the entire temperature range. If instead of constant $\Delta_r H^0_m$ a constant heat capacity is assumed, the experimental data are described accurately for all temperatures ranging from 5 - 200°C (see Fig. 5). The thermodynamic data ($\Delta_r G^0_m$, $\Delta_r H^0_m$, $\Delta_r S^0_m$, and $\Delta_r C^0_{p,m}$) of the formation of $CmNO_3^{2+}$ and $Cm(NO_3)_2^+$ derived from these fits is summarized in Table 3.

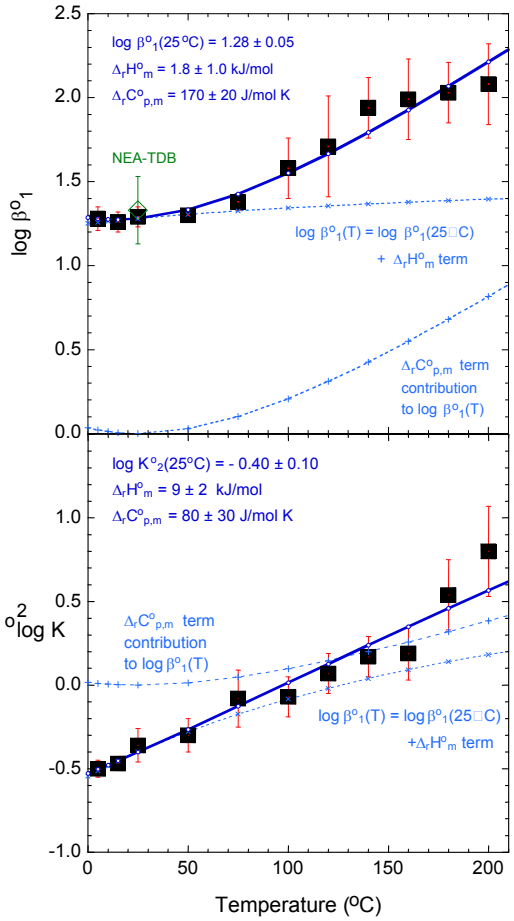

Fig. 5: *Stability constants of $CmNO_3^{2+}$ and $Cm(NO_3)_2^{+}$ as a function of temperature and theoretical fit of the temperature dependency*

Table 3: *Derived thermodynamic data*

	$Cm^{3+} + NO_3^- \rightarrow CmNO_3^{2+}$	$CmNO_3^{2+} + NO_3^- \rightarrow Cm(NO_3)_2^+$
$\log \beta^0$	1.28 ± 0.05	-0.40 ± 0.10
$\Delta_r G^0_m$ [kJ/mol]	-7.3 ± 0,3	2.3 ± 0.6
$\Delta_r H^0_m$ [kJ/mol]	1.8 ± 1.0	9.0 ± 2.0
$\Delta_r S^0_m$ [J/mol·K]	30.5 ± 3.5	22.5 ± 7.0
$\Delta_r C^0_{p,m}$ [J/mol·K]	170 ± 20	80 ± 30

Conclusions

Speciation studies by TRLFS show that the nitrate complexation of Cm(III) and Eu(III) increases with increasing temperature leading to an increase of the stability constants of $CmNO_3^{2+}$ ($\log \beta^0_1$) and $Cm(NO_3)_2^+$ ($\log \beta^0_2$) from 1.28 to 2.08 and -0.50 to 0.80, respectively. In the temperature range from 25 to 75°C the temperature dependency of the stability constants can be described by a mathematical approach using a constant value for $\Delta_r H^0_m$ (van't Hoff-Plot). Fitting of the data at higher temperatures requires an additional constant term, $\Delta_r C^0_{p,m}(298{,}15\ K)$.

Using TRLFS in combination with the high temperature cell, valuable thermodynamic data is derived at elevated temperatures which is crucial for a description of the migration behavior of actinides under near-field conditions.

Speciation of Trivalent Actinides (U, Np, Pu) in aqueous solution

Investigations on the geochemical behaviour of trivalent Pu is often simulated by studying Am(III) or Cm(III) as chemical homologues. In order to verify chemical analogies, it is necessary to perform experiments with Pu(III) directly. Pu(III) is very redox-sensitive against oxygen traces. In this contribution, we have studied different methods for preparation and stabilisation of U(III), Np(III), and Pu(III) at different pH values under anaerobic conditions. Preparation of Np(III) and U(III) is required for fundamental studies on actinide chemistry and in the frame of solvent extraction studies related to partitioning of minor actinides.

For the production of An(III) stock solutions, U(VI), Np(V), Pu(VI) were reduced by electrolysis, with Zn-amalgam, and with Rongalit. The focus of the present study was to stabilize the trivalent oxidation state by using reducing agents. All experiments have been performed with ^{238}U, ^{237}Np, ^{242}Pu in a glove box with 100% argon atmosphere at room temperature. A pH range of 0 – 5.5 was investigated with trivalent actinide concentrations ranging from 2×10^{-3} to 1×10^{-4} M and three different reducing agents (hydroxylamine, acetohydroxymic acid, and Rongalit) were employed. The time dependence of formation and stabilisation of An(III) in solution at different pH values was investigated.

UV-Vis and XAFS absorption spectroscopy have mainly been applied for the speciation of U(III), Np(III), and Pu(III) in organic and aqueous solution. In Fig. 6 typical spectra are shown. Spectroscopic studies in aqueous solution (mainly HCl medium) were carried out at 2.0×10^{-3} – 1.0×10^{-5} M An(III) in presence of the above mentioned redox stabilisation agents. UV-Vis spectra of U(III), Np(III), Pu(III) show main characteristic absorption bands (522, 786, 601 nm, respectively) suggesting that only the aquo ions of U(III), Np(III), and Pu(III) dominate at pH up to 5 and no complex formation with reducing agent could be observed. The effectiveness of stabilisation decreases in the order Pu(III)>Np(III)>U(III).

Pu(III) can be stabilized at pH 4 for 20 h with purity of >85%, Np(III) at pH 2 for 20 h with 88% purity and U(III) at pH 0 for 90 min with 90% purity. The effectiveness of reducing agents depends on the experimental conditions that correlate with the scientific problem. As an example, at higher pH values hydroxylamine seems to be the best choice for Pu(III) stabilisation, whereas Rongalit is preferred for Np(III) at lower pH values.

Because stabilisation of trivalent actinides is achieved for several hours up to two days, EXAFS measurements have been done to characterize U(III), and Np(III) in acidic solution. In Table 4 the EXAFS structural parameters of Np(III) and U(III) are given. For comparison U(IV) results are also listed.

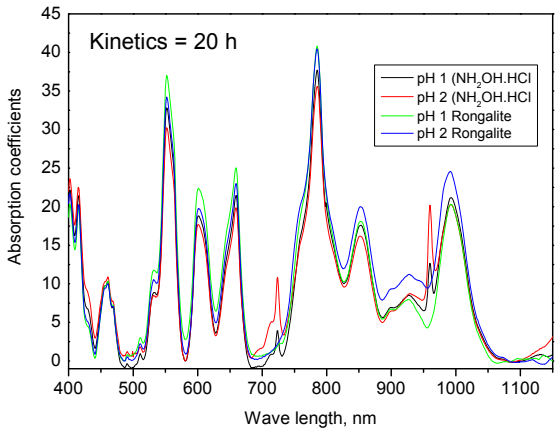

Fig. 6: *Effect of stabilisation agents for Np(III) at pH 1.0-2.0 characterized by UV-Vis spectroscopy, [Np(III)] = $2x10^{-3}$ M, reduced by liq. ZnHg, [NH_2OH·HCl] = 0.1 M, [Rongalit] = 0.01 M.*

Table 4: *EXAFS structural parameters of U(III), U(IV) and Np(III) samples*

Sample		**CN**	**r [Å]**	**σ^2 [Å^2]**	**ΔE_0 [eV]**	**r-factor**
U(III),	pH 0, NH_2OH-HCl (0.1 M)	8.9(1.1)	2.53 (1)	0.009(2)	5.9(1.2)	0.0088
U(IV)	pH 0, HCl	12.6(1)	2.40(1)	0.009(1)	1.9(1)	0.0001
Np(III)	pH 0, HCl	8.4(2)	2.49(1)	0.008(1)	-4.6(2)	0.00011
Np(III)	pH 1, NH_2OH-HCl (0.1 M)	7.9(1)	2.48(2)	0.006(1)	-4.5(1)	0.00001
Np(III)	pH 1, Rongalit (0.01 M)	8.1(2)	2.49(1)	0.006(1)	-5.2(2)	0.00011
Np(III)	pH 1.5, Rongalit (0.01 M)	8.0(1)	2.50(1)	0.008(1)	-3.8(2)	0.00008

References

[1] Brendebach, B., Altmaier, M., Rothe, J., Neck, V., Denecke, M.A., Inorg. Chem. 46 (2007) 6804-6810.

[2] Altmaier, M., Neck, V., Fanghänel, Th., A comprehensive thermodynamic model for the solubility and hydrolysis of Nd(III) and Am(III) in dilute to concentrated NaCl, $MgCl_2$ and $CaCl_2$ solutions. Presented at the conference Migration '07, submitted to Radiochim. Acta (Proceedings Migration '07).

[3] Guillaumont, R., Fanghänel, Th., Fuger, J., Grenthe, I., Neck, V., Palmer, D.A., Rand, M.H.: Chemical Thermodynamics Vol. 5. Update on the Chemical Thermodynamics of Uranium, Neptunium, Plutonium, Americium and Technetium. OECD Nuclear Energy Agency (Eds.: F. Mompean, M. Illemassene, C. Domenech-Orti, K. Ben Said), Elsevier, Amsterdam, 2003.

[4] Vitorge, P., Tran-The, P., Solubility limits of radionuclides in intersticial water - Americium in cement. Task 3 - Characterization of radioactive waste forms. Report EUR 13664, Commission of the European Communities, Luxembourg (1991).

[5] Rabung, Th., Altmaier, M., Neck, V., Fanghänel, Th., A TRLFS study of Cm(III) hydroxide complexes in alkaline $CaCl_2$ solution. Presented at the conference Migration '07, submitted to Radiochim. Acta (Proceedings Migration '07).

[6] Wang, Z., Felmy, A.R., Xia, Y.X., Mason, M.J., Radiochim. Acta 91 (2003) 329-337.

[7] Neck, V., Kim, J.I, Kanellakopulos, B., Radiochim. Acta 56 (1992) 25-30.

[8] Runde, W., Kim, J.I., Chemisches Verhalten von drei- und fünfwertigem Americium in salinen NaCl-Lösungen, Report RCM 01094, Technische Universität München, 1994.

[9] Visyachscheva, G.I., Volkov, Y.F., Simakin, G.A., Kapshukov, G.I., Soviet Radiochem. 26 (1984) 156-160.

[10] Silva, R.J., Nitsche, H., Radiochim. Acta 70/71 (1995) 377.

[11] Breen, P.J., Horrocks, W.D., Inorg. Chem. 22 (1983) 536-540.

[12] Hauser, W., Götz, R., Skerencak, A., Panak, P.J., Rabung T., Geckeis, H., Fanghänel Th., 11th International Conference on the Chemistry and Migration Behaviour of Actinides and Fission Products in the Geosphere, Migration '07, Book of Abstracts, PA7-4, p. 108 (2007).

[13] Ding, R., Gammons, C.H., Wood, S.A. Proceedings of the 9th International Symposium on Water-Rock Interactions – WRI-9, Taupo, New Zealand, 1998.

[14] Yeh, M., Riedener, T., Bray, K.L., Clark, S.B., J. of Alloys Comp. 303-304 (2000) 37-41.

[15] Tertre, E., Berger, G., Simoni, E., Castet, S., Giffaut, E., Loubet, M., Catalette, H., Geochim. Cosmochim. Acta 70, (2006) 4563-78.

[16] Edelstein, N.M., Klenze, R., Fanghänel, T., Hubert, S.,
Coord. Chem. Rev. 250 (2006) 948-73

4.2 Sorption of Cm(III) and Gd(III) onto gibbsite, α-$Al(OH)_3$

N. Huittinen, Th. Rabung, J. Lützenkirchen, M. Plaschke, H. Geckeis

Introduction

Mechanistic insight into radionuclide interaction with mineral surfaces is of great importance for performance assessment of nuclear waste repositories. Beside retardation processes as sorption, precipitation or incorporation reactions at mineral surfaces also an enhanced radionuclide transport via attachment to mobile colloidal phases has to be considered. During the last years a lot of studies have been described in the literature dealing with radionuclide sorption onto a multitude of more or less well characterized minerals. For a fundamental understanding of sorption/incorporation processes and a reliable thermodynamic description by e.g. surface complexation models, all relevant processes have to be identified and quantified. A major point in this respect is the detailed knowledge of the properties and constitution of the reactive mineral surface and the nature, distribution and concentration of surface sites which is not available or only in a limited way for most of the selected minerals.

Extensive studies of metal ion sorption on different aluminum oxides/hydroxides have been performed during the last years [1]. Pure aluminum oxides/hydroxides are rare in nature, but these minerals contain reactive aluminol groups also present on the surfaces of aluminosilicates that are found in vast quantities in natural systems. Furthermore, these aluminum oxides/hydroxides exhibit similar mineralogical structures as iron oxides/ hydroxides which are expected to be very effective substrates for metal ion sorption. The aluminum oxides/hydroxides can therefore be used also as models for the iron containing phases which cannot be investigated by TRLFS as follows from their fluorescent quenching properties. The reactivity of aluminol groups depends on the mineralogical structure, their orientation, acidity and the way they are bound to the surface (singly, doubly or triply coordinated) leading to a slightly different metal ion sorption behaviour on different aluminum oxides/hydroxides. In aqueous solutions the surfaces of suspended oxides are hydrated, and surface transformations of oxides like α-Al_2O_3 and γ-Al_2O_3 have been reported [2-5]. Investigations with γ-alumina show a surface transformation into bayerite, β-$Al(OH)_3$ [2,3]. Also for α-alumina a surface transformation into bayerite and gibbsite, α-$Al(OH)_3$ has been observed [4,5]. The aim of this work is to study trivalent metal ion sorption onto a pure aluminum hydroxide, where surface transformation should be strongly suppressed as compared to pure oxides. For this purpose the mineral gibbsite with high thermodynamic stability in aqueous solution was chosen. Results from previous work by Rabung et al. [6,7] and Stumpf et al. [8], where the sorption of trivalent actinides onto both α- and γ-alumina has been investigated, were chosen as the basis for the study.

Experimental

The gibbsite used in this work was prepared through precipitation of $Al(OH)_3$ followed by subsequent dialysis of the suspension at 70°C for a time span of 4 months. A 0.33 M aluminum chloride solution was titrated with 1 M NaOH until a pH value of 4.5, at which amorphous aluminum hydroxide was precipitated. The precipitation was carried out in a glove box under argon atmosphere (O_2< 1 ppm) to eliminate contamination of atmospheric CO_2. The suspension was dialyzed against MilliQ-water at a temperature of 70°C. Water exchange was done every day for the four first weeks, and 2-3 times per week for the remaining time of three months. The pH and solid content of the final product were 4.2 and 41.9 ± 1 g/l respectively. Gibbsite particles are shaped as hexagonal platelets, with a large basal plane accounting for the majority of the surface area, and short edge planes (Fig.1). The diameter and height of these particles were determined with Atomic Force Microscopy, AFM and an N_2-BET analysis was done to evaluate the specific surface area of the mineral.

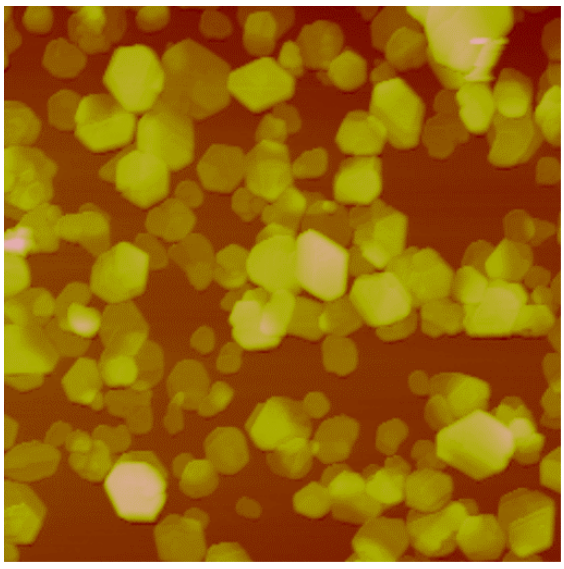

Fig.1: *AFM picture of the synthesized gibbsite particles*

The mineralogical purity and surface composition was examined with XRD and X-ray photoelectron spectroscopy, XPS. To determine the isoelectric point, IEP of the mineral, i.e. the pH value at which the net surface charge equals zero, ζ-potential measurements were performed in 0.1/0.01 M $NaClO_4$ and MilliQ water. The gibbsite suspension was diluted in the three different media to a final concentration of 1 g/l. pH adjustments were done from 4.95 to approximately 12 with NaOH.

- Batch sorption experiments

Batch experiments were conducted in a glove box under Ar atmosphere to exclude CO_2 that influences the speciation of trivalent actinides through the formation of carbonate species at pH values > 6. All reagents were prepared in the glove box. Gadolinium, the lanthanide homologue to curium, was chosen as the metal ion for the study. Gadolinium sorption onto gibbsite was investigated as a function of pH in different electrolytes and ionic strengths; 0.1 M $NaClO_4$ and 0.1 M/0.01 M NaCl. The gibbsite concentration was fixed to 2.2 g/l in each batch, while the Gd^{3+} concentration was varied between $6.4*10^{-9}$ M and $6.4*10^{-5}$ M. pH adjustments were done in small steps by addition of CO_2-free NaOH. The suspensions were shaken periodically for 3-7 days to reach sorption equilibrium. After the equilibration time the samples were centrifuged at 18 000 rpm and the aluminum and gadolinium contents were analyzed in the supernatant with ICP-MS.

- TRLFS study

Two series of three parallel samples were prepared in a glove box in 0.1 M $NaClO_4$ with gibbsite and curium concentrations of 0.5 g/l and $2*10^{-7}$ M respectively. For one sample series the gibbsite suspension was diluted directly in the electrolyte, “gibbsite suspension”. The other series was prepared by using solid gibbsite, (freeze dried gibbsite), re-suspended in the electrolyte, “freeze dried gibbsite”. Solutions were shaken periodically for 2-3 days to reach sorption equilibrium.

Results and discussion

- Gibbsite – synthesis and characterization

The XRD study showed the mineralogical purity and crystalline character of the synthetic gibbsite. Gibbsite surface analysis with XPS revealed the presence of small amounts of chloride (0.16 %) originating from the use of $AlCl_3$ in the Gibbsite synthesis. As the gibbsite surface is positively charged in the stock suspension the presence of small amounts of Cl^- can be explained based on charge neutralization. The aluminum to oxygen ratio was analyzed in the XPS spectrum and was determined to be 0.329, (theoretical value: 0.333). The gibbsite particle diameter and height assessed from 25 particles in the AFM survey were 250 ± 60 nm and 16.8 ± 10.4 nm respectively. The specific surface area of the platelets was determined to be 49.5 m^2/g. The pH value 11.0 was obtained for the IEP of gibbsite (Fig. 2).

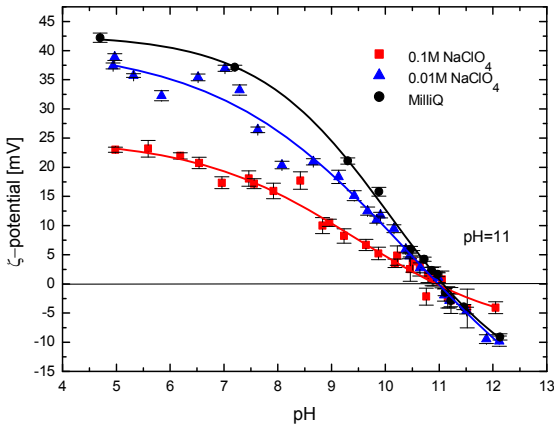

Fig. 2: *Zeta potential diagram. The gibbsite concentration in all three media, 0.1M $NaClO_4$, 0.01M $NaClO_4$ and MilliQ water, was 1 g/l.*

- Gadolinium sorption onto gibbsite

Fig. 3 present the sorption curves for gadolinium concentrations $6.4*10^{-9}$ M - $6.4*10^{-5}$ M in 0.1 M $NaClO_4$. pH curves are congruent at Gd concentrations up to $6.4*10^{-7}$ M, sorption begins above pH 5 and reaches a complete adsorption around pH 7. The two higher metal ion concentrations of $6.4*10^{-6}$ and $6.4*10^{-5}$ M result in a shift of the pH curve to higher pH values, implying that complete sorption is reached at pH 8 instead of 7.

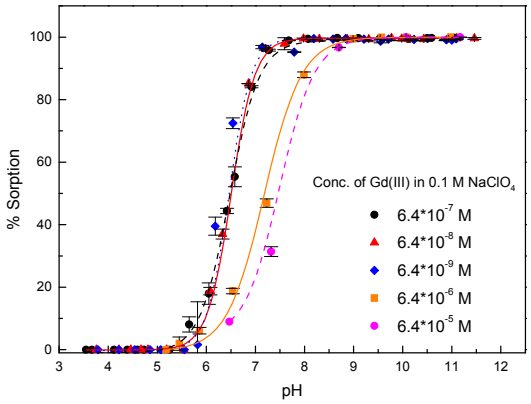

Fig. 3: *pH curves for Gd concentrations $6.4*10^{-9}$ - $6.4*10^{-5}$ M in 0.1 M $NaClO_4$, 2.2 g/l gibbsite*

In the ideal sorption range the position of the pH-edge at a given solid concentration is independent on the metal ion concentration as observed in the present study for concentrations up to $6.4*10^{-7}$ M. At higher metal ion concentrations deviations from the ideal sorption

range result in a shift of the pH edge to higher pH values caused by either saturation effects or binding onto different surface sites. At the highest gadolinium concentration in the present study, a saturation of 35 % of the singly coordinated surface hydroxyl sites on the gibbsite edge planes was calculated, when using a value of 8.5 nm^{-2} for the surface site density. Taking into account the charge of the metal ion of +3 electrostatic interactions can be assumed to be responsible for the saturation effects. Nevertheless, the possibility of gadolinium binding to different sorption sites cannot be excluded, e.g. binding to the doubly coordinated edge and basal plane surface sites. An effect of both the electrolyte anion ClO_4^-/Cl^- and ionic strength 0.1M/0.01M NaCl was investigated but could not be observed.

- Curium emission spectra

Fig. 4 present the curium emission spectra of the gibbsite sample serie "gibbsite suspension" normalized to the highest peak positions. As observed in the previous investigations of curium sorption onto various aluminum oxides by Stumpf et al. [8] and Rabung et al. [6,7] also curium emission spectra in the present study show only one emission peak with a maximum at 593.8 nm for pH < 5. This peak is attributed to the unsorbed curium aquo ion. In accordance with the above mentioned studies, the decrease of the curium aqua ion peak as the pH is raised and sorption onto the mineral surface takes place is being accompanied by a red shift of the emission bands to longer wavelengths and the development of new peak maxima can be observed. Three peak maxima have been identified after peak deconvolution in the investigation of curium sorption onto γ-alumina by Rabung et al. [7], at 600.6 nm, 602.5 nm and 605.7 nm respectively. These peaks were explained to arise from curium inner-sphere complexes bound to the oxide surface in a monodentate fashion. In the present study two peak maxima can be observed at about 603.0 nm and 605.2 nm. A peak maximum that would correlate to the first peak at 600.6 nm in the γ-alumina study could however not be observed. It should be noted that a detailed peak deconvolution should be performed on the emission spectra recorded in the present study in order to determine the correct peak positions of the surface bound Cm species. From the relatively high point of zero charge observed for gibbsite (pH 11.0) follows, that the pH-edge starts at higher pH compared to γ-alumina and therefore the first species is not present or only at a very low concentration. Nevertheless, in the study of curium adsorption onto corundum single crystals the first sorption species was found at about 603.6 nm even at pH 4 [6]. The second surface sorbed species at about 605.2 nm present at higher pH can be explained as a formation of a ternary hydrolyzed Cm species at the mineral surface. The greatest deviation in the emission spectra in this study compared to the previous ones is the inconsistency in spectral evolution with increasing pH and the appearance of a very resolved peak at about 609 nm. This peak is observed in the emission spectra between pH 6 and 11, the range between pH 9-11 however only showing a small shoulder instead of the sharp peak observed at pH 6-9. In addition the Cm emission spectra for the "gibbsite suspension" series show a more evident peak at 609 nm than the "freeze-dried gibbsite" series.

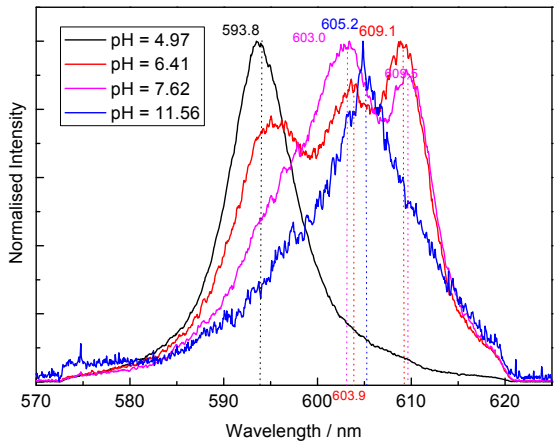

Fig. 4: *Curium emission spectra of the sample series "gibbsite suspension".*

To resolve the origin of this peak and find an explanation for the inconsistency of the emission spectra, additional experiments were performed on a different batch of gibbsite, synthesized and characterized by Mitchell [9], "Mitchell gibbsite". In earlier sorption experiments with this mineral an inconsistency in spectral evolution had only been observed at pH values above 9.5 but no clear peak at 609 nm was present in the emission spectra. Two samples of this gibbsite batch were prepared under the same conditions as described before. One sample was a suspension of the "Mitchell gibbsite" diluted in the electrolyte, the other one re-suspended freeze-dried "Mitchell gibbsite". The pH of both samples was adjusted to approximately 7 and measurements were performed directly after the adjustments. The freeze-dried sample resulted in an emission spectrum consistent with the earlier experiments on the same batch. The suspension sample however developed a very resolved peak just below 609 nm. As reagents and measurement conditions were identical the possibility of contaminated solutions could be ruled out and a hypothesis of a coprecipitation or incorporation phenomenon was suggested.

The TRLFS studies were conducted using sample series with originally very low pH, as both the gibbsite stock suspension was acidic (pH 4.2) as well as the added Cm solution. According to thermodynamic data the solubility of gibbsite is high in the very acidic and very alkaline pH range and showing a solubility minimum between pH 6 and 8. Sorption experiments were thus always performed by increasing the pH from a region of higher to a region of lower Al solubility. At pH > 8 Al solubility increases again as a consequence of the formation of anionic aluminate species. The fact that the new curium species at 609 nm appears in a pH region ranging from 6 to 9 and then decreases again points to the possibility of coprecipitation of curium together with the mineral or incorporation of already adsorbed curium through coverage by the aluminum hydroxide precipitate. When solubility again increases in the very alkaline pH range the coprecipitated/incorporated curium is released and only the metal adsorbed onto the mineral surface can be detected.

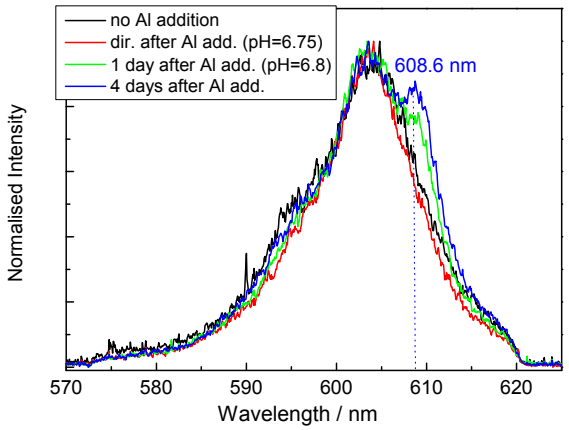

***Fig. 5**: Curium emission spectra of the freeze-dried "Mitchell gibbsite" sample after addition of 10^{-4} M aluminum.*

To support the hypothesis, the freeze dried "Mitchell gibbsite" sample contacted with Cm was allowed to age for 15 days at pH 6.8. After this period of time, the sample was measured again, but no peak at 609 nm could be observed in the emission spectrum. An excess of aluminum, 10^{-4} M, was added to the suspension to exceed the solubility limit of aluminum hydroxide, and the emission spectrum was recorded 0-4 days after the addition. One day after the addition, a peak just below 609 nm had developed and 3 days later the peak was even more resolved, (Fig. 5). This finding supports the hypothesis of incorporation of curium by aluminum hydroxide and explains the inconsistency in spectral evolution with increasing pH. As the mineral solubility increases above pH 9, the concentration of incorporated curium decreases and the emission spectrum shifts back to shorter wavelengths. Furthermore, the fact that the emission peak from incorporated curium was less resolved in the sample series "freeze-dried gibbsite" compared to "gibbsite suspension" and completely absent from the freeze-dried "Mitchell gibbsite" but not the "Mitchell gibbsite" suspension, points to mineral dissolution and precipitation governed by kinetics. Freeze-dried samples, re-suspended and measured within a few days after curium addition do not have time to dissolve in larger amounts and consequently precipitate as the pH is being increased to a region of lower Al solubility. Thus, freeze-dried sample series have less– or no incorporated curium.

Conclusions

The results of the present study showed some similarities in the sorption behaviour of trivalent lanthanides/actinides on gibbsite compared to α- and γ-alumina with respect to surface speciation as studied by TRLFS. Peak positions for observed curium complexes are in accordance with peak positions observed in the γ-alumina study, apart from the first inner-sphere complex at 600.1 nm that could not be found in this work. Similar observations with respect of peak position were made for the Cm sorption study onto corundum single crystals. A clear deviation in the sorption behaviour between the present study and the previous ones caused by pH dependent dissolution and precipitation of the solid phase could however be observed in the spectroscopic study. The main reason for this phenomenon is based on the fact that the gibbsite stock suspension was stored at low pH (4.2) for a long time, thus enabling equilibrium between the solid and liquid phases in the suspension implying the presence of high concentrations of dissolved aluminum. This dissolution and precipitation significantly influences the speciation of surface sorbed metal species as incorporation of curium occurs when adjusting the solution pH from a higher mineral solubility region to a lower one. Further work has to be concentrated on the closer identification of surface species formed at the different gibbsite surfaces.

References

[1] Zhang, H.X., Dong, Z., Tao, Z.Y., Colloids and Surfaces A 278 (2006) 46-52.

[2] Lefevre, G., Duc, M., Lepeut, P., Caplain, R., Fedoroff, M., Langmuir 18 (2002) 7530-7537.

[3] Laiti, E., E., Persson, P., Öhman, L.O., Langmuir 14 (1998) 825-831.

[4] Eng, P.J., Trainor, T.P., Brown, G.E., Waychunas, G.A., Newville, M., Sutton, S.R., Rivers, M.L., Science 288 (2000) 1029.

[5] Liu, P., Kendelewicz, T., Brown, G.E., Nelson, E.J., Chambers, S.A., Surf. Sci. 417 (1998) 53.

[6] Rabung, T., Schild, D., Geckeis, H., Klenze, R., Fanghanel, T., J. Phys. Chem. B. 108 (2004) 17160-17165.

[7] Rabung, T., Geckeis, H., Wang, X.K., Rothe, J., Denecke, M.A., Klenze, R., et al., Radiochim. Acta 94 (2006) 609-618.

[8] Stumpf, T. Rabung, T., Klenze, R., Geckeis, H., Kim J.I., J. Colloid Interface Sci. 238 (2001) 219-224.

[9] Mitchell, S.C., Master Thesis, Brigham Young University (2005).

4.3 Actinide coprecipitation with secondary phases

F.Heberling, M.Schmidt, N.Finck, T.Stumpf, K.Dardenne, D.Bosbach

Introduction

Secondary alteration phases may form during the geochemical evolution within the multibarrier system of a nuclear waste repository system over geological time scales due to the presence of ground water and thermodynamic gradients. Radionuclides, which may have been released from the waste matrix upon contact with groundwater, bind to these secondary phases via various distinct molecular level sorption reactions. Especially, the structural incorporation of radionuclides into secondary phases may present a strong interaction, as the release of radionuclides necessitates the dissolution of the matrix. In principle, secondary phases may be mobile (e.g. colloids) or immobile in the near-field of a nuclear waste repository system as well as in the geosphere, which can result in enhanced or retarded radionuclide migration.

Here we present current R&D activities at INE on coprecipitation and subsequent structural incorporation of actinides with selected secondary phases.

Ln(III)/An(III) – calcite

The interaction of trivalent lanthanides and actinides with the mineral calcite has been intensively studied with various methods in recent years at INE [1-5]. Encouraged by the promising results obtained for Eu(III) by site-selective time-resolved laser fluorescence spectroscopy at low temperatures, the Cm(III) doped system was reinvestigated, applying the same technique. Questions to answer were, how many and which sites are occupied by Cm(III) and how the charge compensation of the replaced Ca(II) is provided.

Calcite powders homogeneously doped with Cm^{3+} and Gd^{3+} were synthesized in a mixed-flow reactor under steady state conditions, at constant pH, ionic strength and temperature. Each calcite is synthesized from three solutions containing Ca^{2+}, $Cm/Gd(ClO_4)_3$ and CO_3^{2-}/HCO_3^-, respectively. The mixed solutions with defined oversaturation with respect to calcite will precipitate in contact with the calcite seeds. The CO_3^{2-}/HCO_3^- solution as well as the background electrolytes are prepared containing either Na^+ or K^+ in order to probe the possible influence of the electrolyte on charge compensation. Cm^{3+} was diluted by the chemical homologous Gd^{3+} to increase the total amount of trivalent cations well above the Na^+ contaminations in the system. Furthermore, this way prevented concentration quenching of Cm^{3+}.

The TRLFS excitation spectra of Cm(III) in calcite (Fig. 1) reveal at low temperature predominantly three resonant transitions from the nearly degenerate ground state to the lowest crystal field level of the first excited electronic level $^7S_{7/2} \leftrightarrow {}^6D_{7/2}$. The transitions of the Cm(III) sites A, B and C at 16.526, 16.213 and 16.015 cm^{-1}, respectively, follow the same sequence of redshifts as found in Eu^{3+}-doped calcite crystals [2]. Also other spectroscopic properties such as coordination symmetry and the emission decay constants (Table 1) show perfect analogy between Cm(III) and Eu(III). The assignment of the respective sites is corroborated by measurements of the lifetimes for each site which are well in line with those measured for Eu^{3+} doped calcites. All results concerning the species identification and characterization are summarized in Table 1.

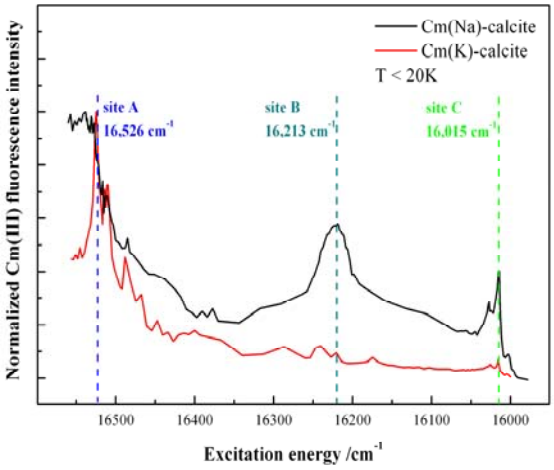

Fig. 1: *Excitation spectra of Cm(K)-calcite and Cm(Na)-calcite. Emission intensities were integrated in the range from 15.980 to 16.550 cm^{-1} at temperatures below 20 K.*

Table 1: *Cm^{3+} sites in calcite. k: Decay constant of the Cm^{3+} fluorescence; the inverse of the emission lifetime: $k = \tau^{-1}$*

	Interaction	Symmetry	k(Cm-calcite) / n(H_2O)[a]
Site A	Sorption	Low	1220 ± 165 s^{-1} / 0.5
Site B	Incorporation	Low	688 ± 55 s^{-1} / 0
Site C	Incorporation	Trigonal	217 ± 18 s^{-1} / 0

The following experiments were performed to shed light on the charge compensation mechanism: if charge compensation is provided by formation of vacancies or incorporation of an anion (e.g. OH^-), a change of the electrolyte during sample preparation should have no effect. If, however, Na^+ was providing for charge compensation, substitution of Na^+ by the much larger K^+ ion should strongly affect charge compensation for both incorporation sites, B and C. The K^+ ion is about one third larger than either of the almost equally sized ions Ca^{2+}, Na^+, Eu^{3+}, Cm^{3+}, and Gd^{3+} (ionic radii in sixfold coordination[6]: Ca^{2+}: 114pm, Eu^{3+}: 109pm, Cm^{3+}: 111pm, Gd^{3+}: 108pm, Na^+: 116pm and K^+: 152pm) and does hardly fit into a Ca^{2+} lattice site.

Comparing the excitation spectra of the samples synthesized with Na^+ (Cm(Na)-calcite) and K^+ (Cm(K)-calcite) reveals the effect of this substitution most clearly (Fig. 1). While in Cm(Na)-calcite a signal for each of the three sites A, B and C is observed, the spectrum of Cm(K)-calcite shows only one prominent peak. The signal for the sorption site A is still present, however, none of the incorporation species' signals is detectable. Obviously, in the absence of Na^+ compensation for the surplus charge of Cm^{3+} is no longer possible, strongly reduced incorporation in the bulk calcite lattice is observed. Sorption onto the crystal's surface site (A), as expected, is more flexible and thus not markedly affected by the substitution of electrolyte.

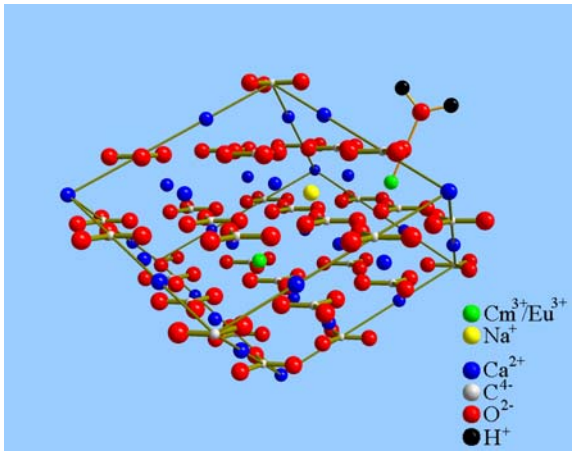

Fig. 2: *Schematic representation of the structure of the doped calcite. One trivalent cation (green) is incorporated into the bulk; its surplus charge is compensated by Na^+ (yellow) on a next neighbour lattice site. Another trivalent cation is sorbed to the surface coordinated by a water molecule.*

These new insights in combination with the results obtained for the Eu^{3+} doped calcite [1-5], clearly show that effective structural incurporation of trivalent cations into calcite requires the presence of a small monovalent alkali metal, such as Na^+. Considering this dependence, it is reasonable to assume Na^+ is providing for the required charge compensation, i.e. a Na^+ ion is incorporated in addition to each trivalent metal ion at a second Ca^{2+} site (Fig. 2).

Np(V) – calcite

In the ongoing study on structural incorporation of Np(V) into calcite several methods were applied in order to corroborate the molecular level picture we gained so far about co-precipitation and structural incorporation of neptunyl in calcite.

In several mixed flow reactor (MFR) experiments neptunyl containing calcite was precipitated under surface reaction controlled conditions at pH ~10.3 at several $Np(V)O_2^+$ to Ca^{2+} ratios. The reaction solutions were undersaturated with respect to all known solid neptunyl phases. The most highly doped calcite containing 1.2 % (mol cations) neptunyl was investigated by low temperature EXAFS, Raman spectroscopy and powder-XRD. As seed crystals for the MFR experiments and for collection of calcite reference spectra we used Merck calcium carbonate suprapur.

Np L3 EXAFS data were collected at the INE-Beamline for actinide research at ANKA in a cryostate at 77 K in fluorescence mode. The EXAFS spectrum in R- Space together with calculated curve fit is shown in Fig. 3.

As annotated in Fig. 3 and Table 2, EXAFS analysis again [7] clearly revealed the fourfold equatorial oxygen coordination around the linear neptunyl moiety. Due to the lower background level of the low temperature data it was for the first time possible to reasonably fit a calcium shell to the data. The low coordination number of the calcium scattering

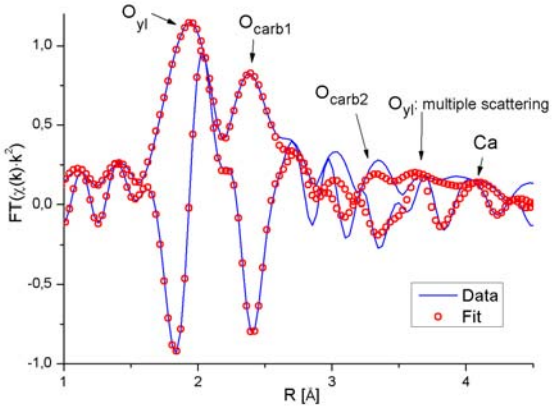

Fig. 3: *Fourier Transform of the k^2 weighted EXAFS data and calculated spectrum, magnitude and imaginary part, for neptunyl doped calcite. Annotations name the scattering paths and corresponding fit parameters with the main contribution to the assigned feature in the spectrum.*

path, fitted after fixation of the Debye-Waller factor, might be an indication for charge compensation by vacant calcium sites, but coordination numbers of distant paths have to be interpreted with great care as indicated by the large standard deviation of this number.

Table 2: *EXAFS fitting parameters: coordination numbers, CN, radii, R, Debye-Waller factors, σ^2.*

	CN	R [Å]	σ^2 [Å^2]
O-yl	2.2 (±0.2)	1.86 (±0.01)	0.00003
O-carb1	3.9 (±0.6)	2.45 (±0.02)	0.006
O-carb2	4.2 (±1.7)	3.43 (±0.04)	0.009
Ca	4.6 (±1.6)	3.97 (±0.04)	0.011

Raman spectra collected on a Bruker Senterra Raman microscope from neptunyl doped and reference calcite are shown in Fig. 4. The additional peak from the $[O=Np=O]^+$ symmetric stretching vibration is clearly visible in the Np-Calcite spectrum. The other typical calcite Raman bands are not significantly influenced by the incorporation of neptunyl. The neptunyl vibration at 753 cm^{-1} is, compared to neptunyl in aqueous solution at 767 cm^{-1} and to aqueous neptunyl carbonate complexes [8] between 762 cm^{-1} and 756 cm^{-1}, shifted towards lower wavenumbers.

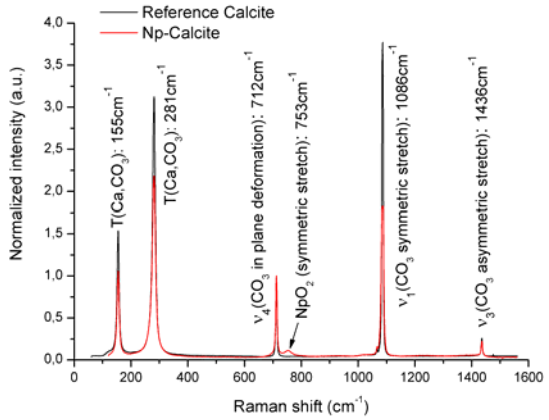

Fig. 4: *Raman spectra of neptunyl doped and reference calcite. The vibrational bands of calcite and neptunyl are annotated in the graph.*

From Rietveld refinement of the XRD powder patterns we deduced the Williamson Hall plots of neptunyl doped and reference calcite shown in Fig. 5. Plotted is the full width at half maximum, β, times cosine of Θ versus the sine of Θ. Evaluated were 68 peaks for each powder pattern. Two conclusions can be drawn from these plots: (i) The slope of the linear fits is directly correlated to the local lattice strain in the crystals, i.e. local lattice strain causes systematic broadening of the diffraction peaks for increasing Θ. (II) The axis intercept is inversely correlated to the scattering domain size, i.e. small scattering domains cause a general increase of the diffraction peak width [9]. Thus what we can see from Fig. 5 is: neptunyl doped calcite has a larger scattering domain size and a higher local lattice strain. This allows the conclusions that calcite precipitates under controlled conditions in the MFR, no homogeneous nucleation occurs, and that local lattice strain is introduced by the incorporation of neptunyl into the crystal structure, which is a strong argument for the structural incorporation. The incorporation of 1.2 % neptunyl into calcite had no significant influence on the scattering peak intensities and the calcite lattice parameters.

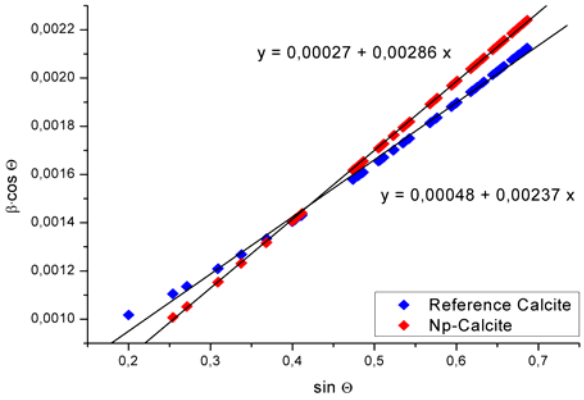

Fig. 5: *Williamson Hall plots of neptunyl doped and reference calcite. Equations of linear fits to the data points are shown.*

Ln(III)/An(III) – clay minerals (hectorite)

Structural incorporation of trivalent lanthanides and actinides into the octahedral layer of clay minerals has been spectroscopically characterized by TRLFS and polarized EXAFS. We have selected hectorite, a magnesian smectite, which has been frequently observed in HLW glass long-term corrosion experiments [10], as a model system. Recent studies about Eu(III) coprecipitation [11] with hectorite suggested a trivalent Ln incorporation into a solid phase: either in a silica phase, or in the clay octahedral layer. A TRLFS study on Cm(III) coprecipitation with hectorite [12] strongly indicated an octahedral substitution mechanism.

Based on this background, hectorite was synthesized [13] in the presence of Eu(III) or Lu(III). Molecular-level structural information was obtained by characterization of the coprecipitated Ln(III) by low temperature (T < 20 K) site selective TRLFS (Eu) and by Polarized-EXAFS (P-EXAFS) spectroscopy (Eu, Lu).

TRLFS – The organo-hectorite multi-step formation allowed to track Eu(III) through the clay mineral synthesis. Excitation and emission data were recorded at low temperature by exciting selectively the $^5D_0 \rightarrow {}^7F_0$ transition for the (Mg/Eu) hydroxide precursor and the Eu(III)-containing organo-clay (Fig. 6). The excitation spectra indicated the presence of more than one Eu species in each sample. The shape of the emission spectra supported an Eu(III) incorporation into a solid phase for both samples. In the precursor, the Eu(III) is bound to 2.5 ± 0.5 H_2O [14] or 5 ± 1 OH^- [15], and in the organo-clay, it is bound to 1.0 ± 0.5 H_2O or 2 ± 1 OH^-. These values match with an oxygen coordinated octahedral site in both solids.

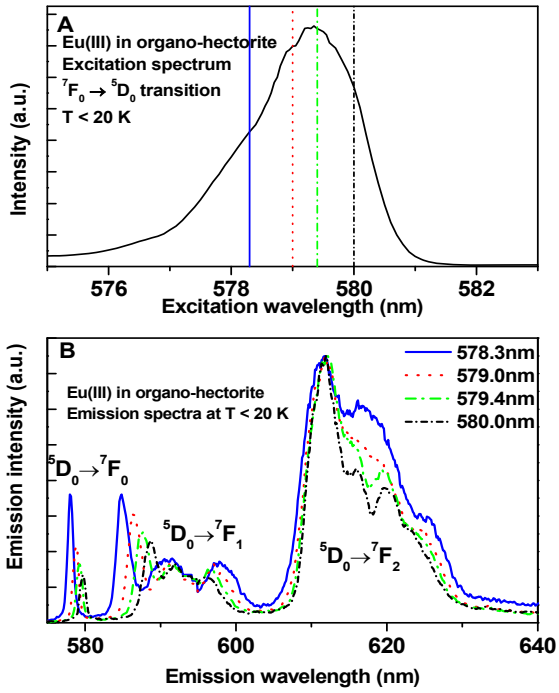

Fig. 6: *Excitation (A) and emission (B) spectra collected for the Eu(III)-containing organo-hectorite.*

EXAFS – Eu(III) or Lu(III)-containing hectorite were prepared as self-supporting films. Different angles between the layer plane and the electric field vector of the x-ray were considered to mitigate the cancelation effects due to backscatterer from the tetrahedral and octahedral layer [16].

Small angular dependences were observed for the P-EXAFS data (Fig. 7). Coordination spheres of 6 O at 2.26 Å and 7 O at 2.40 Å were observed for Lu and Eu, respectively. Further Mg/Si cationic shells were detected at 3.12, 3.25 and 3.85 Å for Lu and 3.24, 3.37 and 4.30 Å for Eu. These results are indicating a clay-related environment. Finally, the Eu incorporation in an amorphous silica phase was ruled out.

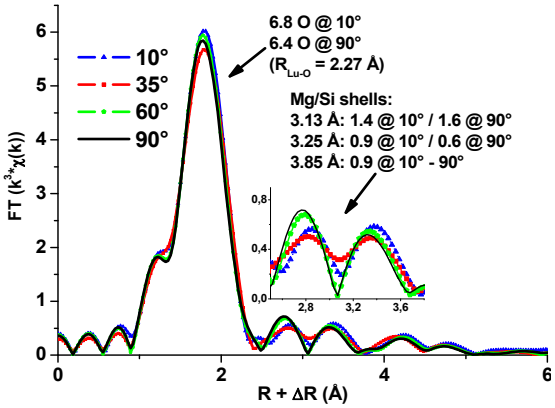

Fig. 7: *Fourier Transform (FT) amplitudes of the k^3-weighted EXAFS data collected at different angles for the Lu(III) coprecipitated organo-hectorite.*

Ln(III)/An(III) – powellite

Powellite ($CaMoO_4$) is one of the secondary phases identified in static batch-type corrosion experiments with HLW glass. The powellite structure exhibits a significant compositional flexibility, which accommodates a wide range of substitutions, including coupled substitutions of Ca^{2+} with monovalent and trivalent cations. Trivalent actinide and lanthanide containing powellite-like molybdate compounds have been synthesized (at high temperature T > 1000°C) and structurally characterized with powder XRD. Under these conditions a complete solid solution series between $Ca_2Mo_2O_8$ and $NaAn(III)/Ln(III)Mo_2O_8$ occurs with significant negative excess volume for La, positive excess volume for Yb and quasi no excess volume for Eu. In order to obtain information on the local ordering in these phases around the La(III), Eu(III), and Yb(III) as substituting lanthanide cations, we investigate a substitution series (1%, 10%, 50%, and 100% Ca replacement) with EXAFS at the La/Eu/Yb L3 edge at varying temperature.

In none of the studied compound, an Ln-Ln interaction has been evidenced in EXAFS excluding the formation of lanthanide clusters in the powellite. The Ln are incorporated in the structure causing more or less crystal disorder (Fig. 8).

The results show that the La-powellite series has a much more disordered structure than the Eu/Yb-powellite series [17,18]. This can be attributed to the size difference between La(III), Na(I), and Ca(II) that introduces perturbations into the local structural arrangement even at low La content. On the contrary, the size similarity between (Eu(III) + Na(I)), and Ca(II) causes this series to have the highest thermal and static structural order. Eu/Yb-powellite

series show an identical trend for the variation of the static disorder with the substitution ratio.

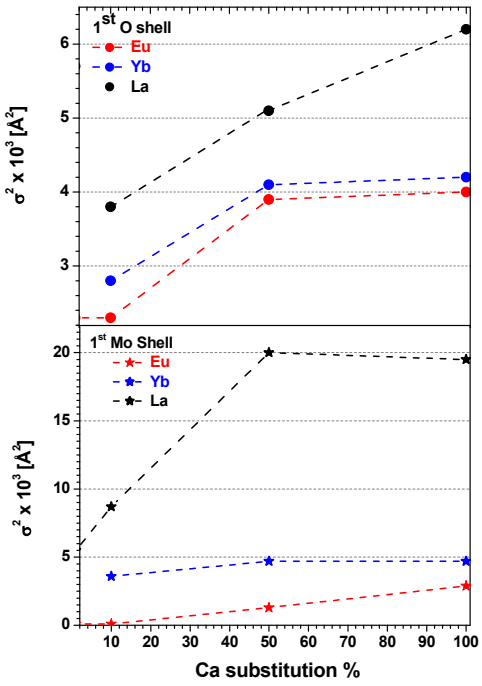

Fig. 8: *Variation of the static part of Debye Waller factor with the Ln molar fraction for the first 2 shells.*

Conclusion and outlook

Combining state-of-the-art mineral synthesis procedures with modern spectroscopic techniques provides a unique molecular level picture of radionuclide uptake mechanisms in aqueous systems. The presented studies will be complemented by thermodynamic modelling of solid solution – aqueous solution equilibria, in order to provide baseline data for geochemical modelling of radionuclide behaviour under waste repository relevant conditions.

References

[1] Stumpf, T., et al., in “Institute for Nuclear Waste Disposal”, H. Geckeis, R. Klenze (Eds.), Annual Report. 2006, Wissenschaftliche Berichte FZKA 7360, Forschungszentrum Karlsruhe (2007).

[2] Fernandes, M.M., Schmidt, M., Stumpf, T., Walther, C., Bosbach, D., Klenze, R., Fanghänel, Th., J. Colloid Interf. Sci. 321 (2008) 323-31.

[3] Fernandes, M.M., Stumpf, T., Rabung, T., Bosbach, D., Fanghänel,Th., Geochim. Cosmochim. Acta 72 (2008) 464-74.

[4] Stumpf, T., Fanghänel, Th., J. Colloid Interf. Sci. 249 (2002) 119-122.

[5] Stumpf, T., Fernandes, M.M., Walther, C., Dardenne, K., Fanghänel, Th., J. Colloid Interf. Sci. 302 (2006) 240-245.

[6] Shannon, R.D., Acta Crystallogr. A32 (1976) 751-767.

[7] Heberling, F., Denecke, M. A., Bosbach, D., Environ. Sci. Technol. 42 (2008) 471-476.

[8] Clark, D. L., Conradson, S. D., Ekberg, S. A., Hess, N. J., Janecky, D. R., Neu, M. P., Palmer, P. D., Tait, C. D., New J. of Chem. 20 (1996) 211-220.

[9] Williamson, G. K., Hall, W. H., Acta Metallurgica 1 (1953) 22-31.

[10] Zwicky H.U. et al., Res. Soc. Symp. Proc. 127 (1989) 129-136.

[11] Pieper H. et al., Clays Clay Miner. 54 (2006) 47-55.

[12] Brandt et al. Geochim. Cosmochim. Acta 71 (2007) 145-154.

[13] Carrado K.A. et al., Clay Miner. 32 (1997) 29-40, Carrado K.A. et al., Langmuir 13 (1997) 2895-902, Carrado K.A. et al., Chem. Mater. 12 (2000) 3052-59.

[14] Horrocks W.deW. and Sudnick D.R., J. Am. Chem. Soc. 101 (1979) 334-340.

[15] Supkwoski R.M. and Horrocks W.deW., Inorg. Chim. Acta 340 (2002) 44-48.

[16] Schlegel M.L. et al., J. Colloids Interface Sci. 215 (1999) 140-158.

[17] Dardenne, K., Bosbach, D., Denecke, M.A., Brendebach, B., Speciation Techniques and Facilities for Radioactive Materials at Synchrotron Light Sources, Workshop Proceedings, Karlsruhe, Germany 18 - 20 September 2006, OECD/NEA (2007) 193 - 201.

[18] K. Dardenne, D. Bosbach, M.A. Denecke, B. Brendebach, 11th Internat. Conf. on the Chemistry and Migration Behaviour of Actinides and Fission Products in the Geosphere, Migration`07, Book of Abstracts, PA2-10, (2007).

5. Applied Studies: Radionuclide retention in the multibarrier system

Investigations reported in this section aim to understand geochemical and geomechanical processes determining mobilization and retention of radionuclides within the individual components of the multi-barrier system. Different to the previous chapter, studies described here focus on the radionuclide behavior in complex systems closer to the "real" repository components. Experiments are thus performed on e.g. real spent fuel corrosion in groundwater, where, however, the aim is to understand underlying processes in detail. Spectroscopic techniques and geochemical data are applied where possible in order to gain speciation information. Geochemical, thermo-mechanical, and hydraulic modeling studies aim at the comprehensive description of radionuclide transport in repository systems.

The present report describes experimental studies on the different impact of α-radiolysis, becoming dominant in spent fuel after decay of most fission products, and α, β, γ-radiolysis, being active in "young" spent fuel on nuclear waste corrosion. Radiolysis has a strong impact on the geochemical conditions of a repository near-field. In order to assess the geochemical behaviour of actinides in the repository far-field, various investigations have been performed in order to understand actinide migration under close to natural conditions. Diffusion of Pu in natural Opalinus clay rock and colloid formation in groundwater-bentonite porewater mixing zones have been studied. Colloids have been quantified in different natural groundwaters by laser-induced breakdown detection (LIBD). Such survey provides data on in-situ stability of natural colloids and thus provides relevant data for the assessment of colloid-mediated radionuclide migration for a wide range of different groundwater geochemical conditions. Natural organic matter is known to influence radionuclide geochemistry due to its redox properties, formation of stable complexes in solution and possible radionuclide retention in case of natural clay-bound organic matter. Latest findings on that issue are discussed.

The final part of this chapter describes model calculations on groundwater and solute transport in a granite shear zone. Those calculations are performed as preparatory work for planned colloid migration experiments in the underground laboratory at the Grimsel-test site (GTS), Switzerland. Thermo-mechanical studies aim at predicting the evolution of the excavation disturbed zone in a rock salt repository.

5.1 Spent fuel matrix dissolution behavior governed by α-,ß-,γ- and α - radiolysis effects: Experimental approach

A. Loida, M. Kelm, N. Müller, E. Bohnert, J. Römer, V. Metz, and B. Kienzler

Introduction

The predominant β- and γ- activity of spent nuclear fuel due to the presence of Cs-137 and Sr-90 will be decayed to a large extent after several hundred years. Corrosion of "old" spent fuel (> 10.000 years) in contact with groundwater will be dominated mainly by radiolysis induced by α-emitting radionuclides. Matrix dissolution and the associated radionuclide release observed in present spent fuel corrosion experiments reflect the presence of a radiation field, generated by α-,ß-,γ-activity. This results in the formation of related radiolysis products, which cause oxidation and subsequent dissolution of the UO_2 matrix. Radiolysis products are expected to be different for "old" and "young" spent fuel with respect to type and concentrations. This can result in a different corrosion behavior. In order to simulate "old" spent fuel, experiments using present spent fuel have been performed, where the β/γ-radiation field is "masked out". As an experimental approach the use of powdered spent fuel, which is only moistened by a thin water film is applied. By this way, far ranging β/γ radiation cannot induce water radiolysis, and α-radiolysis is expected to prevail. In this context, two experimental arrangements were used, where first, 1 g powdered spent fuel was contacted with 20 ml de-ionized water (DIW) (α-,ß-,γ- radiolysis are effective) and second the powder was only covered with 100 µl DIW water (α-radiolysis should prevail).

Special attention was directed on the formation of radiolysis products, the dissolution rate of the matrix and the associated release/retention of radionuclides under both conditions. Moreover, corroded fuel powders are analysed by Raman spectroscopy and SEM/EDS.

Experimental

Powdered spent fuel samples of each 1 g with an average particle size about ~3 µm were corroded over 490 days in DIW (Milli-Q water). In experiment "R1" 20 ml DIW were permanently stirred with spent fuel powder. α-, ß- and γ- radiolysis were active in this experiment. In experiment "R2" only 100 µl DIW were added to the powder to ensure that α-radiolysis will dominate. Fig. 1 shows the arrangement of both experiments mounted on a metal plate and installed within the hot cell.

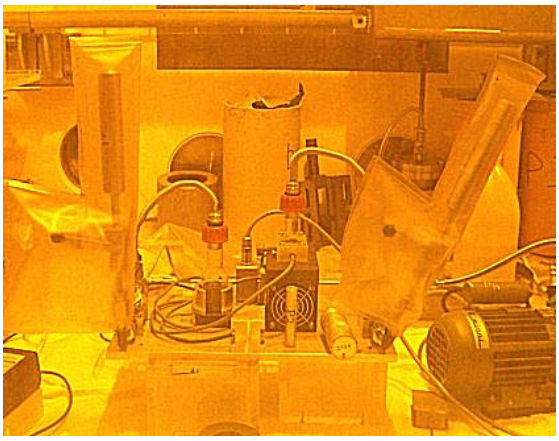

Fig. 1: *Reaction vessels, enveloped gas collection cylinders mounted in the hot cell to study simultaneously the corrosion of spent fuel powder in 20 ml DIW (left - R1: α-,ß-,γ- radiolysis) and 100 µl DIW (right - R2: masking out of ß-,γ- radiolysis).*

At the end of both experiments the gas composition in the headspaces were analyzed by means of mass spectroscopy. To enable sampling of the solution in experiment "R2", it was necessary to replenish the solution of 100 µl to final 20 ml. Afterwards aliquots from both solutions of experiments "R1" and replenished "R2" were analyzed with respect to the amount of dissolved H_2O_2 and dissolved radionuclides. Additionally, a few small particles of the corroded material of about 50 µm in size from both experiments R1 and R2 were selected, by use of micromanipulator technique, and subsequently fixed on a carbon tape for SEM/EDS and Raman studies. Because of the low dose rates (< 50 µSv/h) samples could be transfered to the analytical devices outside the hot cell.

Results and discussion

Fuel powder sampled after experiment "R2" which has been in contact with 100 µl of water was strongly agglomerated, and partly cemented probably due to the formation of newly formed secondary phases.

Formation of radiolysis products

The concentration of radiolytically formed H_2O_2 was found to be below the detection limit of $1x10^{-6}$ M in both experiments. This is in agreement with the well known rapid H_2O_2 decomposition (see also Bruno et al. [1]). Different amounts of H_2 and O_2 were encountered in experiments "R1" and "R2", shown in Fig. 2.

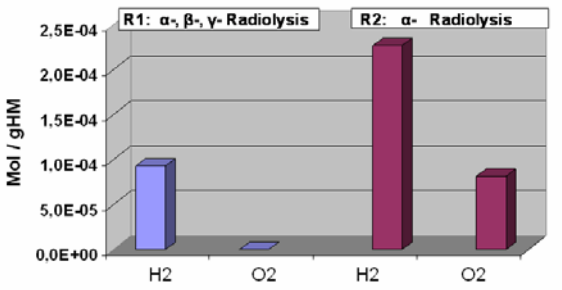

Fig. 2: *Radiolysis gases H_2 and O_2 measured after 490 days of spent fuel powder corrosion in 20 ml DIW ("R1") and in 100 µl DIW ("R2")*

In experiment "R1" (α-, ß-, γ-radiolysis) about $8x10^{-5}$ Mol H_2 and < $1x10^{-5}$ Mol O_2 (<detection limit) were analyzed, whereas in experiment "R2" (α -radiolysis) the amounts of both H_2 ($2.2x10^{-4}$ Mol) and O_2 ($8x10^{-5}$ Mol) were found to be more than twice as high. These lower H_2 and O_2 levels in experiment "R1" may be explained by reactions of radiolytically generated H_2, O_2 and H_2O_2 with radicals produced by ß-, γ -radiolysis thus forming H_2O. O_2 may be in addition consumed by U(IV) oxidation to U(VI) due to effective exposure of the matrix grains to the solution by intense stirring.

Matrix dissolution, release of radionuclides

The UO_2 matrix dissolution progress was quantified by measuring the release of Sr into the aqueous phase [2] in terms of $FIAP_{Sr}$ values (Fraction of the inventory in the aqueous phase). During 490 days of corrosion, it was that about 0.14% of the matrix ($FIAP_{Sr}$ $1.4*10^{-3}$) was dissolved in experiment "R1", and about 0.08 % in experiment "R2" ($FIAP_{Sr}$ $8*10^{-4}$). Differences are smaller than expected. Fig. 3 shows the fractions of radionuclides released into solution and into the gas phase during corrosion for both experiments. Different behaviour is observed for radionuclides (1) located in the fuel matrix such as Sr, Am, Np, Pu, U and radionuclides (2) encountered in matrix and grain boundaries (Cs, Tc, Kr). FIAP values for Am, Np, Pu, U are significantly lower than that for Sr. These differences are visualized by the hatched bars in Figure 3 and indicate sorption, precipitation of secondary phases for those elements. Am, Np, Pu and U concentrations measured in experiment "R2" (100 µl DIW) are distinctly lower than found in experiment "R1" (20 ml DIW). These lower FIAP values for Am, Np, Pu and U are most likely related to solubility limits rather than to differences in radiolysis effects. The limited

solution volume in “R1” experiments prevents further dissolution.

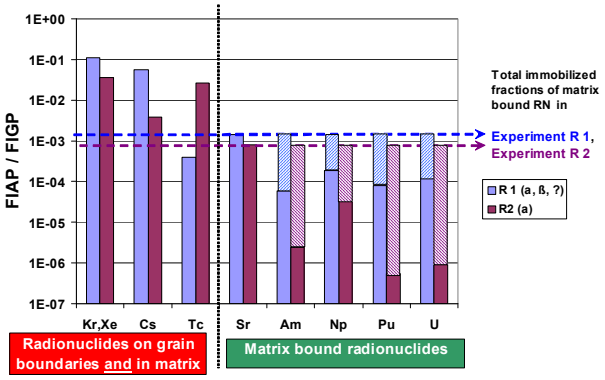

Fig. 3: *Fractions of radionuclides released in the aqueous phase (FIAP) and into the gas phase (FIGP) in experiments R1 and R2 after 490 days corrosion in DIW, shown by filled bars. Hatched bars represent the fractions of re-immobilized matrix bound radionuclides.*

In both experiments U and Pu concentrations lie at the same level (i.e. U 10^{-5} M, Pu 10^{-7} M). Cs and Kr release was higher than matrix dissolution, indicating additional release from grain boundaries. The elevated FIAP values for Cs and Kr in experiment “R1” are again attributed to the more effective grain surface exposure to the solution by permanent stirring. The high fraction of Tc released into solution during experiment “R2” is presently not understood (cf. Fig 3). It may be explained by the heterogeneous Tc distribution in the fuel and possible enrichment at the grain boundaries of the spent fuel powder sample used in experiment “R2”. Preferential dissolution of the exposed Tc phase may rationalize the experimental finding.

Investigation of solid phases

Inspection of corroded fuel particles using SEM/EDS techniques have confirmed the formation of new secondary phases to a high extent. They are of prismatic tabular shape and show frequently an orthorhombic symmetry. EDS reveals U and O as main components. By means of Raman spectroscopy these crystals were identified as meta-schoepite (836 cm^{-1}). Fig. 4 shows SEM micrographs of a non corroded spent fuel powder and the corroded fuel powder sample “R2” with newly formed meta-schoepite crystals. The related Raman spectrum taken from such particles from the corroded SF powder “R2” is shown in Fig. 5 together with a reference spectrum of a synthetic meta-schoepite.

Concluding remarks

Higher amounts of H_2 and O_2 are generated under experiments where the α-radiation field prevails. Radicals produced by far ranging β-

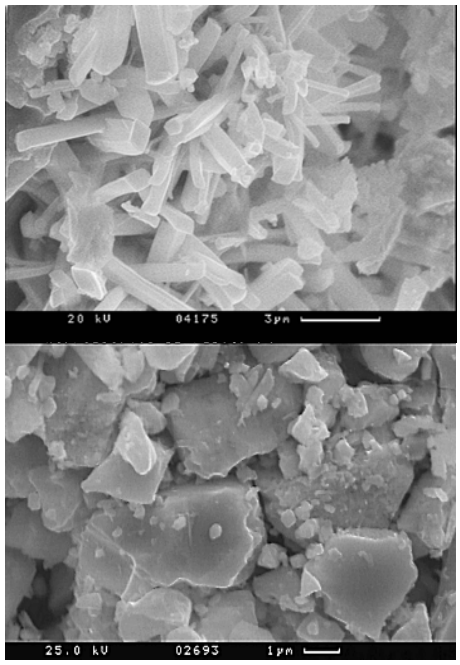

Fig 4: *SEM micrographs of non corroded spent fuel powder (upper) and newly formed secondary phases (lower) containing U and O, probably meta-schoepite.*

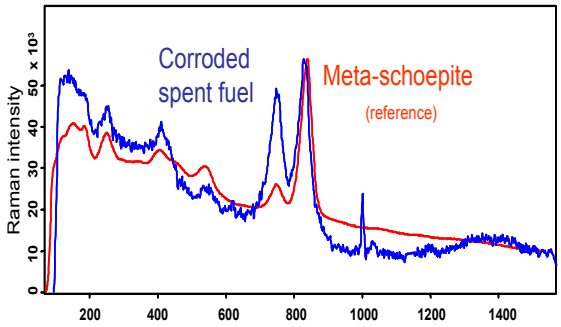

Fig 5: *Raman spectra of meta-schoepite, measured on newly formed secondary phase upon spent fuel sample R2 corroded 490 days in DIW (blue) and reference sample of synthetic meta-schoepite (red).*

and γ-radiation are assumed to react with H_2, O_2, and H_2O_2 to form H_2O thus reducing H_2 and O_2 amounts in the combined α-,ß-,and γ-radiation field. Additional O_2 consumption by UO_2 oxidation is observed in experiments with intense stirring. The reduction of ß/γ radiation effects caused a slightly decreasing matrix degradation. U and Pu concentrations appeared to be controlled by solubility constraints in both experiments. In particular, in experiment “R2”, the formation of newly formed meta-schoepite was observed to a large extent. Radionuclides released into solution appear to be more associated to S/V ratios and solubility limits, rather than by the different radiation fields.

5.2 Pu diffusion in Opalinus Clay

B. Fiehn, N. Banik, C. Marquardt, M. Klein, A. Görtzen, J. Römer, B. Kienzler, A. Bauer

Introduction

Argillaceous media are being considered in many countries as potential host rocks for the final, safe, near surface or at depth disposal of radioactive waste, and/ or as major constituent of the repository system. Countries in Europe with an extensive research program on this option are Belgium, France, Hungary and Switzerland. Argillaceous media have a number of favorable generic properties, e.g. homogeneity, low water flow, chemical buffering, propensity for plastic deformation and self-sealing of fractures, and marked capacity to chemically retard the migration of radionuclides [1].

The Opalinus Clay (OPA) formation in the Züricher Weinland is a potential host rock formation for a repository for spent fuel, vitrified high-level waste and long-lived intermediate level waste in Switzerland. Owing to its small hydraulic conductivity (10^{-14}-10^{-13} m/s), it is expected that transport of solutes will be dominated by diffusion. The objective of this work is to understand actinide diffusion in clay mineral-rich geological formations in order to provide support for improved representation of these processes in performance assessment and to enhance safety case credibility. This study addresses the diffusion of tritiated water (HTO) and ^{238}Plutonium (Pu). The samples were collected in the Mont Terri underground laboratory where the OPA is situated -200 to -300 m below surface. A sample cell - autoclave system (SCAS) was required for carrying out actinide diffusion experiments in clay stones under their natural, confining pressure.

When actinides enter the environment, the chemical interactions are inordinately complex. Precipitation and dissolution of actinide-bearing solids limit the upper actinide concentration in solution, while complexation and redox reactions determine the species distribution and stability. The interaction of a dissolved species with mineral and rock surfacees and/or colloids determines if and how those species will migrate through the environment.

Plutonium exhibits a complex redox chemistry that defines its potential for immobilization and migration. Water is the dominant transport medium and water chemistry determines which actinide oxidation states predominate and which actinide species are stable. Under oxidizing conditions, the most predominant of plutonium is $Pu(V)O_2^+$. $Pu(V)O_2^+$ hydrolysis starts only at pH > 8 and is relatively mobile under oxidizing conditions. The prevalent oxidation state in natural groundwaters, however, is Pu(IV) [2]. The light actinides, including plutonium, form strong complexes in oxidation state IV [3]. Aqueous tetravalent plutonium, Pu(IV), exhibits a solubility of several orders of magnitude lower than Pu(V) or Pu(VI) depending on actual groundwater conditions. In general, actinide solubilities are so low in most natural waters - below micromolar concentrations - that only advanced spectroscopic techniques can detect the species present, a prerequisite for understanding environmental chemistry. An overview of the chemistry of plutonium in aqueous solution is given by [3] and [2].

In our experiments we used ^{238}Pu. ^{238}Pu has a half-life of 87.7 years and is an alpha emitter. Because of its alpha activity (6.3 *10^{11} Bq/g), it can be measured by α-spectrometry down to very low concentrations (detection limit in our experimental set-up 1.5 x 10^{-11} mol/L).

Experimental Set-up

The experimental set-up (Fig. 1) is described in detail in [4].

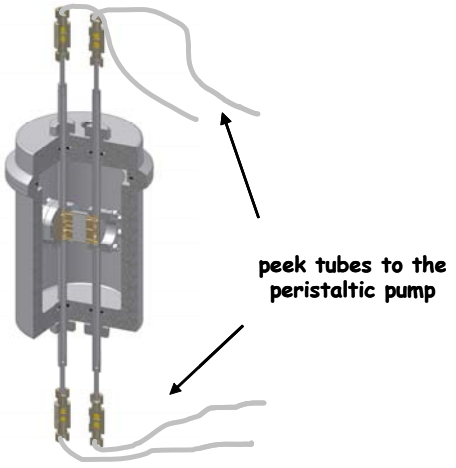

Fig. 1: *Schematic presentation of the INE diffusion cell/autoclave system (SCAS)*

HTO- and Pu diffusion in OPA

The Pu diffusion experiments were performed at four different run times and different initial pH values (see Table 1). All 3 samples were made out of a drill core from Mont Terri provided by NAGRA.

Table 1: *Experimental detail of the Pu diffusion experiments. De is the effective diffusion coefficient [m^2/s].*

			Reservoir		
run number	run time (days)	De HTO OPA (⊥) to bedding (m^2/s)	initial/final ^{238}Pu conc. (mol/L)	inital pH / Eh	final pH/ Eh_{SHE}
HTO Test	100	1.53×10^{-11}	/	7.8 / 360 mV	7.9 / 370 mV
OPA1-SCAS1	150*	1.55×10^{-11}	7.64×10^{-9} / 2.8×10^{-11}	7.8 / 360 mV	8.4 / 30 mV
OPA1-SCAS2	280	1.60×10^{-11}	5.63×10^{-9} / 2.87×10^{-10}	8.4 / 400 mV	8.5 / 390 mV
OPA2-SCAS3	93	1.45×10^{-11}	5.38×10^{-9}/3.12×10^{-10}	7.9 / 380 mV	8.2 / 370mV

*(120 days in and 30 days out diffusion)

With four different OPA samples we measured the effective diffusion coefficient (De) perpendicular to the bedding for HTO. We used HTO to verify if our diffusion cells show any preferential pathways. All values are given in Table 1. The average De was found to be 1.53×10^{-11} m^2/s. All obtained results are within a variation range of 10 % of the average value. According to an autoradiography study HTO diffusion was homogeneous within the core and no preferential pathways were detected.

Evolution of the Pu oxidation states in the OPA porewater

The Pu oxidation states (Fig. 2) as a function of time in the simulated Opalinus porewater were determined by PMBP-extraction [5] for a period of one year. In the Opalinus porewater the pH was adjusted in the beginning to pH 8.2 and the Eh_{SHE} was ~ 350 mV. No change in pH and Eh was observed during the experiment. Whereas in the stock solution 85 % Pu(VI) and 15 % Pu(IV) were observed, the Pu oxidation state changed predominantly to Pu(V/VI) (72 %) after 4 days equilibration time in the OPA porewater.

The evolution of the ^{238}Pu concentration in solution indicates with increasing run time a continuous but steady decrease of the Pu concentration. After one year, only 26 % of the initial Pu was found in solution. After washing the container with HNO_3 at the end of the experiment,74 % of the Pu were found sorbed on the container walls as Pu(IV). Taking sorbed and dissolved Pu into account (Fig. 2) the Pu oxidation states changed to 83 % Pu(IV) and 17 % of Pu(V/VI). In the experiments with porewater in contact with clay no sorption on the container wall was detected.

Pu sorption experiments

We monitored the concentration of Pu (initially 7×10^{-9} mol/L) in solution in batch experiments with clay rock in the pH range 4.75 to 10.23 for one year. Above pH 6 a "steady state concentration" was reached after 12 hours. As a function of time no further evolution of the Pu concentration was observed. In seven batches

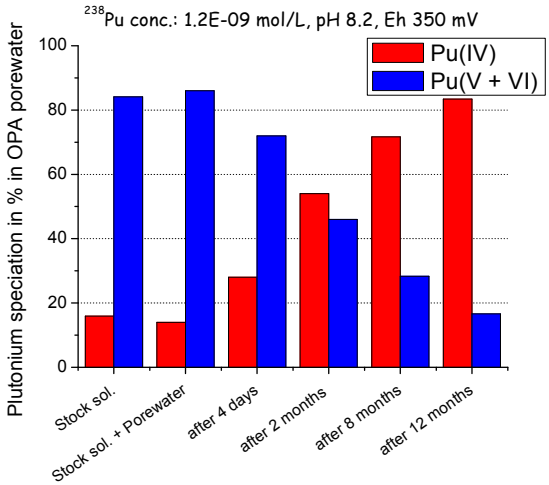

Fig. 2: *Evolution of the Pu speciation in the OPA porewater. The sorbed Pu(IV) from the container walls was added to the Pu(IV) in solution.*

we observed a significant drop of the Pu concentration already after one hour of reaction. The post-mortem XRD analysis of the clay rock by Rietfeld refinement revealed in these samples an unusually high amount of pyrite (~ 40 %) compared to the other samples (~ 1 %). In the "normal samples" the Eh decreased from the initial value of ~ 350 mV to values of around ~ 200 - 150 mV after 12 hours and in the samples rich in pyrite down to a value of ~ 70 mV after one hour. Starting from pH 4.75 the Pu concentration in solution decreases with increasing pH and reaches a sorption maximum at pH 7.2 (Fig. 4). At pH values > 7.2 the Pu concentration in solution increases again. According to the results of the batch sorption experiments a strong Pu sorption under the experimental conditions of the diffusion experiments can be expected. Some batch samples were kept in the glove box and resampled after one year. The Pu concentrations for the samples at pH > 7.2 after one year were close to the detection limit for Pu in our system (detection limit in our experimental set-up 1×10^{-11} mol/L). The pH showed only slight changes and the Eh remained stable within the error of the measurement (± 50 mV).

We measured the evolution of the Pu speciation as a function reaction time in the OPA supernatant porewater and on the solids at pH ~ 8. In the supernatant solution 87 % of the Pu exist as Pu(V/VI) and 13 % as Pu(IV). To determine the oxidation state of clay sorbed Pu we washed the solid with concentrated HNO_3. The Pu removed from the clay after 24 hours consists of Pu(IV) (80 %) and Pu(V/VI) (20 %). After one year all Pu was sorbed on the clay and the oxidation state was found to be IV.

Results on the Pu diffusion in OPA

Three different diffusion experiments are presented. For OPA1-SCAS1 we observed an initial strong and fast decrease in the Pu concentration in the solution reservoir reaching a "steady state" concentration of 2.7 x 10^{-11} mol/L after seven days. During the experimental run time of 150 days the pH shifted from 7.83 to 8.43 and the Eh dropped from 430 to 30 mV. In the two other experiments the pH and the Eh of the OPA porewater remained unchanged throughout the experiment. The Pu concentrations dropped in OPA1-SCAS2 by one order of magnitude to ~ 6 x 10^{-10} mol/L after 16 days. In the OPA2-SCAS3 experiments the Pu solution concentration decreased faster. After 70 days the Pu concentrations for both systems converged and reached a "steady state" concentration of ~ 3 x 10^{-10} mol/L.

At the end of the experiment OPA2-SCAS3 (93 days) the Pu oxidation state in the solution was determined. Like in the OPA porewater in contact with the Opalinus clay, we found as the dominant oxidation state Pu(V/VI) in solution whereas for OPA sorbed species Pu(IV) was dominant.

In the control solution of the all 3 experiments where no radioactive tracer was injected, the first α-activity was measured after 30 days experimental duration. A selective Pu extraction indicated that the detected α-activity was not due to through-diffusion of ^{238}Pu, but came from ^{228}Th released to the solution from the Opalinus clay sample.

At the end of the experiments the autoclave system and connected tubings were washed for two hours with 65 % HNO_3 to check sorption to the experimental set-up. This test showed that around 20-40 % of the initial Pu was sorbed on the container walls and the tubings of the diffusion experiment.

Out diffusion experiments

After 120 days of experimental run time we replaced the Pu spiked OPA porewater of the OPA1-SCAS1 experiment in the in diffusion reservoir by fresh OPA porewater. No increase of Pu concentration in the blank porewater was observed indicating no out diffusion during 30 days.

Analysis of the cores

After the diffusion experiments, bore core samples were taken out and embedded into epoxy-resin. Slices of clay were analysed by autoradiography. Samples of all 3 cores show clearly that no preferential pathways for the migration of Pu exist.

It is, however, evident that the Pu diffusion within the OPA is not homogenous. The Pu is always concentrated in distinct areas which are distributed differently within the core. The highest measured punctual Pu concentration was 200 ppt. In the crosscut through the clay core of OPA2-SCAS3 we found 2 distinct areas where Pu was concentrated. SEM-EDX analysis showed no specific correlation with a specific mineral phase in this area. By measuring the activity of the Pu sorbed on clay particles sticking on the distribution plate of the diffusion cell we were able to show that the solution really covered the whole sample. The profiles measured with autoradiography are different. Whereas one profile shows the diffusion of the Pu over a distance of ~ 5 mm at the end of the experiment (93 days), the diffusion in a second profile in the same core is much more restricted (~ 1 mm). A similar observation was made for OPA2-SCAS2. In OPA1-SCAS1 we found some pyrite in areas of Pu enrichment but also Pu accumulation in areas with no correlation with specific minerals.

Discussion

HTO-diffusion in OPA: The effective diffusion coefficient perpendicular to the bedding was found to be 1.53 x 10-11 m^2/s. This value is in good agreement with the data of [6]. Autoradiography results demonstrated that the HTO diffusion within the core is homogenous. No preferential pathways for the diffusion of HTO and also Pu exist.

Pu in the OPA porewater: To investigate the stability of Pu in the OPA porewater the Pu concentration, oxidation state distribution, pH and redox potentials were monitored as a function of time. At first the Pu(VI) is partly reduced in the OPA porewater to Pu(V) according to the redox equilibrium

$$PuO_2^{2+} + e^- \leftrightarrow PuO_2^+$$

Because of the initial low Pu concentration no change in the Eh can be observed. In the sample the Pu(VI) is nearly completely

reduced to Pu(V) and further to Pu(IV). This observation is in agreement with the observation made by [7]. Because of the reduction of the Pu(V) to Pu(IV) we might exceed the equilibrium concentration and consequently precipitate colloidal Pu(IV) which sorbs on the container walls. With a concentration of 1E-10 mol/L we are at solubility limit of Pu(IV) in the given system [7]

Pu concentration in diffusion & sorption experiments: Two trends for the Pu concentration can be observed in the diffusion experiments. In OPA1-SCAS1 the Eh dropped from 430 to 30 mV during the experiment. After only seven days Pu concentration reached a steady state of ~ 2.7E-11 mol/L. In the other two experiments the Eh-value remains unchanged and the Pu concentration decreased slowly and finally remains one order of magnitude higher than in the OPA1-SCAS1. We explain that by the high amount of pyrite (~ 45%) in the uppermost layer of the core. A similar observation was made for the sorption experiments. In some samples, enriched from the beginning in pyrite, Pu was nearly completely sorbed within one hour of contact time accompanied by a decrease in Eh. At least two different possibilities exist concerning the fate of the initial Pu(VI) in solution.

The Pu(V/VI) was reduced in solution to Pu(IV) [7]. The resulting Pu(IV), possibly present in colloidal form, subsequently sorbed onto mineral surfaces. The other possibility is that Pu(VI) was first sorbed and finally reduced at the mineral surface as it was described for pyrite by [8] or [9] for U(VI).

Because of the very low Pu concentrations in our experiments we have no direct possibility to verify the different possibilities and further experiments are needed.

Conclusions

Diffusion of Pu and HTO in the OPA was studied by the through-diffusion method. The diffusion coefficients for HTO from our experiments were in excellent agreement with those determined in through-diffusion experiments in other laboratories.

The experiments show that (i) about 20-40 % of Pu is sorbed on components of the experimental set-up, (ii) the mobile Pu inventory is dominated by Pu(V), (iii) there is no preferential transport pathway for Pu in the clay sample and Pu is accumulated within the clay core at certain sites. Sorbed Pu was Pu(IV). Futher experiments are needed to determine the reducing and subsequently sorbing mineral phase The experiments indicate that the Pu mobility in claystones is limited. Pu(V/VI) is reduced to Pu(IV) and sorbed by the claystone.

Trustworthy determination of the diffusion behaviour of actinide ions in clay requires carefully designed experimental set-ups and development and application of a series of analytical techniques. Careful cross-checking is required in order to verify that the samples are not subject to undue disturbances, especially those resulting in preferential artificial transport pathways. Trustworthy interpretation of transport experiments also requires batch sorption data and 3D distribution of along the diffusion samples. The present work shows that all these objectives could be reached for the in-house built diffusion experiment system and by the development and application of the required associated analytical techniques.

These ongoing investigations will provide the necessary basis for a credible description of radionuclide mobility in clay for the nuclear waste disposal safety case.

References

[1] Mazurek, M., Pearson, F. J., Volckaert, G., Bock, H., Features, Events and Process Evaluation Catalogue for Argillaceous Media. In: NEA (Ed.). OECD (2003).

[2] Choppin, G. R., Radiochim. Acta 91 (2003) 645-49.

[3] Runde, W., The Chemical Interactions of Actinides in the Environment (2000) Los Alamos Science.

[4] Bauer, A., Fiehn, B., Marquardt, C. M., Klein, M., Römer, J., Schäfer, T., Görtzen, A., Kienzler, B., SKB-Report TR-07-05 (2007) 231-38.

[5] Neu, M.P., Hoffman, D.C., Roberts, K.E., Nitsche, H., Silva, R.J., Radiochim. Acta 66-7 (1994) 251-258.

[6] Van Loon, L. R., Soler, J. M., Bradbury, M. H., J. Contam. Hydrol. 61 (2003) 73-83.

[7] Neck, V., Altmaier, M., Seibert, A., Yun, J.I., Marquardt, C. M., Fanghanel, T., Radiochim. Acta 95 (2007) 193-207.

[8] Eglizaud, N., Miserque, F., Simoni, E., Schlegel, M., Descostes, M., Radiochim. Acta 94 (2006) 651-656.

[9] Wersin, P., Hochella, M. F., Persson, P., Redden, G., Leckie, J. O., Harris, D. W., Geochim. Cosmochim. Acta 58 (1994) 2829-2843.

5.3 Colloid impact on radionuclide migration

P. Kunze[1], H. Seher, P. Panak, W. Hauser, R. Götz, H. Geckeis,T. Schäfer

[1] University of Applied Science (FH), Faculty of Mechanical Engineering, P.O. Box 1455, D-02754 Zittau/Görlitz, Germany

Introduction

Inorganic colloids in groundwater can be either generated in-situ as a consequence of chemical gradients or by dispersion from surrounding rock. The present report describes investigations on colloid formation in the mixing zone of bentonite porewater-groundwater representative for the situation in a granitic environment. The interaction of radionuclides with such type of colloids is studied by filtration experiments and laser fluorescence spectroscopy. But colloids also exist in natural groundwater under non-disturbed conditions. Analysis and characterisation of colloids as a function of groundwater chemistry provides information on colloid relevance under groundwater conditions in the far-field of a repository. The results presented here have been obtained in the frame of a cooperation with the Swedish nuclear waste management organisation SKB and are part of the Swedish site investigation program.

Colloid formation in the Grimsel granite groundwater – Febex bentonite pore-water mixing zone

The engineered barrier system (EBS) of a deep geological repository for high-level nuclear waste foresees in most concepts the use of bentonite as backfill material [1,2]. In the case of granite as host rock formation the bentonite will be most probably in contact with water conduction features (fractures) and consecutively water saturated with the formation of a gel layer. The recently discussed scenario of glacial water intrusion [3] estimates a high erosion of bentonite buffer due to the contact with glacial water of high pH and low salinity favoring the release of bentonite colloids/particles. In the framework of the Grimsel Test Site (GTS) Phase VI the international Colloid Formation and Migration (CFM) project with partners from Japan (JAEA, AIST and CRIEPI), Switzerland (NAGRA), Sweden (SKB) and Germany (FZK-INE) investigate processes related to this bentonite erosion and the possible formation of colloids (see Fig. 1).

The migration of bentonite colloids and associated radionuclides in the shearzone under investigation in CFM has been

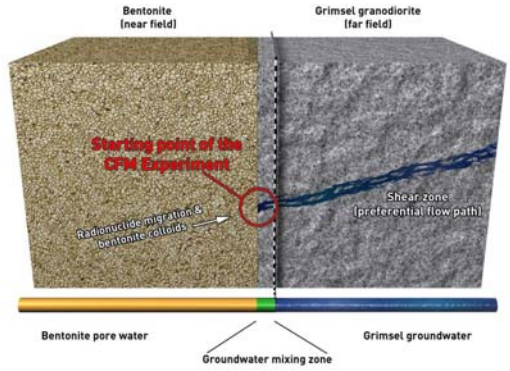

Fig. 1 *Schematic illustration of the bentonite porewater Grimsel groundwater mixing zone investigated in this study (courtesy NAGRA).*

demonstrated in earlier studies [4, 5]. Beside the formation/erosion of colloidal material of smectite type also the neo-formation of colloids due to the geochemical gradients and oversaturation of mixing waters has to be considered. Concerning the formation of aluminosilicate colloids, laboratory studies have already demonstrated that these newly formed phases can have a significant influence on the speciation of trivalent actinides [6].

The focus within this study was particularly on (a) the potential formation of colloids as a function of admixture of Febex porewater to Grimsel groundwater from the so called Migration shearzone (AU Tunnel TM 96) and (b) the influence on the speciation of radionuclides present in the bentonite porewater. A whole suite of techniques was used to investigate the potential formation of colloids, their characterization and the fate of radionuclides in this mixing zone including laser-induced breakdown detection (LIBD), ultrafiltration, ICP-MS, SEM-EDX and time resolved laser fluorescence spectroscopy (TRLFS) as well as geochemical modeling with PHREEQC.

Results and Discussion

A strong pH gradient can be seen in the range of low Febex porewater (FPW)/Grimsel groundwater (GGW) ratios up to approximately 30% before it levels off. In the same region also the highest changes in cation composition could be detected. Interestingly, the oversaturation (saturation index SI > 0) for calcite as well as for fluorite indicates that these phases might be formed in this range of high groundwater admixture. The Febex

porewater is in equilibrium with quartz and under-saturated with respect to chalcedony, whereas it is clearly oversaturated with respect to gibbsite. It is interesting to notice that the simulation of different groundwater/pore water ratios prognoses the potential formation of mineral phases that might re-dissolve with further dilution of porewater with Grimsel groundwater, a phenomenon that has been seen in waste plume fronts [6].

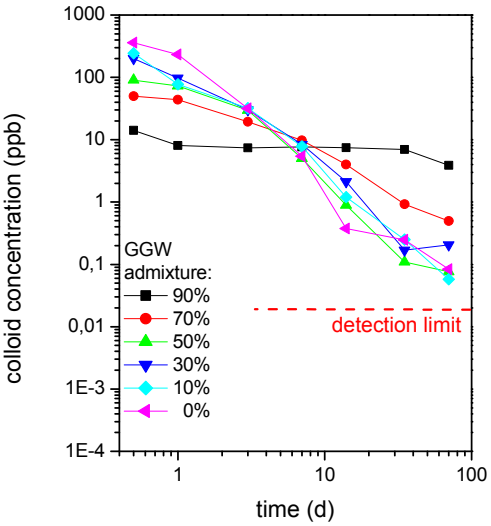

Fig. 2: *Time dependent evolution of colloid concentration as measured by LIBD. The dashed line indicates the detection limit of LIBD.*

The colloids generated in the mixing zone aggregate when the synthetic FPW content exceeds 10%. LIBD analysis of the time-dependent colloid generation/aggregation revealed a low concentration of colloids to be stable with an estimated plateau value around 100 ppt and an average colloid diameter around 30 nm after 70 days reaction time at FPW admixture > 10% (see Figure 2). At a high GGW content of 90% the colloid concentration (~10 ppb) as well as the mean colloid diameter (152 ± 18nm) remains almost unchanged over a period of 70 d.

SEM/EDX identifies predominantly Si/Al containing colloidal phases and additionally some sulfates could be found under certain admixture ratios.

The synthetic FPW was spiked with Eu(III), U(VI) and Th(IV) at a concentration of $1 \cdot 10^{-8}$ mol·L^{-1} for each element prior to GGW admixture. According to the radionuclide speciation and solubility calculations performed for the synthetic Febex porewater used throughout this study [8], the used concentration range is below the calculated solubility limit for Am(III) of $4 \cdot 10^{-6}$ mol·L^{-1} (solid phase $NaAm(CO_3)_2$) and U(VI) of 10^{-4} mol·L^{-1} (solid phase schoepite) and $4 \cdot 10^{-7}$ mol·L^{-1} (solid phase: $Th(OH)_4$). The solution speciation is dominated by $AmCO_3^+$, Am^{3+}, $Th(OH)_3CO_3^-$, $Th(OH)_4$aq and $UO_2(CO_3)_3^{4-}$, $UO_2(CO_3)_2^{2-}$ in the Febex porewater and by $Am(CO_3)^{2-}$, $Am(OH)_2^+$, $Th(OH)_3CO_3^-$, $Th(OH)_4$aq and $UO_2(OH)_3^-$, $UO_2(CO_3)_3^{4+}$ in the GGW (Eh = -70mV) [8], respectively. Eu(III) and Cm(III) have been chosen in our work as chemical homologues to Am(III). The ultrafiltration results show that U(VI), as expected from the speciation calculation, is occurring as dissolved species and passes even the 1 kDa filter to more than 70 % in all experiments. The Th(IV) speciation seems to be dominated by large colloids. In all mixed solutions Th does not pass the 1000 kDa filter by more than 10 %. For solutions containing 30% to 90% pore water, the Eu(III) concentration filtered by 1000 kDa varies between 30 % to 50 % and the fraction filtered by the 1 kDa filter between 35% to 80%, respectively. Due to the strong changes in the pH and the rather dilute solutions, a strong interaction of Th(IV) and Eu(III) with sorption sites of the polyethersulfone filter membranes can not be excluded [9].

To further elucidate the speciation of trivalent actinides/lanthanides in the GGW/ synth. FPW mixing zone Cm^{3+} TRLFS was applied. In a first step the end members GGW and FPW were investigated under variation of the pH from 7.0 to 9.6. Figure 3 shows that the pH variation in GGW does not change significantly the shape or peak position of the fluorescence emission spectra. At a first glance this is somewhat surprising as the speciation calculation predicts a change of the speciation from 42% $Cm(CO_3)_2^-$, 37% $Cm(OH)_2^+$ and 16% $Cm(CO_3)^+$ at pH=9.6 to 48% Cm^{3+}, 27% CmF_2^+ and 20% $Cm(OH)_2^+$ at pH=7.0. The predicted predominant aquo ion at pH=7 with an emission band maximum at 593.8 nm is not visible in the spectrum. All spectra show instead broad emission bands suggesting the co-existence of several species, however, rather independent on pH. In earlier studies, the mainly colloidal character of Cm-species in GGW was already stated [3]. Our present study confirms this observation. Obviously, the Cm-species formed at high pH (=9.6) do not re-equilibrate when pH is adjusted to 7 within hours. Measured fluorescence lifetimes show multi-exponential decay and lifetime values range from ~ 150µs (pH=9.6) to ~170 µs (pH=7.0). Such long lifetimes are characteristic for colloidal species comparable to the Cm-silicate(II) species in [10].

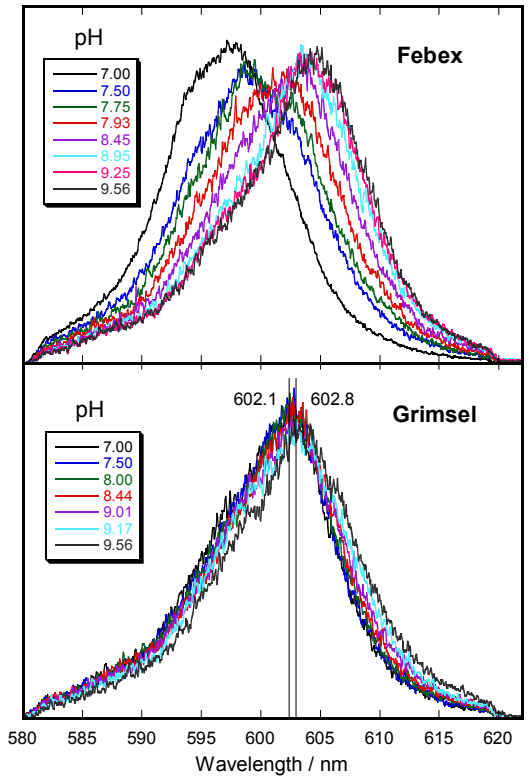

Fig. 3: *TRLFS Cm^{3+} fluorescence spectra for synth. Febex porewater (top) and Grimsel groundwater (bottom) taken at different adjusted pH values.*

In the case of the FPW the pH is varied from low to high pH (7-9.6) accompanied by a significant variation of emission spectra peak position and shape (Fig. 3, top). The spectrum at pH=7 shows a pronounced shoulder at low wavelengths suggesting the existence of a certain percentage of aquo ion. Spectra are red shifted at increasing pH and might be interpreted in agreement with speciation calculations with a change of Cm speciation towards carbonate complexes.

However, measured fluorescence relaxation again follows multi-exponential decay at higher pH, showing a slowly decaying component with a lifetime up to ~410 µs at pH=9.6. The existence or co-existence of colloidal Cm species is therefore evident. In a second step the fluorescence emission spectra of mixed solutions containing different porewater/ groundwater ratios were measured and directly compared with those obtained in the end member solutions at the same pH value (Figure 4). In the solution containing ≥ 30% pore water the fluorescence emission spectra for the mixed solutions and the pure Febex pore water solution are comparable. Interestingly, at lower pore water contents (10-15%) the fluorescence emission spectra deviate significantly from end member spectra at given pH. The fluorescence decay in those solutions contains lifetimes components up to ~200 µs compared to τ=80 µs measured in the porewater. At higher groundwater content lifetimes decrease to 140-170 µs. Considering pure silicate systems, the colloidal Cm-silicate(II) complex found in [10] at pH > 7 has a peak maximum at 603.2 nm and a lifetime of 198.2 ± 7.2 µs (2.4 ± 0.5 hydration water molecules), which is quite comparable to what we find in our mixed solutions with pore water contents of 10-15%. This species is attributed to Cm bound to silicate polymers, which have been observed to form even in silicate solutions being clearly undersaturated with regard to amorphous silica (2.7×10^{-4} mol/L Si) at pH > 5 [10]. Si concentrations in our solutions lie in the same range at 10^{-4} mol/L.

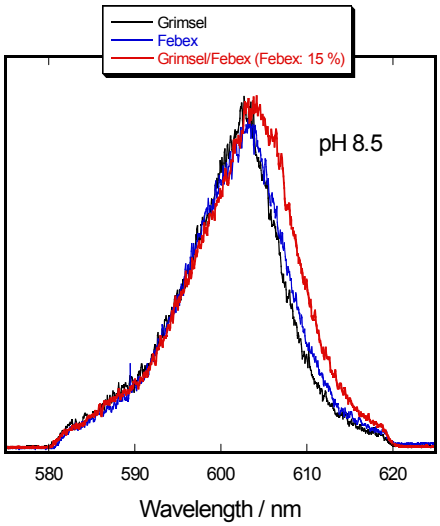

Fig. 4: *Comparison of Cm TRLFS emission spectra in Grimsel groundwater and in synth. Febex porewater at pH=8.5 with spectra taken in mixed solutions at the same pH value.*

To verify the Cm-colloid association the samples with 10% and 15% porewater content were ultra-centrifuged to separate the colloidal fraction and the supernatant was measured by TRLFS. The fluorescence intensity almost disappeared in the supernatant of the solution containing 15% porewater indicating an almost quantitative association of Cm with colloidal phases. Additional tests performed with a higher (85%) porewater content still revealed association with colloids, however not complete.

The presented experiments [11] show clearly the relevance of actinide colloid species in chemically disturbed aquatic systems. Those colloids appear to be stable for the time scale of laboratory investigations. Their long-term stability for e.g. years has to be investigated in future studies in order to assess their relevance for nuclear waste repository safety considerations.

Colloid analysis within the Swedish site investigation program

Beside colloids neo-formed in geochemical gradients, colloids can be found in all natural waters. Colloid analysis has been performed in groundwater samples collected during the site investigation program at Laxemar and Forsmark, close to the nuclear power stations Oskarshamn and Forsmark, Sweden. This study offers the opportunity to gain information in the dependence of natural colloid content on groundwater chemistry. Samples from each borehole position have been collected in two stainless steel cylinders, preventing as much as possible the oxidation of the anoxic groundwater samples. They were sent to INE for laboratory analysis. Colloid analysis was subsequently performed by the laser-induced breakdown detection (LIBD) in the laboratory using a closed flow-through detection cell, again without ambient atmosphere contact. LIBD is known as very sensitive analytical method for notably inorganic colloid counting in natural water. Furthermore, a complete geochemical analysis of the water samples was performed.

In previous measuring campaigns within the Äspö colloid project a series of boreholes along the access tunnel have been sampled and groundwater was directly analyzed with a mobile LIBD system. Colloid concentration was correlated with the groundwater salinity (represented by the Cl^- concentration of the groundwater in Fig. 5. At a Cl^- concentration of about 4000 mg/l a remarkable drop of the natural colloid concentration over 4 orders of magnitude down to the LIBD detection limit of about 10 ng/l was observed.

Data obtained for the Laxemar samples KLX17A, KLX13A fit quite well into this correlation. However, colloid concentrations found in samples taken from the Laxemar (KLX) and Forsmark (KFM) site are partly significantly higher than expected when looking to the corresponding groundwater salinity. This holds notably for samples KLX15A (478 m), KFM08D (~540 m, ~663 m) and KFM11A (~390 m). Closer inspection of the LIBD data obtained for those samples revealed the existence of at least two particle size fractions. Deconvolution of the LIBD data results in the presence of a small 1st colloid fraction with

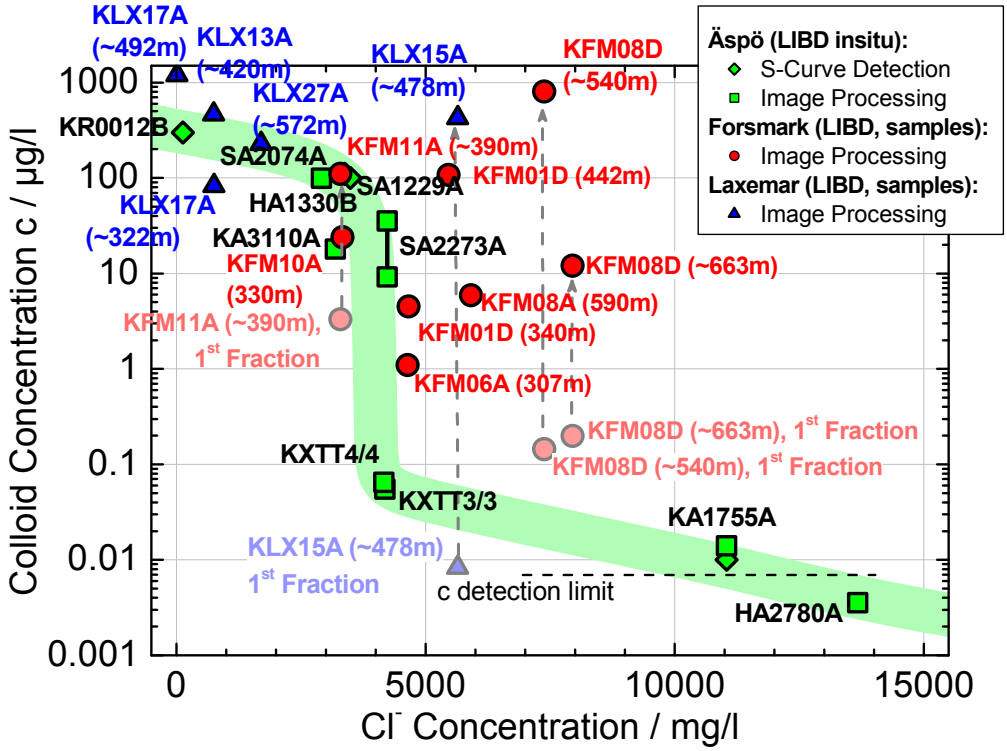

***Fig. 5**: Correlation between colloid concentration and chloride concentration in different groundwater from Äspö, Laxemar and Forsmark samples.( ): sampling depths*

particle sizes around 20 nm at rather low mass concentration levels. A 2nd particle size fraction was identified to show diameters in the µm range. Those large particles, however, dominate the colloid mass concentration determined in the samples. Sizes derived from LIBD deconvolution agrees well with data derived from SEM images. If we assume that the large 2nd colloid fraction consists of mainly mechanically erroded particles (calcite, alumino-silicates, silicates, ..) from borehole drilling, then the smaller sized 1st colloid fraction may represent the undisturbed “real” colloids of the natural groundwater in this borehole zone.

All data suggest the existence of very low inorganic colloid concentration levels in natural groundwater of high salinities > 5 g/l Cl^- (Fig. 5), corresponding to ionic strengths of about > 0.2 mol/l. Inorganic colloids are obviously destabilized at such salinities and prone to agglomeration, sedimentation or attachment to rock surfaces.

References

[1] Nagra, Project Opalinus Clay - Safety Report - Demonstration of disposal feasibility for spent fuel, vitrified high-level waste and long-lived intermediate level waste (Entsorgungsnachweis). NTB 02-05, Nagra, Wettingen (CH) 2003.

[2] SKB, Interim process report for the safety assessment SR-Can.
SKB-Report R-04-33, (S) 2004.

[3] Neretnieks, I., Liu, J., Physical and chemical stability of the bentonite buffer. SKB-report, R-06-103 (S) 2006.

[4] Geckeis, H. et al.,
Radiochim. Acta 92 (2004) 765-774.

[5] Möri, A. et al.,
Colloid Surface A 217 (2003) 33-47.

[6] Kim, M.A., Panak, P.J., Yun, J.I., Priemyshev, A., Kim, J.I., Interaction of actinides(III) with aluminosilicate colloids in "statu nascendi" Part III. Colloid formation from monosilanol and polysilanol.
Colloid Surface A 254 (2005)137-145.

[7] Wan, J. et al., Environ. Sci. Technol. 38 (2004) 6066-6073.

[8] Duro, L., Prediction of the solubility and speciation of radionuclides in Febex and Grimsel waters. Nagra Aktennotiz AN99-218, Nagra, Wettingen, (CH) 1999.

[9] Altmaier, M., Neck, V., Fanghänel, T., Radiochim. Acta 92 (2004) 537-543.

[10] Panak, P.J., Kim, M.A., Klenze, R., Kim, J.I. and Fanghänel, T.,
Radiochim. Acta 93 (2005) 133-139.

[11] Kunze, P., Seher, H., Hauser, W., Panak, P., Geckeis, H., Fanghänel, Th., Schäfer, T., Radionuclide speciation in the Grimsel granite groundwater Febex bentonite pore water mixing zone. J. Contam. Hydrol. (in review).

5.4 Actinides in the far-field: Influence of natural organics

N.L. Banik, G. Buckau, F. Claret, F. Einsiedl[§], St.N. Kalmykov[#], C.M. Marquardt, P. Michel, T. Schäfer, N.S. Shcherbina*

** BRGM, Environment and Process Division, Orleans, France*
[#] Lomonosov Moscow State University, Chemistry dept., Moscow, Russia
[§] GSF, Institute of Groundwater Ecology, Neuherberg, Germany

Introduction

Natural organic matter (NOM) can occur in a wide variety of structures starting with low molecular weight compounds (LMWC) as e.g. found in the porewater of claystone formations (Opalinus clay), humic substances (HS) and finally the immobile most mature organics called kerogen.

The focus of research at INE in the last decade was on the characterization of HS (humic and fulvic acids), their interaction with radionuclides and mobility. Humic and fulvic acids (HA and FA) are a class of organic compounds with a large number of similarities, for example in the comparably long residence time/chemical stability. Special focus is currently on the interaction of redox sensitive functional groups of HA/FA and their influence on speciation of redox sensitive actinide ions. A new aspect within recent years is the characterization of mineral associated organic matter. The fractionation of HA/FA via mineral adsorption might be an approach to explain the observed discrepancies between laboratory data and the predictive modeling of ternary systems (mineral-organics-RN) using linear additive models [1]. The studies on isolation, characterization and reactivity of kerogen found in natural host-rock formations (Callovo-Oxfordian, Opalinus Clay, Toarcien) were continued (see below).

There are still many open questions for adequate description of the overall influence of NOM on the geochemical behavior of actinide ions and their mobility in deep groundwater systems. Three of these topics are discussed in more detail below, namely (a) application and generation of consensus to basic metal humate complexation processes, (b) inventory of redox functional groups and influence on the redox state of actinide ions and (c) the reactivity of mineral bound natural organic matter.

Application and generation of consensus to basic metal humate complexation processes

INE has developed an approach for the systematic description of metal ion humate complexation. The approach was presented, amongst others in the annual report 2006. The description of the complexation process combines the binding capacity, i.e. the amount of complex formed by humic acid under specific physico-chemical conditions with recent findings on the mass distribution of humic acid as well as the number of proton exchanging functional groups per average molecule. The approach shows that strongly complexing metal ions form one complex per humic acid molecule, followed by association of complexes to form larger clusters, finally resulting in the well known flocculation. The protonation induced flocculation also form part of this process description.

One particularity is that the approach does not make use of the frequently assumed polyelectrolyte/double layer properties that cannot be justified reflecting meanwhile generally accepted findings with respect to the much smaller molecules than previously thought.

It has been known already for a long time that the metal ion humate interaction process is described by a simple reaction:

$$M + L \Leftrightarrow ML \quad (1)$$

$$K = [ML] / ([M]_{free} \times ([ML]_{max} - a[ML]^b)) \quad (2)$$

Where $[ML]_{max}$ represents an experimentally determined quantity. For a very broad set of data it is found that a and b are very close to "1" and thus:

- The reaction stoichiometry is 1:1, and
- The number concentration of reactive molecules is decreased by one per complex formed, i.e. only one complex per reactive humic acid molecule.

The key question over many, many years was "What does the measured number $[ML]_{max}$ describe?" Analysis shows that it is the number concentration of reactive humic acid molecules, reduced by the concentration of conescutively protonated molecules and metal ion complexed molecules. Electrolyte cations have a deactivation impact qualitatively comparable to protonation, but with a much weaker influence for comparable concentrations of protons and electrolyte cations.

For the binary system (metal ion and humic acid), $[ML]_{max}$ is easily determined by titration with the metal ion. For application to the ternary system consisting of metal ion, hydroxide and humate, the $[MXL]_{max}$ can be deduced by extrapolation from pH titration data ([2] and Fig. 1), titration with the binary metal ion hydroxo complex [3] or titration with substituent ions [4].

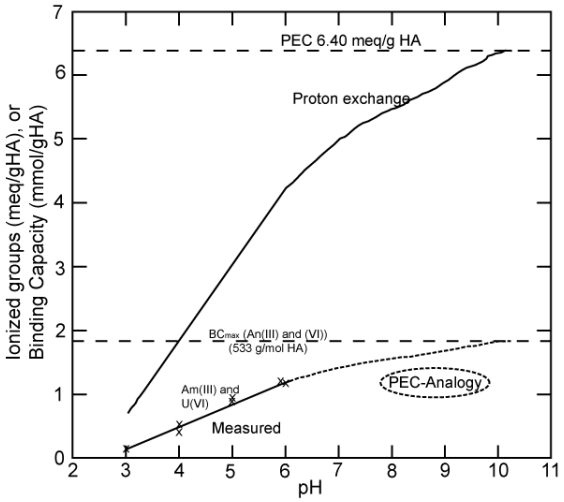

Fig. 1: *The Binding Capacity (BC) (total humate ligand concentration under given physico-chemical conditions); for explanation see text.*

The outcome of complexation studies with Cm(III), Eu(III) and U(VI) show in principle the same processes of reversible, route-independent formation of ternary complexes over different binary pre-steps. This is not self-evident but shows that the process description gives consistent results, including the description of the humic acid ligand function.

Following this significant step towards agreement on this comparably simple, thermodynamically consistent and plausible approach for description of the metal ion humate interaction process, a workshop is planned within the context of the NoE ACTINET Joint Research Project "EXAFS, TRLFS and quantum chemical analysis of An(III) complexes with Humic Acid and organic model ligands". The workshop has the objectives of elaborating upon the degree of consensus in the concerned community with respect to basic properties and processes of humic acid and its formation of complexes.

Redox reactions

(a) Pu with hydroquinones and fulvic acids.

The migration of plutonium in the geological environment of a nuclear repository is governed by its oxidation state. An earlier work showed that plutonium occurs mainly as Pu(III) and Pu(IV) in humic substances containing groundwater [1]. But underlying reaction mechanisms are still unclear. Due to the complexity of natural groundwaters, we have started a study on the plutonium behavior in aqueous solutions of known and simple composition with only one reducing agent. Here, the hydroquinone (HQ) and the 9,10-anthraquinone-2,6-disulfonic acid (AH2DS) with a normal redox potential E_0 of 0.6992 V and 0.228 V [2], respectively, were chosen to cover a broad range of redox conditions. The estimated E_0 of fulvic acids is about 0.5 V [3] and fits in this range.

Our experiments were started with Pu-242, mostly Pu(VI) with small residues of Pu(V), to ensure colloid free start solutions. Colloid formation is expected with reduction of Pu(V, VI) to Pu(IV) at the relatively high Pu concentrations required for spectroscopic studies. To estimate the extent of colloid formation, a concomitant experiment with Pu-238 at tracer concentrations was performed. Pu concentrations were typically [Pu-242] = $1\text{-}2\cdot10^{-4}$ M and [Pu-238] = $2\cdot10^{-8}$ M. The FA concentration was 4 – 200 mg/L ($2.7\cdot10^{-5}$ – $1.7\cdot10^{-3}$ eq/L proton exchange capacity). The hydroquinones were used at concentrations of $2\text{-}3\cdot10^{-3}$ eq/L. The pH of the solutions was between pH 1 and 7. Pu redox species were monitored by UV-Vis spectroscopy and liquid-liquid extraction over a period of at least 100 days.

The results showed that Pu(V) and (VI) are not stable in aqueous solution containing HQ, AH2DS or FA. In presence of 200 mg/L FA the reduction of Pu(VI) to Pu(V) is fast and complete after 30 minutes at pH 3, that is significantly slower as compared to the reduction reaction at similar HQ concentration. Pu(V) in the same solutions is converted totally to Pu(IV) within 20 days. The tetravalent state is the main oxidation state at higher concentrations of plutonium in FA solutions at pH 3 - 7 and in HQ solutions at pH 5 – 7 (relevant to natural aquifers). Partial reduction of Pu(IV) to Pu(III) was found for low concentrations of plutonium at higher pH values. Here, a quasi-equilibrium state of Pu oxidation states is established within 40 days with 50 % Pu(III) (see Fig. 2).

Eh was monitored in all experiments and those measured data were compared with calculated pe values. For pe calculations it was assumed that Pu(III)-species and colloidal $Pu(OH)_4$ are in equilibrium. In agreement with experimental observations, calculations show that Pu(III) can be stabilized in presence of FA at higher pH values.

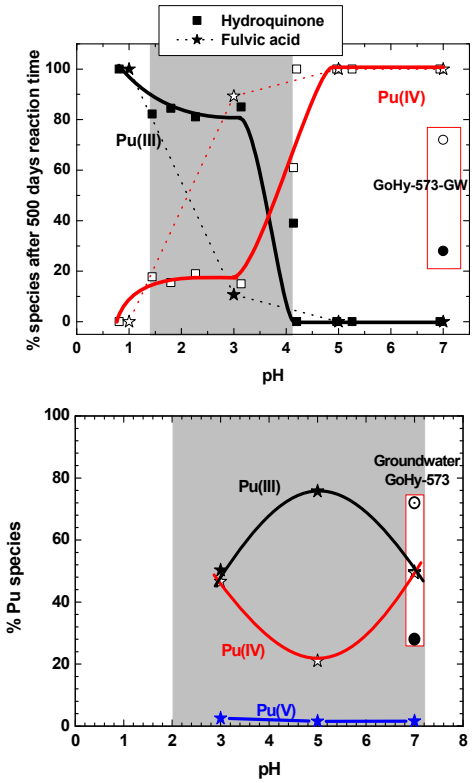

Fig. 2: *Distribution of plutonium oxidation states at two $[Pu]_{tot}$ after interaction with FA and Hydroquinone; top: $[^{242}Pu] = 1\text{-}2x10^{-4}$ M, bottom: $[^{238}Pu] = 2x10^{-8}$ M; [FA] = 1.4 x 10^{-3} eq/L PEC*, [HQ] = 1-2 x 10^{-3} M.*

(b) Sorption of neptunium onto goethite in the presence of humic acids with different hydroquinone group content.

Neptunyl sorption in the ternary system goethite – humic acid (HA) – Np(V) was studied in a series of batch experiments with natural leonardite HA and a hydroquinone enriched derivative. To obtain hydroquinone enriched humic derivative (HQ100), 100 mg of hydroquinone were reacted with 1 g of parent HA. The details concerning synthesis, purification and characterization of both humic materials are given in [8]. The preparation of HQ100 derivatives from leonardite humic acid by enrichment with hydroquinone moieties results in the increase of phenolic hydroxyl groups to maximum values of 4.4 – 4.6 mmol/g, which is a factor of 4 greater than that of the parent leonardite material [8]. Published reducing capacities of IHSS natural peat and soil derived HA samples determined at pH 7 show average values of 1.1 ± 0.2 mmol/g and 1.35 ± 0.25 mmol/g, respectively [9].

The dependence of Np sorption onto goethite upon pH displays s-shaped character typical for surface complexation reactions. No difference was observed for sorption of natural leonardite HA and HQ100 onto goethite. Humic acid sorption decreases with increasing pH, as expected. Separate experiments were undertaken to show that Np did not signifycantly affect HA sorption onto goethite due to the relatively low degree of goethite surface saturation. Considering a site density of 1.7 sites/nm^2 at the goethite surface, the coverage with metal ions was less than 0.2 % (for a total Np concentration of $6•10^{-7}$ M). The addition of natural leonardite HA had only a minor effect on Np solid/liquid distribution. At pH values below 5 a slight increase of Np sorption was observed. However, in the same pH range, the presence of HQ100 caused a considerable increase of Np sorption in this low pH range. One possible explanation for the observed difference in Np distribution upon addition of HQ100 could be the potential neptunyl reduction upon interaction with the hydroquinone enriched leonardite humic acid HQ100. At pH > 6 addition of either natural leonardite HA or HQ100 resulted in a slight decrease of Np sorption onto goethite which was due to the complexation of Np(V) with HA in solution. However, this effect is quite small due to the relatively weak complexation of Np(V) with HA (stability constant of Np(V)-HQ100 complexation: log β = 3.47 ± 0.48 at pH 7.4).

In order to verify spectroscopically the reducetion on Np(V), the 4f electron XPS spectra of Np equilibrated with goethite and HQ100 at pH 3.5 and pH 7.5 were taken. The reduction of Np(V) at low pH upon interaction with hydroquinone-enriched leonardite HA – goethite suspension could be evidenced by XPS. This was not the case when the parent humic acid (leonardite HA) was added. Furthermore, under these low pH conditions the formation of humate coatings at the goethite mineral surface has been identified using scanning transmission X-ray microscopy (STXM) at the carbon K-edge [10]. According to STXM, the humic acid formed surface coatings on goethite colloids and particles at low pH values. Interestingly, comparing the initial HQ100 carbon edge spectra and the extracted spectra of that fraction associated with goethite, a higher aliphaticity is found for the HQ100 associated with goethite. Assuming that the higher density in aliphatic groups are the consequence of a stronger formaldehyde condensation and therefore an enrichment of hydroquinone in leonardite HA, this would consequently mean that redox active groups are selectively enriched at the goethite surface. This would explain the strong and more effecttive Np(V) reduction in the presence of goethite. Therefore, such goethite-humic aggregates could serve as effective scavengers for oxidized actinides, i.e. Np(V) from aqueous solutions.

(c) Evidence for incorporation of H_2S in groundwater fulvic acids

Analysis of isotopic signature of sulphur in natural groundwater and redox speciation of sulphur in natural organic matter determined by K-edge XANES have been used in the past to investigate the generation of humic/fulvic acid from lignite by sulphate reducing bacteria [11]. Such type of studies may be also be helpful for getting insight into the redox state of natural organic matter of different origin, which in turn has impact on the type of interaction with actinide ions.

FA samples were isolated from groundwater samples collected in a shallow oxic and reduced deep karst groundwater system of the Franconian Alb located in southern Germany. Stable isotope compositions of groundwater sulfate and fulvic acid sulfur and sulfur K-edge X-ray absorption near edge structure (XANES) spectroscopy data were used to determine sulfur sources and processes for sulfur binding to FA in the aquifer. The results revealed clearly the influence of dissolved sulfide on the chemical and isotopic composition of fulvic acid associated sulfur [12, 13].

A $\delta^{34}S$ value of 2.2 ‰ for the shallow groundwater sulfate and a $\delta^{34}S$ value of fulvic acids of 4.9 ‰ accompanied by a contribution of up to 49% of the most oxidized sulfur species (S_{+6}, see Fig. 3) documented that fulvic acid sulfur is mainly derived from soil S compounds such as ester sulfates, with $\delta^{34}S$ values similar to those of atmospheric sulfate deposition. In contrast, in the deep groundwater system with elevated $\delta^{34}S$ values in groundwater sulfate of up to 20‰ due to bacterial sulfate reduction, $\delta^{34}S$ values in fulvic acid sulfur were negative and were up to 22‰ lower compared to those of groundwater sulfate. Furthermore, reduced sulfur compounds constituted a significantly higher proportion of total fulvic acid sulfur in the deep groundwater compared to fulvic acids in shallow groundwater (see Fig. 3), supporting the hypothesis that fulvic acids act as a sink for dissolved hydrogen sulfide in the deep aquifer.

The results indicate that a significant proportion of sulfide enriched in the lighter ^{32}S isotope must have been incorporated into FA in the deep aquifer, and we conclude that the combination of traditional stable isotope techniques and sulfur K-edge XANES spectroscopy is a powerful tool to elucidate the role of FA in the sulfur cycle of groundwater systems. Future research will focus on the influence of the observed variable FA sulfur inventory on sorptive reduction of redox sensitive radionuclides.

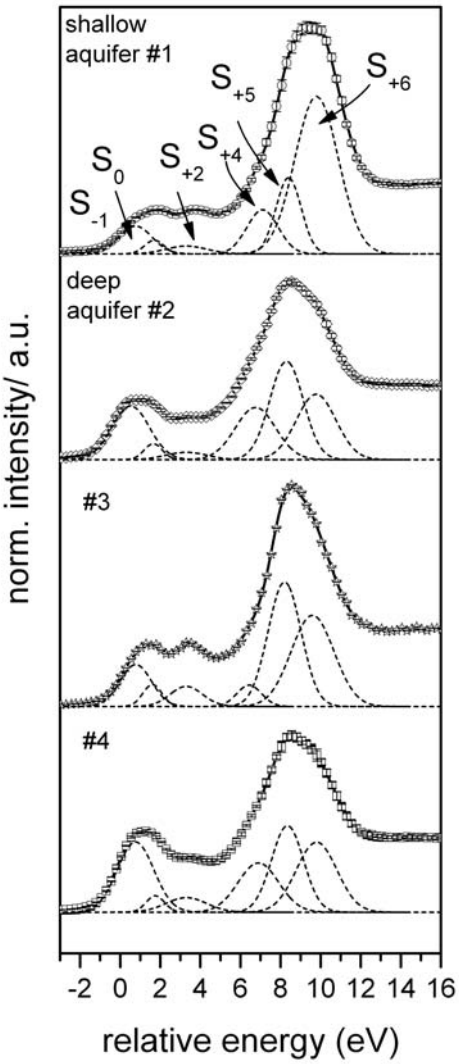

Fig. 3. *Deconvolution of different oxidation states (S_{-1}, thiol; S_0, thiophene and disulfide; S_{+2}, sulfoxide; S_{+4}, sulfone; S_{+5}, sulfonate; and S_{+6}, sulfate) by sulfur K-edge XANES. Samples #2, #3, #4 derive from deep aquifers.*

Radiation sensitivity of natural polymerized organic matter: Clay mineral association effects in the Callovo-Oxfordian argillite

Clay-rich low-organic carbon formations (e.g. Callovo-Oxfordian argillite in France and Opalinus Clay in Switzerland) are considered as host rocks for radioactive waste disposal. The clay organic carbon has a strong impact on the chemical stability of the clays. For this reason, the nature of the clay organic carbon, the release of hydrophilic organic compounds, namely humic (HA) and fulvic acids (FA) and the radiation sensitivity of the undisturbed host rock organics were investigated. The clay sample originates from Oxfordian argillite (447 m depth, borehole EST 104). HA and FA were extracted following the standard International

Humic Substance Society (IHSS) isolation proce-dure. Synchrotron based (C-, K-, Ca-, O- and Fe-edge XANES) Scanning Transmission X-Ray microscopy (STXM) and synchrotron based FT-IR microspectroscopy was used to identify under high spatial resolution the distribution of clay organic matter with different functionality using principal component and cluster analysis. The results show that in this old (Jurassic) geological formation, small parts of the organic inventory (1-5%) keeps the structure/functionality and can be mobilized as hydrophilic humic substance type material (HA and FA). Target spectra analysis shows best correlation for isolated humic acids with organics found in smectite rich regions, whereas the extractable FA has better spectral similarities with the illite mixed layer minerals (MLM) regions. Spectral similarities to extracted kerogen could be localized in both regions.

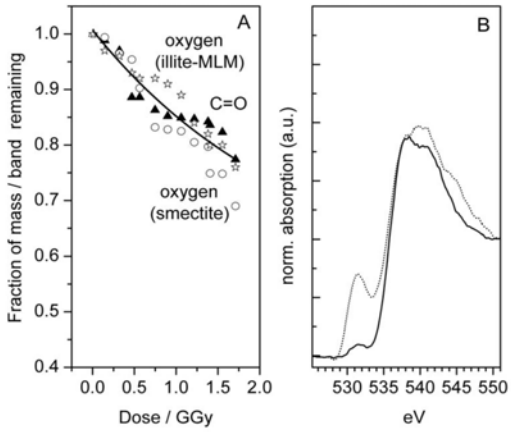

Fig. 4. *(A) Fraction of oxygen mass/ C=O band remaining after indicated dose. (Illite-MLM region oxygen mass loss (open stars), smectite region oxygen mass loss (open circles), smectite C=O band intensity loss (filled triangles)). The solid line represents the exponential fit for critical dose determination. (B) Oxygen K-edge spectra before dose scans of smectite region (dotted line) and illite-MLM region (solid line) [14].*

After irradiation by 1.7 GGy under helium atmosphere the same rock sample area was investigated for radiation damage (see Fig. 4). Radiation damage in the smectite and illite-MLM associated organic matter is comparably low with 20-30 % total oxygen mass loss and 13-18 % total carbon mass loss. A critical dose d_c of 2.5 GGy and an optical density after infinite radiation (OD_∞) of 54 % was calculated under room temperature conditions. C(1s) XANES show a clear increase in C=C bonds especially in the illite-mixed layer mineral associated organics. This results suggests a combination of the formation of C=C bond due to crosslinking via polymerization and mass loss due to bond breaking (scissioning) in the main chain or in side groups of the organic macromolecules upon irradiation. Furthermore, the results indicate a rather low sensitivity of the Callovo-Oxfordian organic matter independent of clay type to high radiation doses (1.7 GGy) under helium atmosphere [14].

References

[1] Claret, F., Schäfer, T., Reiller, P., Environ. Sci. Technol. (2008) in review.

[2] Pashalidis, I. and Buckau, G., J. Radioanal. Nuclear Chem. 273 (2007) 315–322.

[3] Sachs, S., Brendler, V. and Geipel, G., Radiochim. Acta 95 (2007) 103 – 110.

[4] Maes, A., De Brabandere, J., Cremers, A., Radiochim. Acta 44/45 (1988) 51.

[5] Marquardt, C.M., Seibert, A., Artinger, R., Denecke, M.A., Kuczewski, B., Schild, D., Fanghänel, Th.,
Radiochim. Acta 92 (2004) 617.

[6] Clark, W. M., Oxidation-Reduction potentials of organic systems. Baltimore, MD, The Williams & Wilkins Company (1960).

[7] Skogerboe, R.K., Wilson, S.A.,
Anal. Chem. 53 (1981) 228.

[8]. Perminova, I.V., Kovalenko, A.N., Schmitt-Kopplin, Ph., Hatfield, K., Hertcorn, N., Belyaeva, E.Y., Petrosyan, V.,
Environ. Sci. Technol. 39 (2005) 8518.

[9]. Peretyazhko, T. and Sposito, G.,
Geoderma, 137 (2006) 140-146.

[10] Kalmykov, S., Schäfer, T., Claret, F., Khasanova, A., Shcherbina, N., Perminova, I., Teterin, Y., Radiochim. Acta (2008) accepted.

[11] Schäfer, T., Buckau, G., Artinger, R., Kim, J.I., Geyer, S., Wolf, M., Bleam, W.F., Wirick, S., Jacobsen, C.,
Organic Geochem. 36 (2005) 567–582

[12] Einsiedl, F., Schäfer, T., Northrup, P., Chemical Geology 238 (2007) 268-276.

[13] Einsiedl, F., Mayer, F., Schäfer, T., Environ. Sci. Technol. 42 (2008) 2439-2444.

[14] Schäfer, T., Michel, P., Claret, F., Beetz, T., Wirick, S., Jacobsen, C., Fanghänel, Th., J. Electron Spectroscopy A (2008) accepted.

5.5 Numerical simulation of the hydro-mechanical processes in the repository environment

A. Pudewills

Introduction

This section describes research activities performed on modeling of hydro-mechanical processes relevant to radionuclide migration in fractured rock and related to the evolution of the excavated disturbed zone of a repository in rock salt. In both cases the infinite element code ADINA F is applied [1].

Numerical simulation of the ground-water flow and solute transport in a shear zone at the CFM location

In the framework of the Grimsel Test Site (GTS) Phase VI, the international Colloid Formation and Migration (CFM) project with partners from Japan (JAEA, AIST and CRIEPI), Switzerland (NAGRA), Sweden (SKB) and Germany (FZK-INE) investigates processes related to colloid generation from the engineered bentonite barrier and migration of colloid-borne radionuclides. Colloid migration experiments require an exact description of the given hydraulic situation. The present contribution reports a numerical analysis of the groundwater flow field through the shear zone around the CFM experimental tunnel at the Grimsel Test Site. In order to judge how well the model fits the hydro-geological conditions at the CFM test location, a calibration of the model parameters of the long-term tracer tests was performed. The influence of the characteristic flow and transport parameters has also been studied. The overall objective of this work is to understand the flow path geometry and the relevant transport processes within the water conducting shear zone, considering the low hydraulic gradients.

Tracer tests description

The use of transport models requires a number of parameter values. Some of them may be determined in the laboratory and other by field measurements. Recently, tracer tests were performed in a low gradient flow field within the shear zone at the CFM location [2, 3]. The tunnel was equipped with a 3m-diameter surface packer system. The scope of this packer was to avoid uncontrolled flow rates towards the drift, to reduce the hydraulic gradient in the shear zone and to achieve longer tracer travel times. The first tracer test (Run #1) was performed using uranine as conservative tracer. The tracer was injected at borehole BOMI 87.0010 and recovered at the tunnel surface interval packer named "Pinkel". The distance between the injection and extraction wells is about 4 m. The groundwater was injected with a rate of 5ml/min and extracted with a rate of about 650 ml/min. After the steady-state flow conditions were established, the injection of a tracer solution (~5.6 ppm) was performed. The second tracer test (run 07-02) was performed at the same location with a restricted outflow rate field of about 120ml/min. Figure 1 shows the location of the injection boreholes and extraction point (Pinkel) at the surface packer in the plane of the shear zone around the experimental drift.

Numerical modelling

For numerical simulation of the uranine tests, it was assumed that the groundwater flow and the solute transport take place only in fractures filled with fault gouges, and the shear zone at the test location is plane. This allows a two dimensional

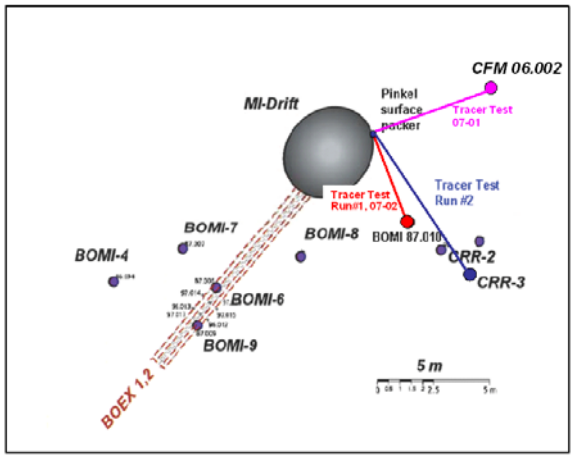

Fig. 1: *Location of the tracer tests and the different observation boreholes in the plane of the shear zone around the experimental drift.*

(2D) porous medium approach for the calculation. The medium is assumed to be homogeneous but anisotropic. The groundwater flow is governed by Darcy's law and the solute transport is described by the standard advection/dispersion equation. All numerical investigations were performed with the ADINA-F finite element code.

The present finite element model extends the relatively simple model used in an early stage of the CFM project. The problem examined here represents a vertical cross section perpendicular to the horizontal axis of the tunnel. The domain around the gallery including the injection and extraction wells is modelled explicitly.

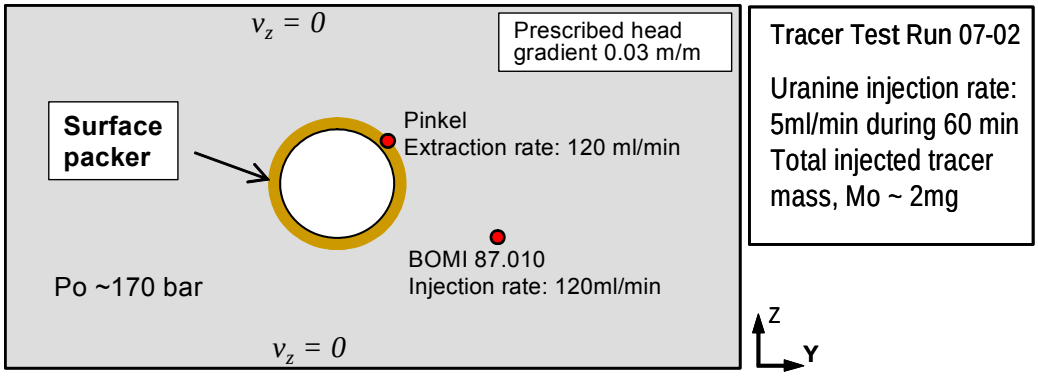

Fig. 2: *Schematic diagram of the 2D model and the boundary conditions used for simulation of test Run 07-02*

For the tracer test run 07-02 a section-view of the model with the assumed boundary conditions and the tracer test location is shown in Figure 2. The uranine injection rate and the total injected tracer mass are also given in this figure.

The hydraulic parameters obtained from preview simulation of Run 1 (same dipole but different flow rates) were used firstly. However, it was necessary to perform further adjustments of these parameters due to the new test conditions (i.e. smaller pumping and extraction rates) to be able to fit the measured breakthrough curves. The calibrated parameter values are given in the Table 1.

Tab. 1: *Hydraulic and transport parameters used to model the tracer test Run #1 and Run 07-02*

	Run # 1	Run 07-02
Flow porosity	0.1	0.1
Horizontal permeability (m^2)	2E-11	1E-11
Vertical permeability (m^2)	1E-11	1E-11
Longitudinal dispersion (m)	0.0025	0.005
Transversal dispersion (m)	0.0002	0.0005
Diffusion coefficient (m^2/s)	2E-11	2E-11

Calculation results and discussions

Figure 3 depicts the calculated and measured uranine breakthrough curves at the extraction hole. As can be seen, the model produces a reasonable fit to the experiments. There is clearly good agreement between curves regarding in the peak arrival time and the tail. The long tailing seems to be induced by progressive release of the tracer late in the injection interval. It should be noted that the fit of the experiment is not unique. Certainly, it would be possible to obtain further acceptable fits of the measurements assuming another set of hydraulic and transport parameters.

These results suggest that the use of an anisotropic hydraulic permeability of the shear zone, which was successfully applied to fit early tracer experiments [4], does not work in this case. However, it seems that the heterogeneity of the shear zone material with respect to porosity and permeability in the model domain will influence the transport processes under the low or natural hydraulic gradients.

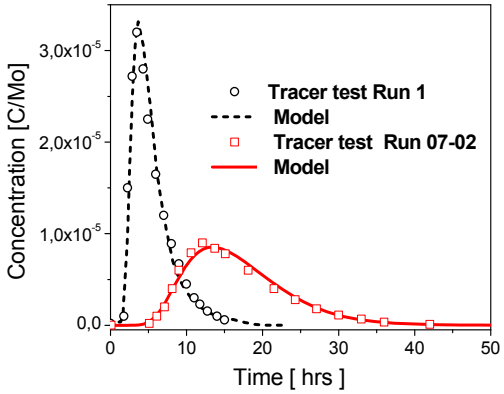

Fig 3: *Comparison of measured and calculated uranine breakthrough curves.*

A series of simulations with varying permeability and dispersion coefficients of the shear zone are also done. The evolution of computed uranine concentration in the shear zone is illustrated in Figure 4. The plots show that the mean flow pathway of the tracer is toward the extraction well.

Conclusions

The comparison of the numerical results and the experimental data was presented as breakthrough curves where the uranine concentration is plotted versus time. The simulation results match the experimental data fairly well. However, the previous assumed anisotropy in the permeability of the shear-zone material is not confirmed yet. In the next project step, further work is required to explore how the uncertainties on parameter estimation and the subsequent predictions at lower hydraulic gradients are affected by the choice of the present conceptual model. However, the

improvement of the large scale model taking in to account the heterogeneous hydraulic conductivity of the shear zone will be performed.

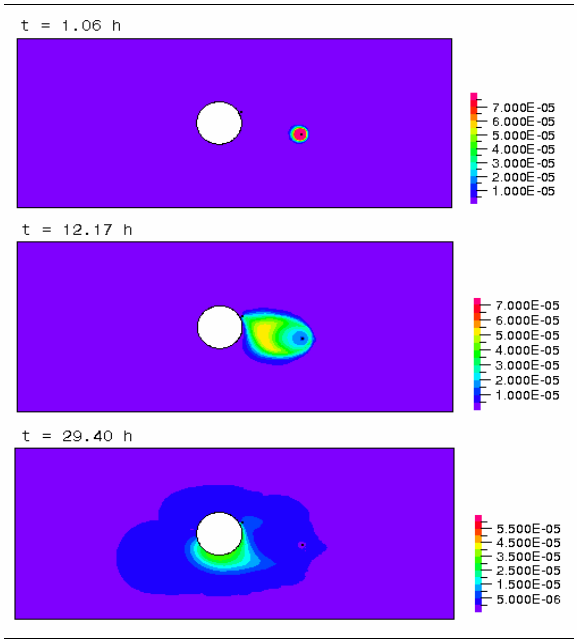

Fig. 4: *Distribution of the uranine concentration (C/Co) around the drift after different times*

Modelling the long-term evolution of the EDZ in a repository in rock salt

For the long-term performance of an underground repository in rock salt, the evolution of the "Excavation Disturbed Zone" (EDZ) and the hydro-mechanical behaviour of this zone represent important issues with respect to the integrity of the geological and technical barriers. Within the framework of the NF-PRO project, attention focuses on the mathematical modelling of the development and evolution of the EDZ in the rock near a disposal drift.

The finite-element codes containing a set of time- and temperature-dependent constitutive models have been improved. A new viscoplastic constitutive model for rock salt that can describe the damage of the rock has been implemented in the available finite-element codes. According to this model, the total strain rate is given as the sum of elastic and viscoplastic strain rates. The viscoplastic strain rate is decomposed into a part without volume changes of the material and a second one taking into account the volume changes due to the damage. In this case, the viscoplastic flow function depends on mean stress, deviatoric stress, and volumetric strain. A preliminary relationship between permeability and the dilatant volumetric strain is employed to calculate the hydraulic properties of the EDZ. The model parameters were evaluated based on experimental results. Additionally, the long-term evolution of the EDZ around a circular gallery in a salt mine at about 700 m below the surface was analysed and the numerical results were compared with in-situ measurements [5]. The calculated closing of open space, stress distribution and the increase of rock permeability in the EDZ were compared with in situ data, thus providing confidence in the model used. In the next step the work concentrates on the mathematical modelling of the development and evolution of the EDZ in the rock salt around a disposal drift in a repository for heat generating radioactive waste and their interaction with the backfill material.

Modelling of the hydro-mechanical behavior of rock salt around a disposal drift

Repository concepts for disposal of heat generating radioactive waste are based on multiple barriers for protection of the environment against the radioactive nuclides. According to one of these concepts, the containers with the radioactive waste will be placed on the floor of long parallel drifts at a depth of about 850 m below the surface in a rock salt formation. The remaining space between the containers and host rock will be filled with crushed salt. It is expected that in response to the thermally induced creep closure of the excavations the backfill material will compact sufficiently to serve as an efficient seal for the radioactive waste.

The numerical simulation started with the calculation of the isothermal drift closure and the stress distribution around the disposal drift prior to the emplacement of the heat generating casks. After about 200 days, the temperature development and the backfill material in the drift were taken into account. The thermomechanical analysis was continued over a period of 50 years. In Figure 5 the distribution of the effective stresses and the volumetric strains (porosity) in the vicinity of the disposal drift at different times after excavation are presented. The region in the pillar next to the drifts shows the highest effective stress just after excavation. The compression-dilation boundary near the drift surface has almost been reached and the extension of this disturbed zone is about 2 m after about 250 days. The calculated magnitude of the porosity is quite small with the maximum of about 1.2 % in the elements near the drift corners after 250 days. The calculated permeability of the rock salt around

the drift is in the order of magnitude with the few in situ measurements available [6], (10^{-16} - 10^{-17} m^2).

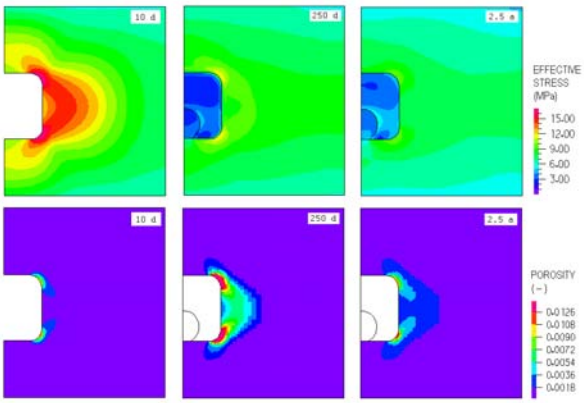

Fig 5: *Distribution of the effective stress and the porosity in the vicinity of a disposal drift 10, 250 days and 2.5 years after excavation.*

After emplacement of the waste and the backfill in the disposal drift, the closure rates and the compaction of the backfill material are mainly determined by the temperature development and the thermomechanical behaviour of the crushed salt [7]. The compaction pressure in the crushed salt increases and becomes large enough to support substantially the rock salt around the drift. The development of the mean stress (i. e. compaction pressure in the backfill) along the horizontal distance at the mid-height of the drift for several time intervals is shown in Figure 6. The calculated porosity of the backfill reduces already from 30% to about 2% after about 20 years of heating.

Due to the new stress conditions (i.e. nearly a hydrostatic stress state) the accumulated porosity of the rock salt into the EDZ zone reduces slowly to values less than 0.3 % after about two years at the drift mid-plane. The beginning of the reconsolidation of the damaged salt represents also the start self-sealing process.

Conclusions

The proposed constitutive model has predicted the extent of the damaged or dilated zone reasonably well during the operational phase. Further work will improve this model and to adapt the material parameters on the new laboratory data for a reliable analysis of the interaction between EDZ and the backfill. Nevertheless more complex material laws taking into account the temperature dependency of the damage and also the healing of rock salt have to be considered.

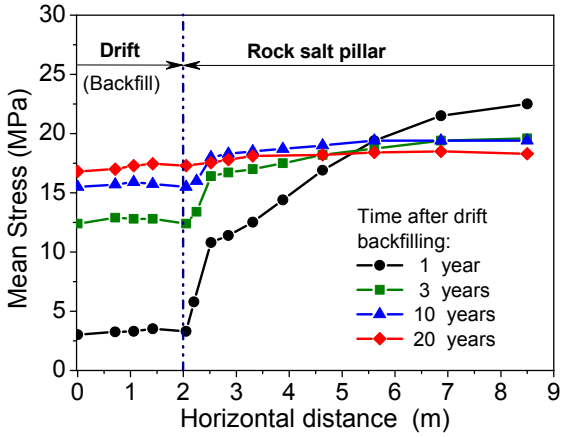

Fig 6: *Development of the mean pressure along an horizontal traverse at the drift mid-height after different times from backfilling*

References

[1] Adina R & D Inc., ADINA (Automatic Dynamic Incremental Nonlinear Analysis), Report ARD 01-9, Watertown, MA, USA, (2006).

[2] Trick, T., GTS-CFM: Tracer Test Run #1,QLR (2005).

[3] Trick, T. Blechschmidt, I., GTS-CFM: Tracer Test Run 07-02, PH6-CFM, AN 07-342 (2007).

[4] Guimera, J., Kosakowski, G., Iijima, K., Pudewills, A., Smith, P., The CRR final project report series: 3 - results of the supporting modelling programme, NAGRA Technical Report NTB 02-04, Wettingen (CH) (2008) in press).

[5] Pudewills, A., Modelling of the hydro-mechanical processes around excavations in rock salt, EUROCK 2007- Multiphysics Coupling and Long Term Behaviour in Rock Mechanics, Proc. of the Internt. Symp. of the Inter. Soc. for Rock Mechanics, Liège (B) May 9-12 (2006) 527-530.

[6] Bechthold, W. et al., Backfilling and sealing of underground repositories for radioactive waste in salt, (Bambus-II project), Final report, EUR-20621-EN, Brussels (2004).

[7] Pudewills, A., Modelling of hydro-mechanical behaviour of rock salt in the near field of repository excavations, The Mechanical Behavior of Salt: Understanding of THMC Processes in Salt, Proc. of the 6th Conf., Hannover (D), May 22-25, (2007) 195-2.

6. Development of speciation methods: Speciation of actinides at trace concentrations

The application of sensitive speciation techniques is crucial for the elucidation of radionuclide reactions on a molecular level. INE has invested substantial efforts in the past and will continue this strategy in the future to further develop advanced tools for the characterization of radionuclide species. Application of hard synchrotron radiation for speciation of actinides and other radioactive material at the INE-Beamline for Actinide Research at ANKA is reported and includes recent achievements in developing micro X-ray techniques for spatially resolved speciation. In the field of laser spectroscopy the focus was on vibrational spectroscopy. Vibronic sidebands spectroscopy yields valuable structural information on the ligands in the first and second coordination sphere and is highly sensitive for Cm(III). Sum frequency vibration spectroscopy provided detailed information about Al-OH dipoles at the corundum(001)/water interface, especially on their orientations, which may control the hydrophilic properties of the surface. The distribution of polymeric Th(IV) species as a function of Th-concentration and pH has been determined by nano-electrospray - mass spectrometry. Various examples of theoretical quantum chemical calculations to interpret or complement experimental spectroscopic findings are given in the last section of this chapter.

6.1 Speciation of Actinides Using X-Ray synchrotron Radiation

M. A. Denecke, B. Brendebach, K. Dardenne, J. Rothe

The INE-Beamline for Actinide Research at ANKA

Introduction

As in the past, since official operation began in October 2005, the major activities at the INE-Beamline involve in-house research and support of external users. These activities have lead to twenty-five contributions to the ANKA Annual Report 2007, as well as technical improvements and upgrades to the beamline to meet users scientific demands. The following report summarizes these activities, concentrating on technical highlights in 2007. In addition, an outlook of upgrades planned for the near future is given at the conclusion.

In-house research

The INE-Beamline is designed to ensure variability, primarily in order to optimize conditions for diverse actinide speciation applications associated with in-house research related to safe disposal of high level nuclear waste, but also for basic actinide research. The in-house investigations performed in 2007 (eight projects) cover a broad range of themes including, for example, colloid formation and stability [1], studies of actinide incorporation into secondary phases [2,3,4], high-level waste glasses [5], characterization of partitioning ligand-actinide complexes [6], actinide oxide/ hydroxide solubility [7], actinide chemistry, and identification of corrosion products on UO_2 fuel pellets [8]. The results of many of these investigations can be found elsewhere in this report. Selected results, which are specifically associated with technical upgrades of the INE-Beamline are described below.

External users

A total of fifteen external groups came to use the INE-Beamline in 2007. The beamtime delivered to external users in 2007 represents 57% of the total available beamtime. A large percentage of the guests coming to the beamline were/are students and young researchers.

INE-Beamline external users fall into three main categories: ACTINET users, ANKA proposal users, or INE cooperation partners. INE active laboratories, including the INE-Beamline, are one of the pooled facilities of the

Cooperation at the INE-Beamline 2007 (ACTINET projects are indicated)

- University of Bonn, Physikalisches Institut (20% of all shifts)
- FZK – Institute for Nanotechnology
- FZK – Institute for Microstructure Technology
- University of Karlsruhe
- Universität Mainz, Kernchemie
- University of Erlangen
- European Commission Joint Research Center – Institute for Transuranium Elements (ITU) (ACTINET)
- CEA Grenoble (ACTINET)
- Paul Scherrer Institute, Villigen (ACTINET)
- Institut de Recherches Subatomiques, Strasbourg (ACTINET)
- Subatech, Nantes
- University of Manchester (ACTINET)
- University of Helsinki
- University of Bari

European Network of Excellence for Actinide Science (ACTINET). Six groups with approved ACTINET projects having team members from four different countries (Germany, France, England, and Switzerland) performed experiments at the INE-Beamline in 2007. Thirty percent of annual INE-Beamline beamtime is available to external users through the standard ANKA facility proposal system (for details see [9]). In 2007 eleven projects accessed the INE-Beamline via this route. A measure of the INE-Beamline success is a near doubling of requested beamtime for the first cycle of 2008 (12 projects are submitted for the period April-September 2008). Access to the INE-Beamline is also possible through cooperation with INE. One of the strongest cooperation is between INE and the University of Bonn, Physikalisches Institut (PI-Uni Bonn), covering not only scientific investigations performed by students, but also continued efforts in instrumentation development and beamline improvement.

Upgrades in 2007

This year a number of beamline improvements and technical upgrades were installed [10,11,12]. These include both hardware and software, as well as technical improvements and upgrades, which are primarily driven by in-house and external users' needs. For example, ACTINET projects with expressed scientific intentions partially financed a liquid N_2 cryostat, XIA digital electronics for INE's Canberra LEGe fluorescence detector, and a new Vortex silicon drift detector.

The following discussion of hardware and software upgrades at the INE-Beamline in 2007 are arranged according to the beamline's beam path, starting with components in the optical hutch, followed by those in the experimental hutch, and finishing with the sample environment.

To increase flux at low energies (S and P K-edges), the 100 µm Be window was replaced by a 50 µm window. Following installation of the thinner window, the first systematic study at the P K-edge was successfully conducted [13]. For this purpose a new low energy sample holder was also designed and built. The beamline design is such that one can theoretically reach energies down to the Si K-edge (1.8 keV) and first tests at this energy have already been performed in 2007.

An additional crystal alignment stage for the second monochromator crystal, allowing the fine tuning of the roll adjustment, was installed in cooperation with the PI-Uni Bonn. This upgrade allows precise beam adjustment, which facilitates optimization of the primary beam focus from the second mirror. Optimization of the primary focus is necessary for successful installation of a secondary focusing optic for achieving beam spots in the micrometer range (µ-focus). The first step towards a µ-focus at the INE-Beamline was performed with focusing in one dimension (vertical) using planar compound refractive lens (CRL) arrays fabricated by the Institute for Microstructure Technology (FZK-IMT) (Fig. 1).

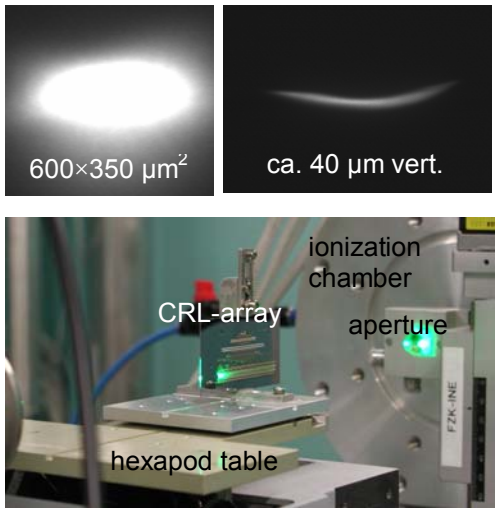

Fig.1: *Top : 1D µ-focus (right) of the originall beam spot (left) at 18keV (Ge 422 crystals). Compound refractive lens array mounted on a hexapod positioning table (bottom).*

The CRL serves as a virtual slit and was first applied in surface specific grazing incidence (GI-) XAFS investigations of the corrosion layer on a UO_2 pellet [8]. The advantage of using a virtual slit over a conventional slit system is to increase the photon flux. In our case a gain factor of approximately two was achieved.

The next important upgrade involved the replacement of the Canberra LEGe five pixel fluorescence detector analogue read-out by a fully digital XIA system. This upgrade was performed in cooperation with the Institute for Synchrotron Radiation (FZK-ISS) and 50% funded by ACTINET. The digital electronics permits storing the complete fluorescence spectrum in digitized form for single scans (as opposed to storing windowed counts in selected regions of interest = single channel analyzer). This will enable scanning µ-XRF to, e.g., determine elemental distributions through multi-line peak fitting of the digital multi-channel MCA data recorded while scanning a sample area. IGOR PRO visualization software already in use at other ANKA beamlines for the digital electronics has also been implemented at the INE-Beamline (Fig. 2).

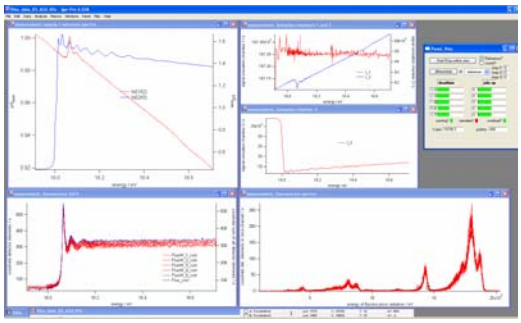

Fig. 2: *Screen dump of the digital electronic visualization software. The complete fluorescence spectrum of the sample at a given energy is shown at the bottom right.*

The XIA electronics also exhibits a lower noise level than the previous analogue read-out. Recording XAFS data at lower concentrations was crucial for in-house investigations. For example, Th oxy-hydroxide polynuclear species identified by nano-electrospray mass-spectrometry (sect. 6.4) as a function of the pH value and Th total concentration was corroborated by XAFS results of a Th 0.7 mM solution with good statistics (Fig. 3).

The following upgrades of sample environment were made in 2007:

An Oxford Instruments (OptistatDN) liquid N_2 cryostat, partially financed through an ACTINET project with ITU, was commissioned and first active measurements performed. The low temperature enhances the EXAFS signal by dampening atomic thermal vibrations. For example, in the U L3 EXAFS of a pentavalent uranyl coordination polymer (ACTINET project between INE, CEA-Grenoble, and Uni Manchester), pronounced oscillations are still visible in the EXAFS up to k=20 $Å^{-1}$ (Fig. 4). Low temperature measurements have also been performed on the Np L3 edge of Np(V) incorporated into calcite (F. Heberling, PhD work). In these studies, combined XRD /XAFS measurements were also performed. Details on the XRD setup are given in the Annual Report 2006.

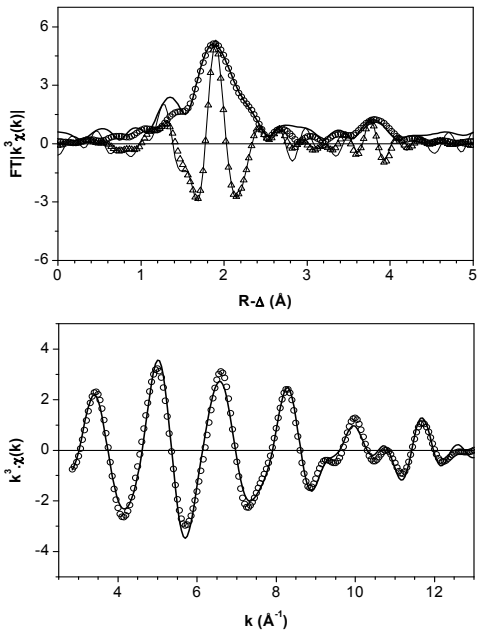

Fig. 3: *Th L3-edge XAFS spectrum of a 0.7mM Th solution. Top: Fourier Transform with fit result (symbols); bottom: corresponding Fourier filtered EXAFS $\chi(k)$.*

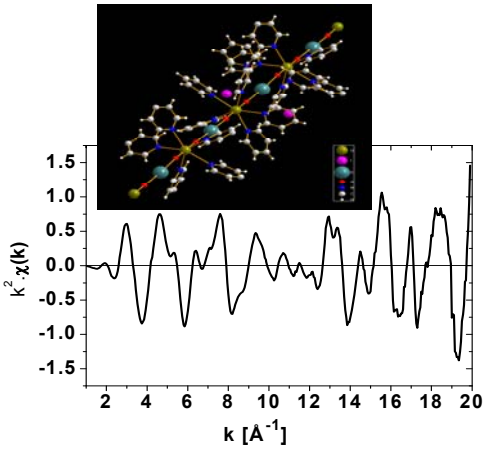

Fig. 4: *Top: U L3 EXAFS spectrum of $\{[UO_2Py_5][KI_2Py_2]\}_n$, containing polymeric dioxo-uranium(V) units linked by potassium atoms.*

Following first measurements on U(III) samples in 2006 [6] using a prototype inert gas sample environment, an inert gas sample cell with standard INE sample holder design was constructed and successfully tested on U(III), Np(III) and Pu(III) containing systems linked to both ACTINET and in-house projects (A. Geist, N. Banik, Ch. Marquardt). The inert gas holder is loaded with samples inside inert gas glove boxes in INE's active laboratories, transported under Ar to the beamline, and connected to an appropriate gas supply (Ar, He, N) upon arrival to guarantee constant inert gas flow. For example, using this inert gas holder Np(III) samples were observed to remain stable over

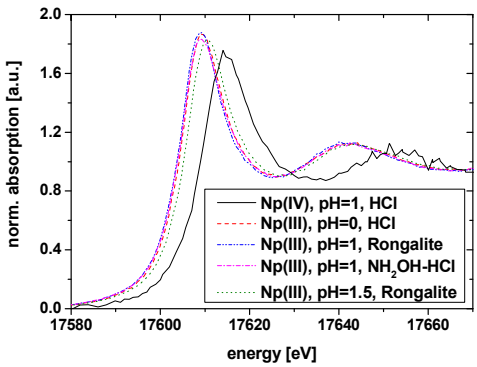

Fig. 5: *Np L3 edge XANES of Np(III) samples compared to Np(IV) aquo ion (N. Banik, Ch. Marquardt).*

a period of several hours (Fig. 5).

The first high pressure measurements with a diamond anvil cell (DAC; Fig. 6) were performed in cooperation with ITU in 2007 at the INE-Beamline. This project has recently been approved as a long term (three year) project through the ANKA proposal system, starting in 2008. In the initial studies, the pressure dependant B1 → B2 transition in USb was investigated by means of XANES spectroscopy. The pressure inside the DAC was calibrated by in situ monitoring of wavelength changes in the fluorescence emission line of a ruby crystal.

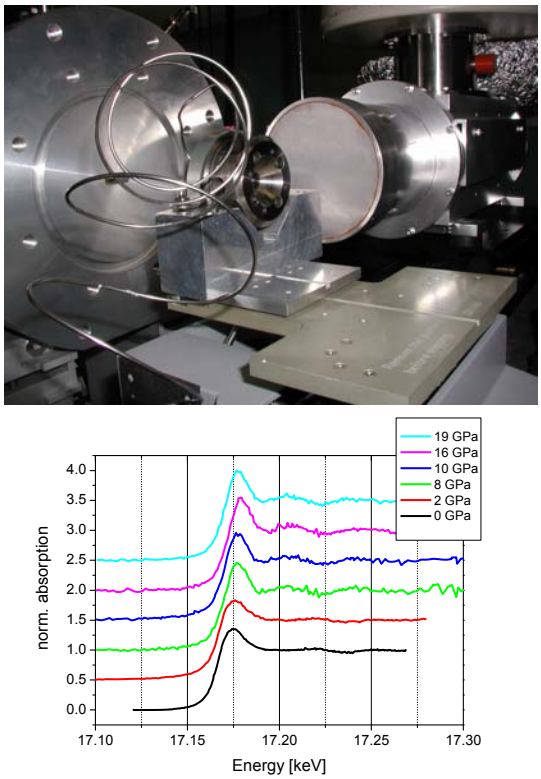

Fig. 6: *Top: Experimental setup for investigating the pressure dependant B1 → B2 transition in USb. Bottom: U L3 XANES recorded at varying pressures.*

Outlook for 2008

Instrumentation development and upgrades planned at the INE-Beamline for 2008 are related to optimizing low energy measurements, implementation a µ-focus option at the beamline, initiation of a project to develop, construct and test an high resolution energy dispersive fluorescence detector (HRXES), and designing new sample holders for special requirements. The planned activities involve specifically:

- Increase the monochromator stabilization unit (MOSTAB) time stability. The incident beam intensity as MOSTAB feedback input parameter will be normalized to the ring current.
- Installation of new low energy ionization chambers (OKEN chambers). This setup has an improved sensitivity and will allow, e.g., better P and S K-edge measurements and 5f element M4,5-edge studies.
- Continue activities to implement a µ-focus option. These include tests of the Vortex Si-drift detector, first measurements with a polycapillary focusing optic (on loan from HASYLAB), tests of confocal irradiation-detection geometry, characterization of beam-size and beam-profile at different energies for two dimensional CRL arrays (possibly including a new mosaic CRL design).
- Purchase and installation of a CCD camera for XRD characterization of small crystallites, for spatially resolved measurements, as well as for tomography experiments.
- Development of a Johann spectrometer for HRXES and for resonant inelastic X-ray scattering (RIXS). Initial RIXS investigations of Eu incorporation into hematite and goethite crystalline phases were performed at the W1 Beamline at HASYLAB in 2007.
- Development, fabrication, and test of an electrochemical cell for in situ XAFS investigations.

Actinide speciation investigations with microfocused X-ray beams

Introduction

Over the past four years INE has embarked on a program using micro-focused synchrotron-generated X-rays for performing spatially resolved actinide speciation investigations. The goal of these investigations is to identify and characterize long term determinant behavior of actinide transport in geological media, requisite to reliable performance assessment of proposed waste disposal strategies for high-level, heat producing nuclear waste. Because these studies involve natural systems with inherent heterogeneity (multi-component systems), application of spatially resolved speciation techniques is essential. Our studies concentrate on natural analogue samples, which mimic repository geochemical and geological conditions on a geological time scale, and on transport in column tracer studies, which are model systems simulating actinide release (plume). The discussion below is divided into two parts according to these two major investigative themes.

Natural analogue Ruprechtov

We investigate U-rich argillaceous Tertiary sediment bore core sections originating from the natural analogue Ruprechtov site in the Czech Republic using micro-focused synchrotron radiation. The aim is to assess mechanisms leading to immobilization of the U by determining the uranium speciation in the sediment and characterizing the spatial distribution of uranium relative to other elements and mineral phases. This is done by means of scanning X-ray fluorescence analysis (XRF) with a micro-focused X-ray beam to obtain elemental distributions. Chemical state maps of an element are obtained by scanning with excitation energies, which selectively ionize single oxidation states. X-ray absorption fine structure (XAFS, both XANES and EXAFS) spectroscopy is used for characterizing chemical speciation and scanning diffraction (XRD) techniques for phase distribution mapping.

Measurements are recorded at Beamline L at HASYLAB, at the Fluo-Topo Beamline at ANKA, and at ID22 at the ESRF. Various X-ray imaging (reflective and refractive) micro-focusing optics are used: polycapillary lenses, new planar compound refractive lenses (CRL) fabricated at FZK-IMT [14], and Kirkpatrick-Baez (KB) mirrors. Most measurements are performed in a confocal irradiation-detection geometry, providing added depth information; the confocal set up allows probing defined volumes below the sample surface with a µm scale resolution. By scanning arbitrary sample areas (x,y scans) at different depths (z), stacks of tomographic cross sections can be easily recorded [15, 16].

We summarize the results from these investigations [17,18,19,20] in the following. Uranium U L3 µ-XANES results (Fig. 7) reveal uranium in the sediment to be present in tetravalent form. Analysis of a µ-EXAFS spectrum (Fig. 8) recorded at a U hot spot below the sample surface to avoid oxidation artifacts on the surface from cutting the bore column shows the U(IV) phase to be a U-phosphate/sulfate. The presence of uraninite observed in bulk XRD and EDAX is also confirmed from µ-XRD measurements on thin section samples.

The analyses of a number of tomographic cross-sections of elemental distributions recorded over different sample areas shows a strong correlation between uranium and As. Arsenic K-edge µ-XANES measurements reveal As to be present mostly as As(0), with some As(V); no As(III) is found. From comparison of measured uranium, As(0), and

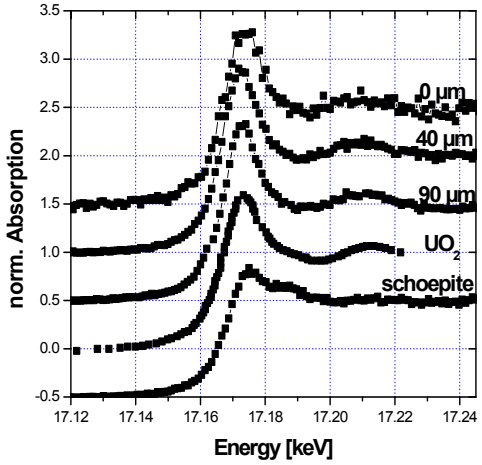

Fig. 7: *U L3 µ-XANES recorded at various positions of the bore core section, at indicated depths below the surface, and compared to U(IV) and U(VI) reference sample XANES.*

As(V) distributions, a positive correlation between uranium and As(V) is found. The As K-XANES of As(0)-rich areas in the sample show a fingerprint comparable to that for arsenopyrite, AsFeS. Supporting the presence of AsFeS is the observed linear correlation between As(0) and Fe. Further evidence of AsFeS is seen in elemental distribution maps recorded with a high lateral resolution, where an As-rich boundary layer or rim surrounding Fe framboidal nodules is observed (Fig. 9). Uranium occurs in direct vicinity of these As-rich boundary layers.

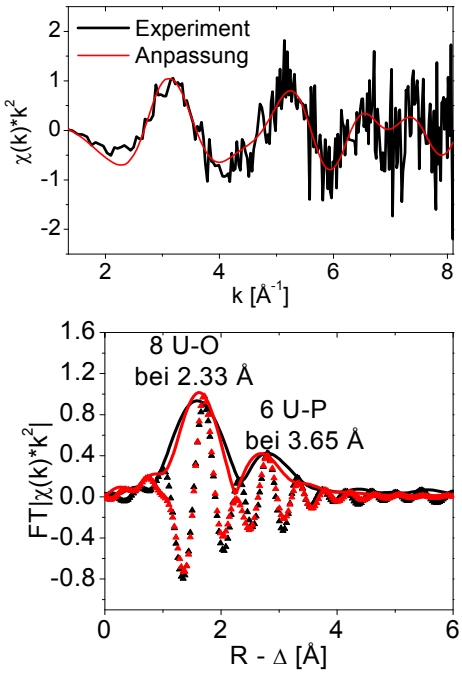

Fig. 8: *U L3 µ-EXAFS and corresponding Fourier transformed data (top right; magnitude in solid lines and imaginary part as symbols). Experimental data is shown in black and the fit result in red.*

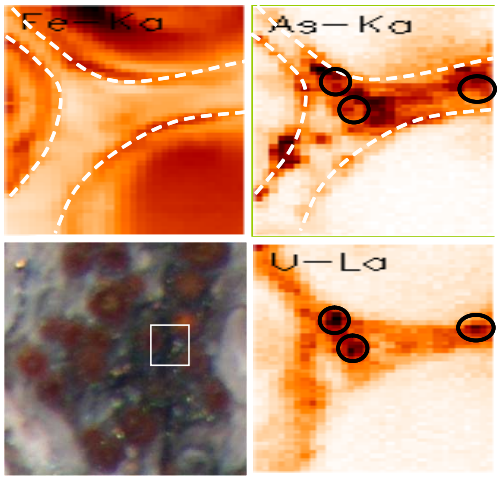

Fig. 9: *Confocal µ-XRF maps of a 120 µm ×120 µm section (2 µm×4 µm v × h step size; 15 s counting time) -60µm below the surface. Circles indicate U hot-spots found in the U map. Dashed lines indicate an As-rich rim around a Fe(II)-nodule. The marked region in the microscopic image shows the area studied.*

Upon comparison of As distribution maps with scanning µ-XRD results (Fig. 10) we find As to be associated with pyrite. We find no XRD evidence for AsFeS, indicating that arsenopyrite is present as thin amorphous or nanocrystalline coating on pyrite framboids, which formed secondary to the original framboid nodules. The observation that both pyrite and siderite occur in the same sediment allows us to assume that the pH was near neutral during formation of these minerals.

These results together allow us to formulate one of the mechanisms for uranium-enrichment of secondary U(IV) minerals in the sediment. The AsFeS in the sediment reduced mobile groundwater-dissolved U(VI) to less-soluble U(IV), thereby immobilizing the uranium as U(IV). As a consequence As(V) was formed.

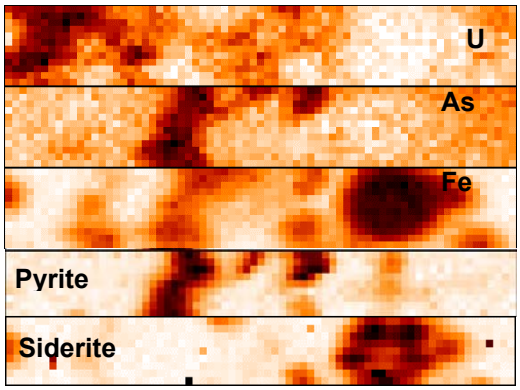

Fig. 10*: Top: Fe, As, and U distributions in a 710 µm × 120 µm thin section (10 µm × 10 µm, counting time = 10s). Bottom: Distribution of d-spacing intensities expected for pyrite and siderite for the first 9 rows (i.e. top 90 µm) of the elemental distribution images. The darker the pixel, the higher the measured intensity in all images.*

Tracer study of Aspö granite

We investigate Np speciation and spatial distribution in a fractured granite bore section from the Swedish Äspö Hard Rock Laboratory following a radiotracer experiment [21]. A polished slice of a fractured granite bore core column (52 mm in diameter) used in a radiotracer experiment is studied. The actinide tracer cocktail contained long-lived radioisotopes, including 10^{-5} mol/dm^3 237-Np (added as Np(V)). The slice studied is where most of the tracer activity was recovered and contains ~3 nmol Np/g; >1ppm.

Analysis of Np L3 µ-XAFS results (Fig. 11) allows us to conclude that Np, originally introduced as Np(V) onto the column, is reduced to Np(IV) in the fractured granite. We note that without the spatial resolution of the experimental setup and the confocal geometry it would not have been possible to obtain this information on such a dilute tracer concentration. Use of confocal geometry is especially important in these experiments as probing volumes below the sample surface not only avoids potential speciation changes caused by sample preparation, it also limits the sample volume probed, which minimizes spectral interference from other elements (in this case energetically close lying Np Lα1 and Sr Kα1 emission lines).

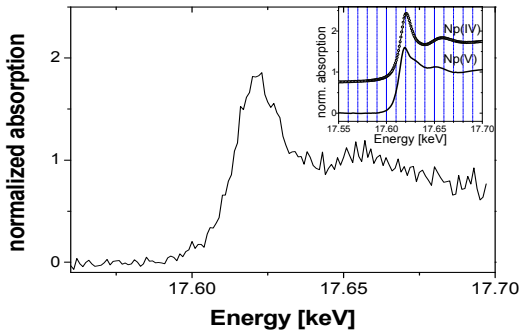

Fig. 11: *Np L3 µ-XANES measured at a Np hot spot around –50 µm below the sample surface. Inset: Np(IV) and Np(V) reference spectra.*

The distribution of Np(IV) is apparently associated with Zn (Fig. 12). We assume This may indicate that ZnS played a role in Np(V) reduction to Np(IV) and subsequent immobilization as the less soluble tetravalent form. There are sample areas where a correlation between Np and Fe is observed, but other areas with none (Fig. 12). The correlation between Np and Fe may indicate

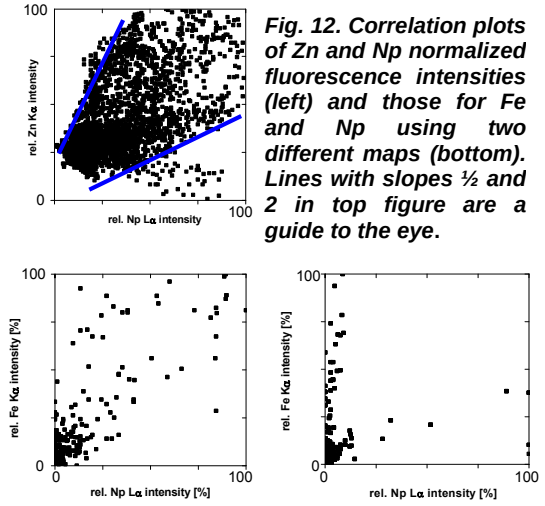

Fig. 12. Correlation plots of Zn and Np normalized fluorescence intensities (left) and those for Fe and Np using two different maps (bottom). Lines with slopes ½ and 2 in top figure are a guide to the eye.

one or both of two things: Np(V) was immobilized by reduction by Fe(II) and/or the Np is located in fissures, as Fe is an indicator element for granite fracture material. The sample regions, where no correlation between Fe and Np is found, may be associated with fissures not easily accessible by inflowing groundwater carrying the Np tracer.

The highest Np concentrations were found clustered in 1—3 pixels (pixel size of 20µm or 10µm) of scanned areas associated with small granite fissures of less than 100 µm width. That high activity is localized in the smallest fissures may indicate that during the tracer experiment inflowing Np has a shorter residence time in large fractures, while in the small fissures migration is slower, leading to longer residence times, i.e., reaction times, resulting in Np(V) reduction and immobilization to less soluble Np(IV). That a clustering of pixels with high Np intensity can be interpreted as either formation of precipitate or presence of a sorbed species at highly localized areas on the fissure walls.

This study has implications for modeling scenarios of actinide release in a nuclear waste repository placed in a granite host rock formation. The redox conditions of the groundwater/granite obviously play a role, but this is coupled to varying hydrological transport affected by the size and interconnectivity of the fractures and fissures in the granite.

Outlook

At the INE-Beamline for actinide research at ANKA we are presently installing the necessary equipment and instrumentation for achieving a beam focus in the micrometer range. First experimental results of the setup are expected in 2008.

References

[1] Walther, C., Rothe, J., Fuss, M., Büchner, B., Koltsov, S., Bergmann, T. Anal. Bioanal. Chem. 388 (2007) 409-431.

[2] Stumpf, T., Curtius, H., Walther, C., Dardenne, K., Ufer, K., Fanghänel, Th. Env. Sci. Technol. 417 (2007) 3186-3191.

[3] Dardenne, K., Bosbach, D., Denecke, M.A., Brendebach, B. Workshop Proceedings, Karlsruhe, Germany 18.-20. September 2006, OECD/NEA (2007) 193 – 201.

[4] Heberling, F., Denecke, M.A., Bosbach, D., Env. Sci. Technol. (2008) 42(7) 471-476.

[5] Brendebach, B., Denecke, M.A., Dardenne, K., Rothe, J., Luckscheiter, B., Weisenburger, S., Roth, G., Nesovic, M., Mangold, S., Workshop Proceedings, Karlsruhe (D) 18.-20. Sept. 2006, OECD/NEA (2007) 183-191.

[6] Denecke, M.A., Panak, P.J., Burdet, F., Weigl, M., Geist, A., Klenze, R., Mazzanti, M. Gompper, K., Comptes Rendus Chimie Academie des Sciences 10 (2007) 872-882.

[7] Brendebach, B., Altmaier, M., Rothe, J., Neck, V., Denecke, M.A., Inorg. Chem. 46 (2007) 6804-6810.

[8] Metz, V., Bohnert, E., Dardenne, K., Brendebach, B., Rothe, J., Denecke, M.A., Nazmov, V., ANKA Annual Report (2007) 168-170.

[9] http://ankaweb.fzk.de/

[10] Brendebach, B., Dardenne, K., Denecke, M.A., Rothe, J., Vitova, T., Nucl. Instrum. Methods Phys. Res. A, 582 (2007) 80-81.

[11] Brendebach, B., Denecke, M.A., Rothe, J., Dardenne, K., Römer, J., in X-ray Absorption Fine Structure – XAFS13, B. Hedman, P. Pianetta Eds., American Institute of Physics, Melville, NY (2007) 875-877.

[12] Brendebach, B., Dardenne, K., Denecke, M.A., Rothe, J., ANKA Annual Report (2007) 284-285.

[13] Löble, M. (Diplom) "Synthese tripodaler N-Donor-Ligandensysteme und deren Verwendung zur Komplexierung von Übergangsmetallen und Lanthanoiden", Fakultät für Chemie und Biowissenschaftender Universität Fridericiana Karlsruhe (TH), Jan.2008.

[14] Nazmov, V., Reznikova, E., Boerner, M., Mohr, J., Saile, V., Snigirev, A., Snigireva, I., DiMichiel, M., Drakopoulos, M., Simon, R., Grigoriev, M., AIP conference proceedings 705, 752-755 (2004).

[15] Janssens, K., Proost, K., Falkenberg, G., Spectrochimica Acta B. 59, 1637-1645 (2004).

[16] Smit, Z., Janssens, K., Proost, K., Langus, I., Nucl. Instrum. Methods Phys. Res. B 35, 219-220, (2004).

[17] Denecke, M.A., Janssens, K., Proost, K., Rothe, J., Noseck, U., Environ. Sci. Technol. 39(7), 2049-2058 (2005).

[18] Denecke, M.A., Janssens, K., Brendebach, B., De Nolf, W., Falkenberg, G., Rothe, J., Simon, R., Somogyi, A., Vekemans, B., Noseck, U. in X-ray Absorption Fine Structure – XAFS13, B. Hedman, P. Pianetta Eds., AIP, Melville, NY (2007), p.187-189.

[19] Denecke, M.A., Somogyi, A., Janssens, K., Simon, R., Dardenne, K., Noseck, U., Microscopy Microanal. 13(3), 165-172 (2007).

[20] Denecke, M.A., De Nolf, W., Janssens, B. Brendebach, B., Rothkirch, A., Falkenberg, G., Noseck, U.,
Spectrochim. Acta B. 63, 484-492 (2008).

[21] Römer, J., Kienzler, B., Vejmelka, P., Soballa, E., Görtzen, A., Fuß, M., FZK-Wissenschaftliche Berichte FZKA6770 (Oct. 2002).

6.2 Laser spectroscopy: Selective speciation of the actinide solvation shell and of aluminol groups at the corundum/water interface

A. Abdelmonem, M. Flörsheimer, R. Klenze, K. Kruse, P. Lindqvist-Reis, R. Polly, B. Schimmelpfennig, C. Walther,

Introduction

Emphasis of laser spectroscopy was placed on the vibrational spectroscopy of the ligand interaction within actinide complexes (vibronic side band spectroscopy) and of OH oscillators at the water/α-Al_2O_3 (001) interface (sum-frequency vibrational spectroscopy). Both methods provide important information with high selectivity and sensitivity, which is not accessible by other techniques.

Outer shell speciation of actinide ions by vibronic sideband spectroscopy

Time-resolved laser-induced fluorescence spectroscopy (TRLFS) is a valuable tool for characterization and quantification of trace amounts of luminescent trivalent lanthanide and actinide (Cm^{3+}, UO_2^{2+}) species in solution. For example, the emission bands of Eu^{3+} reveal the number of different species and their symmetry, while the emission lifetime provides the number of H_2O or OH^- ligands. Similar information is obtained for Cm^{3+}. However, since the f-f electronic transitions of lanthanides and actinides are sensitive only to the local structure, TRLFS is less suited for detecting changes in their second coordination shells. Another drawback is that these transitions provide no direct information about the ligand type. Spectroscopic methods such as infrared and Raman are indeed sensitive to internal molecular vibrations but are of little relevance for very dilute systems.

However, several of these problems can be overcome by means of vibronic side band spectroscopy (VSBS). This method provides infrared-like spectra in the direct environment of the luminescent ion and has been used, e.g., to derive vibrational information of Ca^{2+} binding sites in biological macromolecules, replacing Ca^{2+} by luminescence probes such as Gd^{3+} or Yb^{3+} [1,2]. VSBs arise due to the coupling between the f-f electronic transitions and the various localized vibrational modes (e.g. stretching and bending modes of H_2O ligands), and appear at the low energy side (Stoke shift) of the parent electronic transition (zero phonon line, ZPL) in the emission spectra (Fig.1). Although VSBs have generally extremely low intensities and therefore are difficult to detect, when observed in the spectra they may provide valuable information about the nature of the ligand.

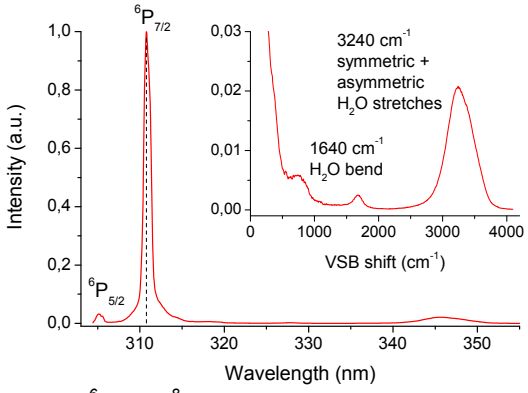

Fig. 1: *$^6P_{7/2} \rightarrow {}^8S_{7/2}$ fluorescence emission spectrum of Gd^{3+}(aq) (75 mM $Gd(ClO_4)_3$ in 0.1 M $HClO_4$); the inset shows the vibronic side band spectrum.*

We have studied VSBS of Cm(III) for the first time and compared the results with Gd(III) to obtain spectroscopic information about solvent-shared and contact ion-pairs formations of both ions in aqueous perchlorate solutions. Our previous TRLFS studies on the hydration of Eu(III) and Cm(III) in 0.1-12 M $HClO_4$ solution have shown an increase in the fluorescence decay rates with increasing concentration up to ~ 8.8 M, but no changes in the spectra [3]. This was interpreted as the formation of solvent-shared ion-pairs (M^{3+}-H_2O···ClO_4^-), because as perchlorate ions progressively enter the second coordination spheres of the metal ions the hydrogen bonding to the first hydration spheres weakens, which does not necessarily affect the coordination geometries. At higher concentrations the decay rates decrease significantly followed by major spectral changes as perchlorate ions penetrate the first hydration spheres to form contact ion pairs (M^{3+}-ClO_4^- ···H_2O), presumably in monodentate fashions by replacing 2-3 water ligands (Fig. 2).

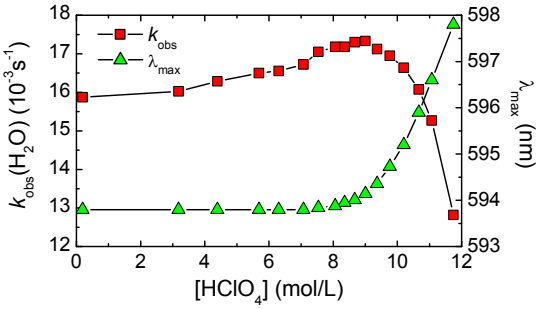

Fig. 2: *Fluorescence decay rate constant k_{obs} (■) and peak maximum λ_{max} (▲) of the $^6D_{7/2} \rightarrow {}^8S_{7/2}$ fluorescence emission spectrum of Cm^{3+}(aq) at different concentrations of added $HClO_4$.*

The formation of solvent-shared and contact ion-pairs are clearly seen in the Gd^{3+} and Cm^{3+} vibronic spectra as a Cl-O stretching band at about 1020 and 980 cm^{-1}, respectively, whose intensity increases markedly above ~ 8.8 M $HClO_4$ due to contact ion-pair formation (Figs. 3 and 4). This is in agreement with reported infrared frequencies of monodentately coordinated ClO_4^- [4]. In addition, with increasing $HClO_4$ concentration the OH stretching vibrations of the water ligands shift ~ 270 cm^{-1} to higher frequencies. These large blue-shifts indicate significant strengthening of the O-H bonds of the water ligands due to the simultaneous weakening of the hydrogen bonds to the perchlorate ions in the second coordination shells. It is noteworthy that VSBS on Cm(III) is much more sensitive compared to Gd(III). The vibronic intensities normalized to the ZPL intensities shown in Fig. 3 ([Gd(III)] = 0.075 M) and Fig. 4 ([Cm(III)] = 0.5×10^{-6} M) is about 2-3 times higher for Gd, however the noise level is comparable in both spectra. This indicates that the sensitivity of VSBS is more than four orders of magnitude higher for Cm(III) compared to Gd(III).

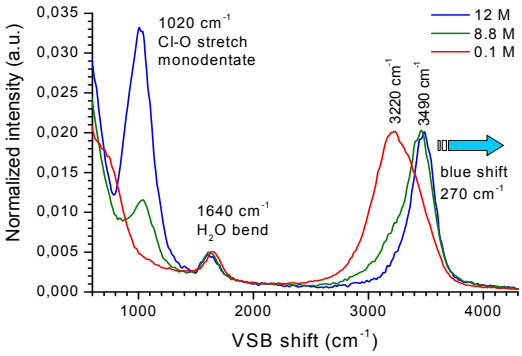

Fig. 3: *Vibronic spectra associated with the parent $^6P_{7/2} \rightarrow {}^8S_{7/2}$ electronic transition of 75 mM $Gd(ClO_4)_3$ in 0.1, 8.8, and 12 M aqueous $HClO_4$.*

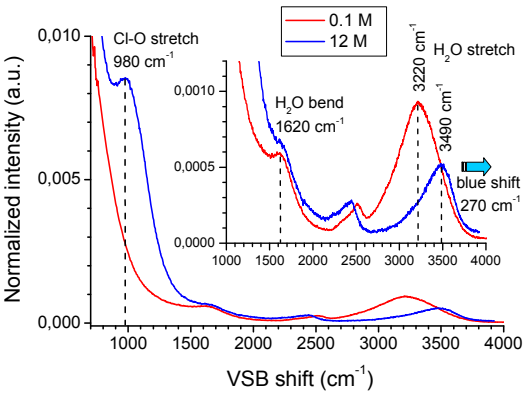

Fig. 4: *Vibronic spectra associated with the parent $^6D_{7/2} \rightarrow {}^8S_{7/2}$ electronic transition of 0.5 μM Cm^{3+}(aq) in 0.1 and 12 M aqueous $HClO_4$.*

VSBS has also been used for Gd^{3+} and Cm^{3+} doped into solids. In the spectra recorded at 20 K the bands are rather sharp and have intensities well above the noise level, but are still much lower than the ZPL. For example, the intensity of the VSBs normalized to the ZPL of $[Cm{:}Y(H_2O)_9](CF_3SO_3)_3$ ranges from 0.015 to 2 %, where the higher intensities are found in the low frequency part of the spectrum (Fig. 5). This is due to that fact that the VSB intensity depends on the infrared oscillator strength for a given molecular vibration and R^{-6}, where R is the distance between the emissive Cm^{3+} ion and the vibrational centre at the molecule (H_2O, $CF_3SO_3^-$). Thus, the higher intensities originate from the CmO_9 skeletal modes appearing at lower frequencies (< 400 cm^{-1}), whereas the more distant vibrational centers of $CF_3SO_3^-$ give rise to bands of much lower intensity. Interestingly, the intensity ratios (VSB/ZPL) for several of the VSBs in Fig. 5 are similar to the corresponding bands of $[Gd(H_2O)_9](CF_3SO_3)_3$.

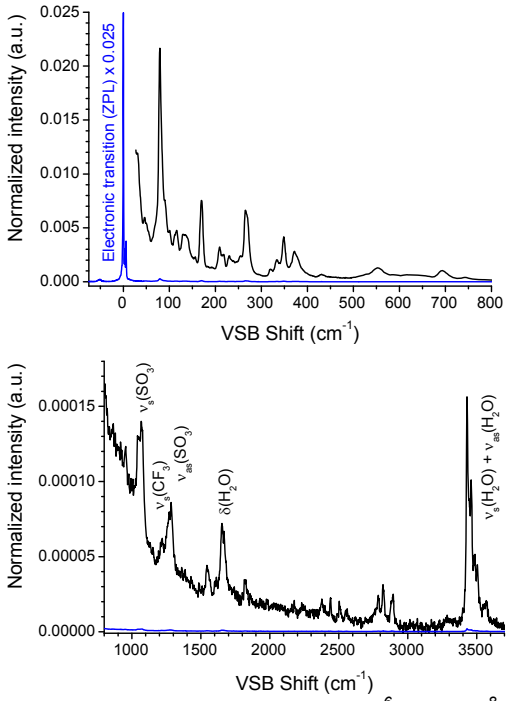

Fig. 5: *Vibronic spectrum of the $^6D_{7/2} \rightarrow {}^8S_{7/2}$ transition of $[Cm{:}Y(H_2O)_9](CF_3SO_3)_3$ at 20 K in the two frequency regions 0-800 and 800-3700 cm^{-1}.*

In summary, we have shown that VSBS of Gd^{3+} and Cm^{3+} can provide infrared-like spectra of the local structure around these ions both in solution and in solids. This was demonstrated by the first spectroscopic evidence of solvent-shared and contact ion-pairs formations in aqueous Gd(III) and Cm(III) perchlorate solutions at high $HClO_4$ concentration. The vibronic spectrum of Cm^{3+} in $[Y(H_2O)_9](CF_3SO_3)_3$ at 20 K contains several sharp lines originating from different localized phonon modes in the crystal.

Speciation and hydration of mineral surfaces probed by vibrational sum frequency spectroscopy and quantum chemistry

Introduction

The adsorption of radioisotopes at mineral surfaces of the aquifer is an important process which leads to the retention of the contaminants. That means that their transport by the ground water is either suppressed or considerably slowed down. For the reliable long-term modelling of the elements' migration, the adsorption/desorption properties and the reactivity of the mineral surfaces must be understood at the molecular level.

The interaction of a mineral with an electrolyte is controlled by the surface functional species. We use corundum (α-Al_2O_3) as a model mineral which is related to natural clay minerals and analogous iron phases. At the surfaces, there are aluminol groups. At a corundum (001) surface, for example, a single type of a doubly coordinated OH species (see middle structure in Fig. 6) is expected to occur [5]. The most basic and most important reaction of the surface functional species is their protonation

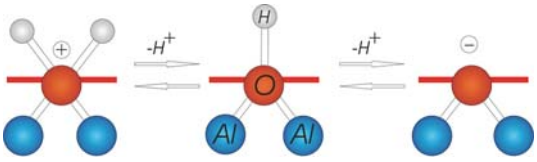

***Fig. 6**: Scheme of expected speciation corundum/ water interface, protonation and deprotonation of aluminol species.*

and deprotonation which occurs upon the change of the pH of the water. As a result, the surface properties change dramatically, for example the interaction capability with actinide and lanthanide ions. In our combined experimental and theoretical study we observe a surprising diversity of species and unexpected processes at the interface leading to a picture of the interface at the molecular level which is much more detailed as compared to the simple model assumed in Fig. 6.

Speciation of functional groups obtained by Sum Frequency Spectroscopy

In order to obtain chemical analytical information *selectively* from a mineral surface *in situ* in water we apply the nonlinear optical technique of sum frequency (SF) vibrational spectroscopy [6, 7]. This method is the only experimental technique for direct and selective probing of small functional surface species such as OH groups.

The spectral positions of the vibrational bands provide information on the chemical composition of the species. From the band positions, we can also obtain the coordination number of the atom, which binds the functional species to the crystal lattice. The quantitative comparison of the amplitudes in spectra, taken at different polarization configurations, allows us to determine the bond tilt angles of the functional species.

We can also use the method for measuring the net *polar* orientation of the water molecules adjacent to the mineral surface. This information is not accessible in a corresponding linear optical experiment. Polar water ordering near the interface is due to the interaction of the water molecules with the functional species of the hydrophilic mineral. The SF signal thus provides information on the interaction mechanism.

The following results are obtained:

- The corundum (001) surface exhibits different aluminol groups. They are all doubly coordinated with Al atoms. As shown in Fig. 7, the species differ in their OH bond tilt angle.
- The tilt angles do not depend significantly on the pH in the region between pH 12 and 4.
- The surface concentrations of the flat oriented species increase with decreasing pH.
- At high pH, the mineral surface is partially deprotonated as expected (Fig. 6). At high pH, mineral/water interaction is controlled electrostatically.
- Within the broad pH range from 7 to 2, the preferential polar orientation of the water molecules at the interface cannot be explained by electrostatic interactions.

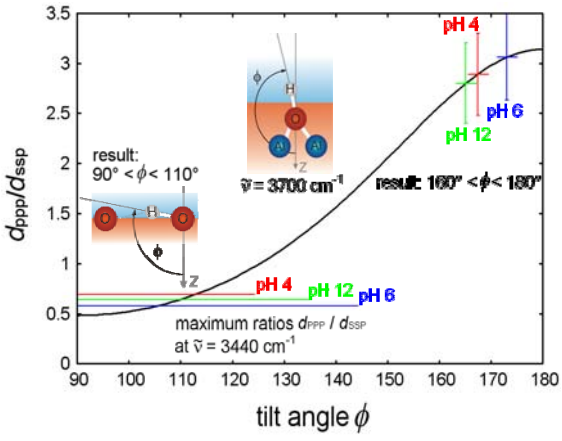

***Fig. 7:** Tilt angles for the examples of the steepest and flattest aluminol species observed in the SF spectra at different pH. tilt is calculated from the ratio of two nonlinear susceptibility tensor elements obtained in two different experimental geometries.*

Hydrophilic hydration observed by SFG

If mineral/water interaction between pH 7 and 2 is not due to electrostatic forces it must be due to hydrogen bonding. The hydrogen bonding The interaction between water and *hydrophobic* surfaces (hydrophobic hydration), which is responsible for key biological phenomena such as protein folding and self assembly of membranes, could be well understood at the molecular level in the recent years [8]. For *hydrophilic* hydration, however, which is a key phenomenon in mineral/water interaction, no predictive theory exists so far. There are only indications from computer simulations in the literature [9-11] on the parameters at the molecular level which probably control hydrophilic hydration:

- The relative concentration of hydrogen bond donor species and acceptor species of the surface was stated to be essential [9,10].
- Not only the chemical composition but also the geometry of the functional species determines their ability to act as hydrogen bond donor or acceptor [11].
- The relation between the surface lattice constants and the size of the water molecule is crucial.

The unique observation of various functional surface species in our experiments, which differ only in one geometric parameter, can now be applied for the first experimental study of hydrophilic hydration as a function of the species' geometry. To this end we determine the net polar orientation of the water molecules near the interface. The net water dipole moment is normal to the interface. It points into the water phase at medium pH and to the mineral surface at pH 3. The different polar orientations are due to different hydrogen bonding caused by the density variation of the flat oriented OH groups upon a pH change. An OH species can serve as a hydrogen bond acceptor and as a donor. Flat oriented species, however, favour the action as acceptors in contrast to steeper oriented species which preferentially serve as donors. (See Fig. 8) As a result, the hydrogens of the water molecules are favoured to be bonded to the surface at pH 3, where the density of the flat OH species is increased, leading to the net water dipole moment in agreement with the measurement. At medium pH, the oxygens of the water molecules are favoured to be bonded to the hydrogens of steeper oriented OH groups, leading again to the net water dipole moment to be in agreement with the measurement.

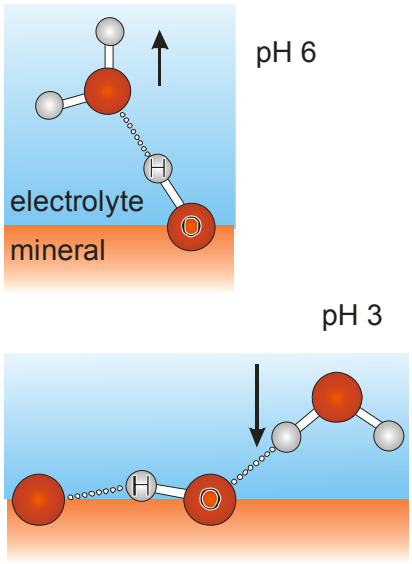

Fig. 8: *The aluminol species of the surface can act as hydrogen bond donors and acceptors. Flat oriented species, whose surface concentrations increase with decreasing pH, favour to serve as acceptors. Steeper species favour acting as donors. The observed change of the net polar water orientation with decreasing pH is a consequence of the increase in the flat oriented species' concentration.*

The interpretation of the SF data leads to a detailed, consistent model. For a verification, we need, however, the results of an independent method.

Quantum chemical calculations

For the task of supporting and confirming the experimental results we complemented the spectroscopic study with *ab initio* and *first principles* quantum chemical computations. We considered aluminium oxide and hydroxide clusters whose sizes were increased successively in order to approximate the real mineral surface. We calculated the minimum energy structures, bond angles, and vibrational frequencies. Details are given in Section 6.4 of this report. We obtained surfaces, composed of doubly coordinated species which differ in their OH bond tilt angle. From the calculated tilt angles and resonance frequencies of the different OH species, we computed SF spectra which are in excellent agreement with the measured ones (see Section 6.4). The calculations provided also two water populations at the cluster surfaces with opposite net dipole orientation. The water molecules are bonded to flat oriented aluminol species which act as hydrogen bond acceptors and to steep oriented donors similar as obtained experimentally. The calculations represent a completely independent theoretical proof of the experimental findings.

Conclusion and Outlook

Applying two independent methods, we obtained a detailed, consistent model on the speciation of the functional groups of a mineral surface and on the interaction of the functional species with the adjacent water molecules. The results are important for geochemical transport modelling which depends on reliable information on the real chemical composition and geometric structure of the mineral/water interfaces. High impact is also expected for the understanding of hydrophilic hydration. In the next steps we include actinide ions as well as organic molecules

References

[1] Iben, I.E.T., Stavola, M., Macgregor, R.B., Zhang, X.Y., Friedman, J.M., Biophys. J. 59 (1991) 1040-1049.

[2] Roselli, C., Boussac, A., Mattioli, T. A., Griffiths, J. A., El-Sayed, M.A., Proc. Natl. Acad. Sci. USA 93 (1996) 14333-14337.

[3] Lindqvist-Reis, P., Klenze, R., Fanghänel, Th., Influence of temperature and ionic strength on the hydration of curium(III) in aqueous solution studied with TRLFS, Proc. of the Conference Actinides 2005, Manchester, UK, July 4-8, 2005, in: Recent Advances in Actinide Science (Eds. R. Alvarez, N. D. Bryan, I. May), Royal Society of Chemistry, Spec. Pub. No 305, RCS Publishing Cambridge, UK, (2006) 500-502.

[4] Bünzli, J.-C.G., Yersin, J.-R., Mabillard, C., Inorg. Chem. 21 (1982) 1471-1476.

[5] Barrón, V., Torrent, J., J. Colloid Interface Sci 177 (1996) 407.

[6] Shen, Y.R., Nature, 337 (2004) 519.

[7] Flörsheimer, M., Kruse, K., Polly, R., Abdelmonem, A., Schimmelpfennig, B., Klenze, R., Fanghänel, Th., submitted to Langmuir (2008).

[8] Chandler, D., Nature 437 (2005) 640.

[9] Besseling, N.A.M., Langmuir 13 (1997) 2113.

[10] Hayashi, T., Pertsin, A.J., Grunze, M., J. Chem. Phys. 117 (2002) 6271.

[11] Janeček, J., Netz, R. R., Langmuir 23 (2007) 8417.

6.3 Formation and hydrolysis of polynuclear Th(IV) complexes

C. Walther, J. Rothe, M. Fuß and S. Büchner

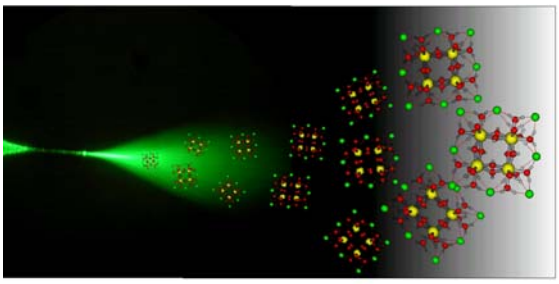

Introduction

Polynuclear complexes play an important role for the hydrolysis of tetravalent thorium ions in aqueous solution [1-3], in particular, for Th(IV) concentrations in excess of [Th(IV)]=10^{-4} M. Consequently, these polymers ($Th_x(OH)_y^{4x-y}$, denominated (x,y)) must be considered when describing hydrolysis of Th(IV) or dissolution processes of Th(IV) solids, even in undersaturated solutions [4,5]. In the past, considerable efforts were made to obtain equilibrium formation constants of these polymers and different stoichiometries for dimers (x=2) [6,7], tetramers and hexamers have been suggested. However, most information was obtained from indirect methods, in particular, from potentiometric titrations. Here, we use nano-electrospray mass-spectrometry [8,9] to directly quantify the degrees of polymerization, *i.e.* the numbers of Th^{4+} ions, the numbers of hydroxide ligands, and as a consequence, also the charges of the complexes. All mono- and polynuclear species which are present in solution are quantified simultaneously down to species contributing less than 0.1% of the total [Th(IV)] concentration.

Experimental methods and sample preparation

The electrospray time-of-flight mass-spectrometer [10] consists of a home built nanospray ion source equipped with spray capillaries from PROXEON (boro-silicate, thick metal coating, inner tip diameter 2 μm). Droplets of less than 100nm in diameter form [11] and shrink within a few microseconds to tiny droplets of some 50 water molecules each containing only one thorium hydroxide complex $\{Th_x(OH)_y^{4x-y} \cdot mCl^- \, nH_2O\}^{4x-y-m}$. The chloride ions, presumably located in an outer shell, compensate part of the charge of the complex. The source is operated at conditions preventing polynucleation in the spray [10]. The ions are analyzed in the time-of-flight mass-spectrometer with a maximum mass resolution of $m/\Delta m$ = 26000 which provides isobaric resolution and allows us to identify, as a function of pH_C, not only size and polymerization x, but also the number of hydroxide groups y and via q=4x-y the charge of each oligomer [10]. Often several hydroxide complexes with the same degree of polymerization x but different number of hydroxide groups y are present simultaneously. In this case, a number weighted mean charge y is calculated. Though Th has only one long lived isotope (^{232}Th), the natural isotope abundances of ^{35,37}Cl cause isotopic patterns unique for each complex in the mass spectrum ($\{^{232}Th_x(OH)_y.^{35}Cl_p{}^{37}Cl_q \, n(H_2O)\}^{4x-y-p-q}$) which facilitates unequivocal identifcation.

Thorium nitrate ($Th(NO_3)_4 \cdot nH_2O$, analytical grade) was dissolved in $HClO_4$ and upon pH increase by addition of NaOH, amorphous thorium hydroxide was precipitated. The precipitate was repeatedly washed with distilled water and centrifuged. Subsequently, the precipitate was redissolved in HCl resulting in a stock solution of $[Th(IV)]_{tot}$ = 0.3M at pH_C 3.1. (pH_C denominates –log[H+], not activity). The samples were prepared in two steps: First, small amounts of stock solution were diluted with HCl (pH_C 0.3-4), and subsequently were titrated with MQ water very slowly (10μl min^{-1}) with vigorous stirring in order to avoid colloid formation due to local pH gradients. All samples were undersaturated with respect to the formation of amorphous thorium hydroxide.

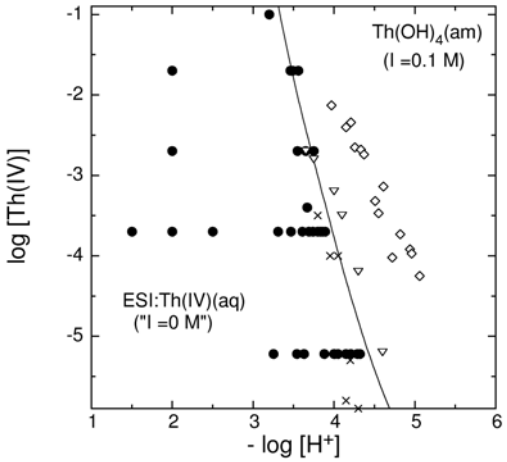

***Fig. 1**: Solubility diagram for $Th(OH)_4$(am). Samples measured by ESI (•). Solid line: solubility calculated for Th(IV) in HCl without addition of electrolytes denominated ("I=0 M"). Formation constants and SIT parameters from [3]. Open symbols represent experimental solubility data at I=0.1M from Nabivanets et al. [12], Ryan et al. [13], and Rai et al. [14].*

Oversaturated samples can not be measured by nano-ESI due to clogging of the 2 μm capillary, restricting the present investigations to 1 < pH_C < 4.5 (Fig. 1, •). Samples between $[Th(IV)]_{tot}$ = 6×10^{-6}M and $[Th(IV)]_{tot}$ = 1×10^{-1}M are measured up to the solubility of amorphous Th(IV) hydroxide ([12-14]). The frequently used approach of working at rather high, but constant, ionic strength, *e.g.* at I = 1M is not possible here, since the amount of electrolyte present in solution is limited by the ESI technique: Salt deposition clogs the small orifice were the spray enters the vacuum chamber and strongly reduces the measurement time between cleaning cycles. Hence, no electrolyte was added to the samples, and the ionic strength of the solution is determined by the molality of H^+, Cl^- and the thorium hydroxide complexes.

Results

In the following, the dependence of hydrolysis and complex formation on Th(IV) concentration and on acidity are discussed by means of the time-of-flight spectra of seven selected samples (Fig. 2). All but spectrum (h) are plotted in a logarithmic representation due to the large difference in abundance of the various species. The Th(IV) complexes remain embedded in small water droplets during all stages of the detection to minimize the invasiveness of the electrospray process. However, since the number of water molecules in the detected droplet may vary between some 10 < n < 50, each complex (x,y) gives rise to a cluster of peaks rather than one single line in the spectrum.

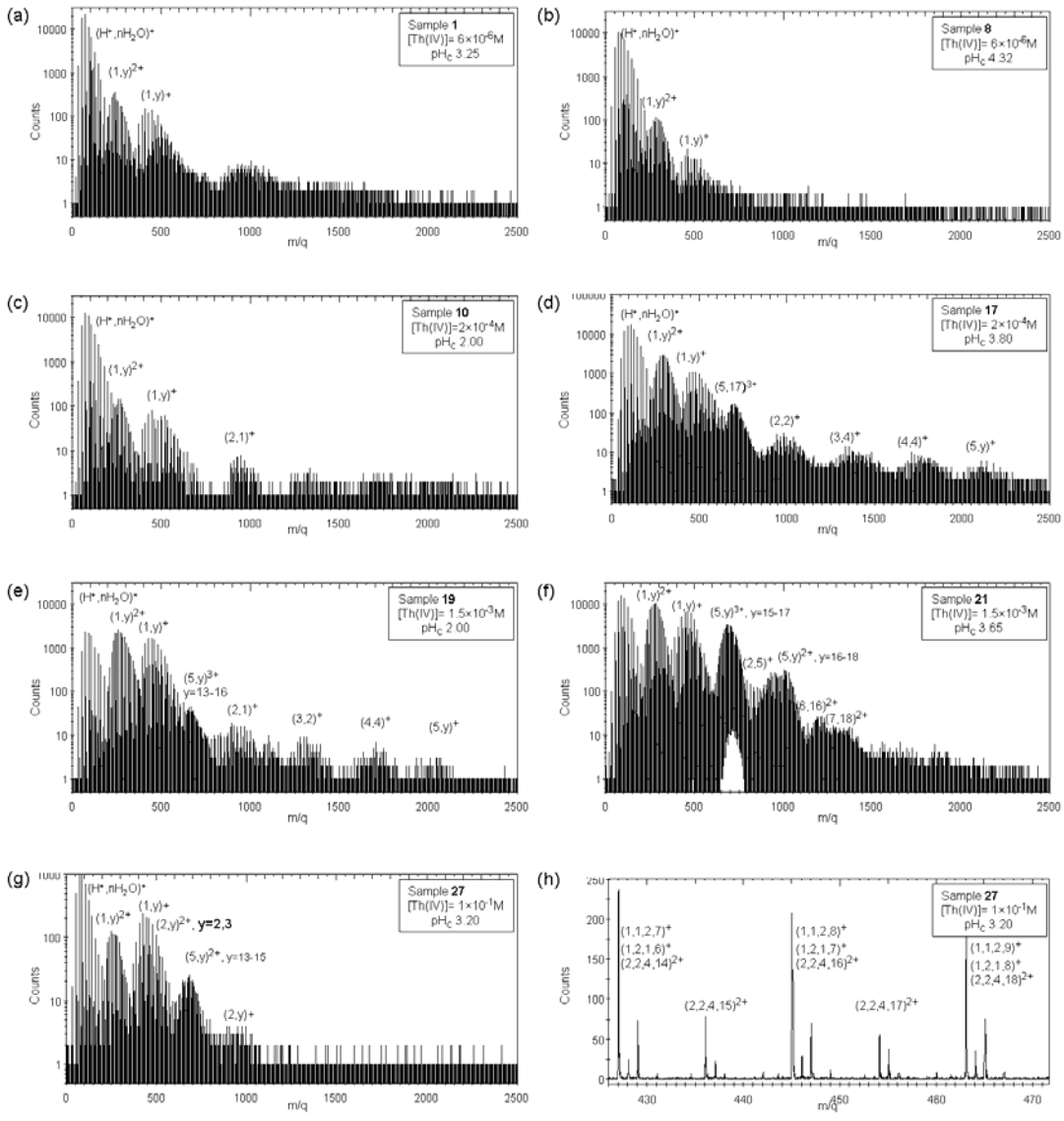

Fig.2: *ESI Mass-spectra of selected samples. With increasing Th(IV) concentration and with increasing pH_C the abundance of polymers increases. Details on the peak structure are discussed in the text.*

At $[Th(IV)]_{tot}$ = 6×10^{-6}M (a),(b) only monomeric complexes $Th(OH)_y^{4-y}$ are detected: the singly charged $(1,y)^+$ and the doubly charged $(1,y)^{2+}$. These charges, however, are not the charges of the complexes in solution but the charge of the droplet containing the complex and in addition some charge compensating chloride ions. The species $(1,0)^+$, for instance, corresponds to $\{Th^{4+}\cdot Cl^-_3\ nH_2O\}^+$, whereas loss of one chloride ion leads to the doubly charged species $(1,0)^{2+}$ ($\{Th^{4+}\cdot Cl^-_2\ nH_2O\}^{2+}$).

At $[Th(IV)]_{tot}$ = 2×10^{-4}M, initially polymer free solutions (c) form polymers upon pH increase (d). The most abundant species is the pentamer $Th_5(OH)_y^{20-y}$, a rather surprising finding, since most models of Th(IV) polymerization include only even sized polymers, *i.e.* dimers, tetramers, and hexamers.

Increase of Th(IV) concentration ($[Th(IV)]_{tot}$ = 1.5×10^{-3}M), shifts the stability range of polynuclear hydroxide complexes to higher acidity (Fig.2e: pH_C 2.0) and polymers dominate the spectrum close to the solubility limit of $Th(OH)_4$(am) at pH_C 3.65 (f). Moreover, the hydrolysis of pentamers is clearly visible: The number of hydroxide ligands increases from y=13-16 at pH_C 2.0 (e) to y = 16−18 at pH_C 3.65 (f). While the pentamer is the most abundant polymer up to $[Th(IV)]_{tot}$ = 1.5×10^{-2}M, the dimer becomes equally abundant at $[Th(IV)]_{tot}$ = 1×10^{-1}M (g) in agreement with recent X-ray scattering experiments on solutions of comparable concentration [6,7].

Fig. 2(h) shows a magnified section of spectrum (g) in order to visualize how doubly charged dimers can be quantified in spite of the massspectrometric interference of the mononuclear hydroxide complexes (h) by making use of the unique isotope distribution of the charge compensating chloride ions.

Discussion

Fig. 3 compares the species distributions of the two series at $[Th(IV)]_{tot}$=6×10^{-6}M and $[Th(IV)]_{tot}$=2×10^{-4}M to the model of [3].

At $[Th(IV)]_{tot}$=6×10^{-6}M (top), no polymers are detected which is in accordance with a potentiometric study performed at twofold higher concentration [15]. With increasing pH_C 3.0−4.3, the dihydroxide complex $Th(OH)_2^{2+}$ forms at the expense of the hydrated ion Th^{4+} and the first complex $Th(OH)^{3+}$ which is in quantitative agreement with the hydrolysis model of [3] (solid, dotted and dashed lines, respectively). Moreover, it also agrees with the model that no polymers are detected. The concentration of the most abundant polymer predicted by the model, the tetramer, should

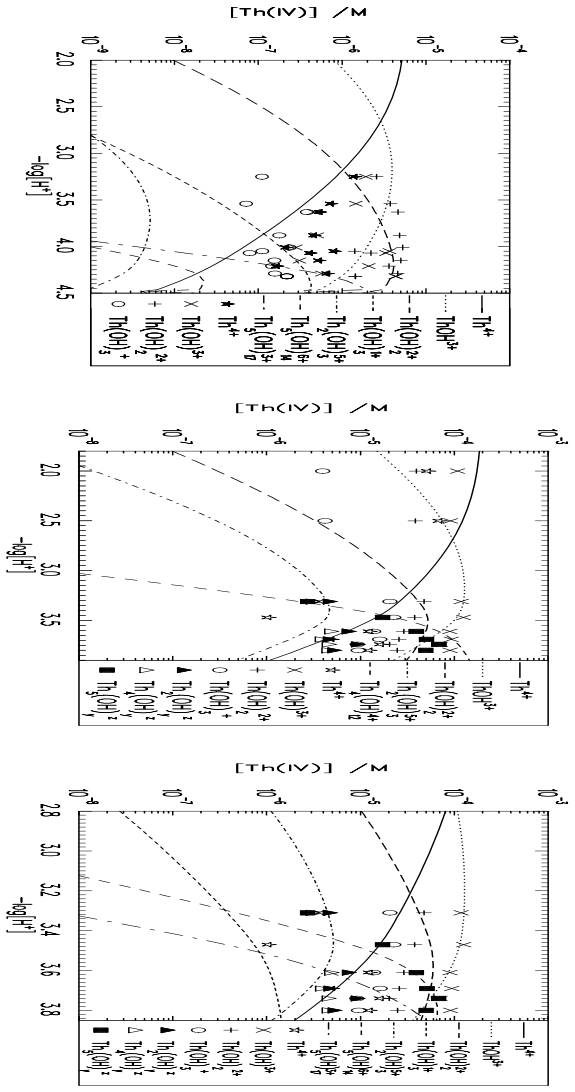

***Fig. 3**: Distribution in Th(IV) solutions measured by ESI-TOF (symbols) compared to model predictions (lines): top: At $[Th(IV)]_{tot}$=6×10^{-6}M only monomeric hydroxide complexes are detected. Middle: At $[Th(IV)]_{tot}$=2×10^{-4}M , polynuclear complexes form close to the solubility limit. The formation of pentamers coincides with the prediction of tetramer formation by [3] (dashed line). Bottom: The same data, compared to a modified model taking into account pentamer formation and hydrolysis.*

be $[Th_4(OH)_{12}^{4+}]$ = 1×10^{-8}M which is below the detection limit of our ESI mass spectrometer. In Fig.3 (middle) the series at $[Th(IV)]_{tot}$=2×10^{-4} M is compared to the NEA model [3]. At pH_C 2.5, Th^{4+} and $Th(OH)_{3+}$ contribute approximately 40% of the total Th(IV) concentration each, which is in accordance with the NEA model (solid and dotted lines, respectively). The fraction of dimers remains below the detection level. At pH_C 3.3, dimer,

tetramer and pentamer form at approximately equal amounts, though they are clearly minor to the mononuclear complexes Th^{4+} and $Th(OH)_3^+$. With increasing pH, the relative abundance of the pentamer increases strongly and eventually accounts for almost 50% of the $[Th(IV)]_{tot}$ concentration at *pHC* > 3.6. In this pH range, the fraction of Th(IV) pentamers agrees very well with the polymer fraction predicted by the NEA model (dashed line). That pentamers are observed instead of the predicted tetramers must not necessarily be regarded as a contradiction. For one, the present study was conducted at low ionic strength, whereas the equilibrium constants at zero ionic strength used for the model [3] were obtained by extrapolating conditional constants from experiments performed at typically molar ionic strength. Supposed, a species were of minor relevance or of low stability at high ionic strength it would not be described correctly by extrapolation to zero ionic strength. Second, to our knowledge, up to now no direct observation of the polynuclear species of Th(IV) in millimolar concentrations was reported. The introduction of the tetramer is based on analogy considerations for Zr(IV) and Hf(IV) [3]. It might very well be possible to model earlier experiments by formation of $Th_5(OH)_y^{20-y}$ complexes instead of by formation of tetramers and hexamers.

In the lower part of Fig. 3 the data of the middle part is compared to a slightly refined model, including two pentamers (5,14) and (5,17). Data from $[Th(IV)]_{tot}$= 6×10^{-6} M – 0.1 M is well described by one set of equilibrium constants [16].

At pH_C 3.5, the pentamer coordinates 16 hydroxide ligands in average, and 17 at pH_C > 3.7: $Th_5(OH)_{17}^{3+}$. This finding agrees with solubility data: According to the solubility curve for amorphous Th hydroxide close to pH_C 4, $d\log[Th]_{tot}/d(-\log[H^+]) = -3 \ldots -4$ (Fig.1), the most abundant species must be threefold charged, for dilute solutions this is the monomer $Th(OH)^{3+}$ in more concentrated samples $Th_5(OH)_{17}^{3+}$. In addition, the total charge of q=3 of (5,17) is similar to q=4 of the predicted tetramer (4,12) and the hydroxide to metal ratios are y/x = 3.4 (5,17), and y/x =3.0 (4,12), respectively.

XAFS measurements

Th L3-edge (16.3 keV) XAFS measurements of selected samples are performed at the INE-Beamline with the same sample solutions parallel to or immediately following ESI-TOF investigations. Spectra are recorded in fluorescence yield detection mode using the 5-pixel solid state Ge detector recently upgraded with a fully digital data acquisition system (cf. section 6.1). XAFS data analysis is based on standard procedures implemented in *autobk* and *feffit* using scattering functions derived from FEFF8.2 [17]. Here we show exemplarily results obtained for two samples: $[Th(IV)]_{tot}=7.0\times10^{-4}$M at pH_C 3.67 and $[Th(IV)]_{tot}=1.6\times10^{-3}$M at pH_C 3.49. The Th(IV) species distribution measured by ESI-TOF indicates the presence of ~43% pentamers ($Th_5(OH)_{17}^{3+}$), ~36% $Th(OH)^{3+}$ and ~14% $Th(OH)_2^{2+}$ in the former and ~71% pentamers ($Th_5(OH)_{17}^{3+}$), ~16% $Th(OH)^{3+}$ and ~9% $Th(OH)_2^{2+}$ in the latter sample solution. EXAFS fit parameters for these samples are summarized in Tab.1; R- and backtransformed k-space data and best fit results for the sample with $[Th(IV)]_{tot}=7.0\times10^{-4}$M are shown in section 6.1 covering the INE-Beamline in this report.

Table 1: *EXAFS fit parameters for Th samples described in the text.*

$[Th]_{tot}$	shell	R [Å]	CN	σ^2	ΔE_0[eV]	*r-fact*
0.68 mM	O1	2.40	3.8	0.0020	8.9	0.03
	O2	2.55	3.4	0.0020	8.9	
	Th	3.87	1.7	0.0061	5.2	
16 mM	O	2.48	9.2	0.0128	8.1	0.03
	Th	3.94	3.0	0.0091	8.6	

In both cases Th absorbers are surrounded by a first shell of oxygen neighbors and a clearly visible second shell of Th backscatterers. We observe only a single Th-Th distance at around 3.9 Å. The Th-Th coordination number is significantly reduced for the lower concentrated sample (1.7) compared to the sample with higher Th concentration (3.0). This trend is in good agreement with ESI-TOF species distribution results. Based on a pyramidal Th arrangement in the polymers one predicts an average coordination number of 1.3 in a sample consisting of ~40% pentamers and ~60% monomers (i.e., the sum of aquo ions and monomeric hydrolysis products) and 3.2 in a sample consisting of ~70% pentamers and 30 % monomers. The splitting of the next neighbor oxygen shell in the sample with lower Th concentration indicates the different environments of Th species. Thorium is predominantly coordinated by water in the monomers and by bridging or terminal hydroxyl groups in the pentamers.

Conclusions

The following general trends for Th(IV) hydrolysis and polymerization are observed:

While at high acidity monomeric species account for the majority of $[Th(IV)]_{tot}$ in solution, the fraction of polynuclear hydroxide comple-

xes increases with increasing pH. Close to the limit of solubility for amorphous thorium hydroxide, polymers often dominate the solutions.

The relevance of polymers increases for increasing $[Th(IV)]_{tot}$ concentration. At $[Th(IV)]_{tot} = 6\times10^{-6}$M no significant amount of polymers is observed at any pH that was measured in the present work, for $[Th(IV)]_{tot} > 10^{-4}$M, however, polynuclear species form with increasing pH. In solutions of millimolar Th(IV) concentration the stability field of polymers extends from pH 2 up to the limit of solubility of $Th(OH)_4(am)$.

Pentamers ($Th_5(OH)_y^{20-y}$) were found to dominate the species distribution of acidic Th(IV) solutions over a wide range of concentrations. In contrast to most models, tetramers and hexamers were observed only as minor species or in freshly prepared non-equilibrated solutions.

However, the latter species were introduced in order to fit solubility data and were never proved to exist directly. The present mass spectrometric detection is the first actual observation of Th(IV) complexes in rather dilute solutions and it is most likely possible to model solubility data with a series of pentamers.

The largest polymers measured are the decamer $Th_{10}(OH)_{32}^{8+}$, the undecamer $Th_{11}(OH)_{38}^{6+}$ and the dodecamer $Th_{12}(OH)_{42}^{6+}$. Since their contribution to the total Th(IV) concentration was very minor and since these complexes were observed only for the first few hours after preparation of the samples they are not discussed. Formation of larger polymers eventually culminates in the generation of amorphous $Th(OH)_4$ – like colloids.

One central result of this work is the direct proof that the mean number of hydroxide ligands of Th(IV) complexes increases quasi continuously with increasing pH_C, not only in the case of monomeric species, $Th(OH)_y^{4-y}$, but also in the case of polymers $Th_x(OH)_y^{4x-y}$. The simultaneous presence of three or four different complexes with the same degree of polymerization x (for instance (5,13), (5,14), (5,15), (5,16)) is frequently observed.

This has direct consequences for the understanding of potentiometric data or solubility experiments. It is difficult to obtain reliable equilibrium constants and SIT parameters for such a large number of species and most present models restrict to only a few complexes. For instance, a recent review on Th(IV) hydrolysis [3] models a great manifold of data with high precision including only six polymers. However, one should keep in mind, that, though this model is very successfully applied, it does not reflect the high complexity of the real system and that for an understanding of reactions on a molecular level the exact stoichiometry of the species in solution needs to be known.

References

[1] Johnson, G. L., Toth, L. M., Plutonium(IV) and thorium(IV) hydrous polymer chemistry. ORNL Technical Report TM-6365, (1978).

[2] Wickleder, M., Fourest, B., Dorhout, P., Chapter 3: Thorium. In L. R. Morss, N. M. Edelstein, J. Fuger, J. J. Katz, (Eds), The chemistry of actinide and transactinide elements, vol. 1,. Springer, 3 edition (2006) pp. 117-129.

[3] Rand, M. H., Fuger, J., Grenthe, I., Neck, V., Rai, D. Chemical thermodynamics of thorium., vol. 11 of Chemical Thermodynamics. Elsevier, North-Holland, Amsterdam (2007).

[4] Katz, J. J., Chemistry of the actinide elements. Chapman and Hall., London (1986).

[5] Kim, J. I., Mat. Res. Soc. Bulletin 19 (1994) 47-53.

[6] Johannson, G., Acta Chem. Scand. 22 (1968) 389-398.

[7] Wilson, R. E., Skanthakumar, S., Sigmon, G., Burns, P. C., Soderholm, L., Inorg. Chem. 46 (2007) 2368-2372.

[8] Di Marco, V. B., Bombi, G. G., Mass Spec. Rev. 25 (2006) 347-379.

[9] Moulin, C., Amekraz, B., Hubert, S., Moulin, V., Anal. Chim. Acta 441 (2001) 269-279.

[10] Walther, C., Rothe, J., Fuss, M., Büchner, S., Koltsov, S., Bergmann, T., Anal. Bioanal. Chem. 388 (2007) 409-431.

[11] Wilm, M., Mann, M., Anal. Chem. 68 (1996) 1-8.

[12] Nabivanets, B., Kudritskaya, L., Ukr. Khim. Zh. 30 (1964) 891.

[13] Ryan, J. L., Rai, D., Inorg. Chem. 26 (1987) 4140-4142.

[14] Rai, D., Moore, D. A., Oakes, C. S., Yui, M., Radiochim. Acta 88 (2000) 297-306.

[15] Ekberg, C., Albinsson, Y., Comarmond, M. J., Brown, P. L., J. Sol. Chem. 29 (2000) 63-86.

[16] Walther, C.,Fuss, M., Büchner, S., Radiochim. Acta (in print).

[17] Ankudinov, A.L., Rehr, J.J. Phys. Rev. B 56 (1997) 1712-1728.

6.4 Computational Chemistry

B. Schimmelpfennig, M. Armbruster, R. Polly

Introduction

Computational Chemistry has been established at INE in various research fields covering a broad range of problems and employing appropriate theoretical tools to tackle them. Recently, ab initio ADC(2) calculations on C(1s) →π * have been applied to benzoic systems, here we present results on much larger system to understand the NEXAFS spectra of polyacrylic and humic acid. Interactions at the corundum/water interface are studied at INE with various experimental methods. DFT calculations on Al/O/H-clusters supported the interpretation of SFG-results on the aluminol groups at the surface but also of coordinated lanthanide ions and small organic molecules, such as butanol. However, for actinide the main and most demanding challenge is to provide a reliable description of the three- and tetravalent hydrated ions with the currently available soft- and hardware.

Metal-Ion Complexation Effects in C 1s-NEXAFS Spectra of Carboxylic Acids

The experimental NEXAFS spectra of humic acids (HA) and polyacrylic acid (PAA) are dominated by the C 1s (COOH)→$\pi_{C=O}$* transition appearing at ~288.4 eV [1]. The carboxyl resonance undergoes distinct changes upon reaction of HA or PAA with higher charged metal cations such as Eu^{3+} or Zr^{4+}. As shown in Fig. 1 for PAA the resonance intensity decreases while at the same time a shoulder at slightly lower energy (~0.5 – 0.8 eV) appears adjacent to the C 1s (COOH)→$\pi_{C=O}$* transition. To corroborate quantum mechanically this complexation effect we consider some simple carboxylic metal complexes as model compounds for the HA and PAA metal complexes. As model compounds, we investigated the hydrated acetate complexes of the type $[M(OOCCH_3)(H_2O)_6]^{(n-1)+}$ and $[M(OOCCH_3)(H_2O)_7]^{(n-1)+}$ with Zr^{4+}, La^{3+}, Eu^{3+} and Ac^{3+}, the uranyl acetate complexes $[UO_2(OOCCH_3)(H_2O)_4]^{2+}$,$[UO_2(OOCCH_3)_2(H_2O)_2]$,as well as La^{3+} complexes with glutaric acid ($HOOC(CH_2)_3COOH$), which is structurally related to PAA. As an example, in Fig. 2 some BP86/def2-TZVPP optimized structures of the model compounds are shown.

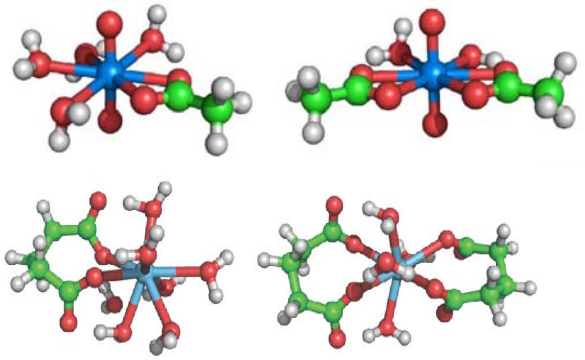

***Fig. 2**: Structures of some metal carboxylate complexes studied. The left corresponds to the 8-fold and the right one to the 9-fold coordinated complex: $[UO_2(OOCCH_3)(H_2O)_4]^{2+}$, $[UO_2(OOCCH_3)_2(H_2O)_2]^{2+}$, $[La(O_2C(CH_2)_3CO_2)(H_2O)_7]$,$[La(O_2C(CH_2)_3CO_2)_2(H_2O)_4]$*

The calculations of the vertical C 1s (COOH)→ $\pi_{C=O}$* excitations energies and transition strengths were done within the ADC(2) method [2]. The ADC (Algebraic Diagrammatic Construction) method is a specific reformulation of the diagrammatic perturbation theory for the polarization propagator. It combines diagonalization of a Hermitean secular matrix with Rayleigh-Schrödinger perturbation theory for the secular matrix elements. The ADC(2) approach contains the core-hole relaxation and the response of the ionic core to the presence of an excited electron consistently through second order in the electronic repulsion. The ADC(2) implementtation in the program package TURBOMOLE with the very useful resolution-of-the-identity (RI) approximation for the two-electron integrals allows the calculation of core-excitation spectra of comparatively large molecules with adequate basis sets. We compare the transition energies of the optimized structures of the model metal complexes mentioned above with the associated free anions (both in the gas phase). All investigated complexes show, independent of the metal center, qualitatively the same behavior: the C 1s (COOH)→$\pi_{C=O}$* transition in the metal complexes appears at lower energies than the transition in the free

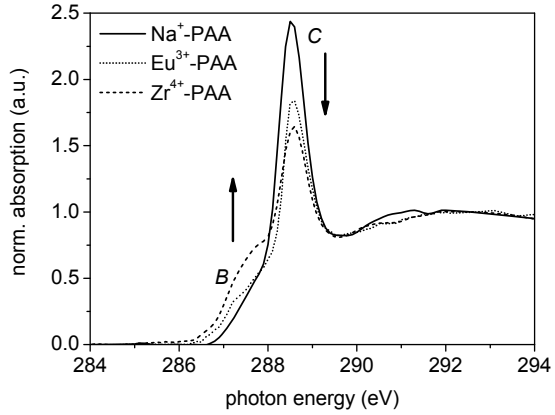

***Fig. 1:** NEXAFS spectra at the C 1s edge of metal complexes of polyacrylic acid with Na^+, Eu^{3+} and Zr^{4+}.*

anions. The shift of the C 1s (COOH)→$\pi_{C=O}$* transition to lower energies lie in the range between 0.33 eV for the uranyl acetates and 1.01 eV for $[Zr(OOCCH_3)(H_2O)_6]^{3+}$. The complexation shift of the other investigated metal species lie between these values. The coordinating water molecules have a minor effect on the energetical position of the C 1s (COOH)→$\pi_{C=O}$* transition: the excitation energies of the 8- and 9-fold coordinated species differ by 0.08eV only. The excitation is therefore very localized despite the fact that the excited state have $\pi_{C=O}$* character, but contains to a lesser extent orbital contributions from the metal center and the water ligands.

The geometry of the organic ligand in the metal complex plays an important role. The comparison of the transition energies for three different alignments of the glutaric anion (free-optimized in the gas phase, with the same structure as in the complex with/without water sphere) with the whole complex $[La(OOC(CH_2)_3COO)(H_2O)_7]^{2+}$ show that the C 1s (COOH)→$\pi_{C=O}$* transition shift comes from the geometry of the organic ligand in the complex. The influence of the water ligand shell is small. The remaining fraction of the energy shift is due to the electronic structure of the metal cation and the distance between the carbonyl C atom and the metal center.

For consistency a different basis set, the cc-pwCVTZ basis, which is especially constructed for core excitations, is compared for the La and Ac acetates with the def2-TZVPP basis set. The differences in the transition energy (0.01 eV) are small and therefore negligible. We conclude the def2-TZVPP basis is an adequate basis set for the study of core excitations of metal containing systems. Based on this quantum chemical investigation the experimentally observed complexation effect can be interpreted as associated ligand structure and metal cation electronic changes.

Theoretical investigation of the interaction of the corundum (0001) surface in contact with water, organic substances and metal ions

Interaction of water with the corundum (0001) surface: These calculations are aimed to assist an experimental effort understanding the structure of the corundum surface in contact with water. Sum-frequency spectroscopy experiments determines the orientations (tilt angles) and vibrational frequencies of the surface OH groups. In our calculations we focused on these experimental observables. We performed a theoretical study employing the cluster model for the surface using different ab initio methods (MP2, CCSD(T)) along with Density functional theory (DFT). The clusters are Al_4O_8+H_2O, $Al_7O_{12}H_3$, $Al_{12}O_{22}H_6$, $Al_{21}O_{38}H_{12}$ and $Al_{31}O_{60}H_{21}$. At the smaller clusters the DFT results were assessed with highly accurate CCSD(T) and MP2 calculations. With this benchmark study we established that the results obtained with DFT agree very well with the ab initio methods for this class of systems. Accordingly we were safely able to proceed with DFT for the larger clusters.

The results of this study were used to simulate the experimental spectra [3]. The excellent agreement of the simulated spectra with the measured spectra provides a complete independent theoretical proof of our model of the corundum (0001) surface in contact with water (Fig. 3).

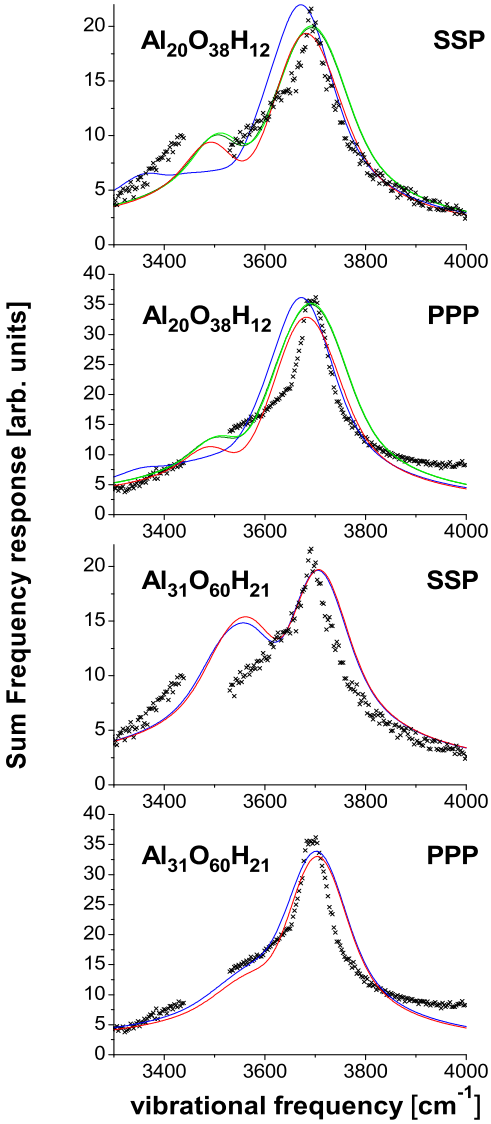

Fig 3: *Simulation of the sum frequency spectra of the OH- vibration at the corundum (001) surface by various DFT / ab initio calculations of Al_2O_3 clusters.*

A further point of this work was the determination of the average distance of the water molecules to the surface. Eng et al. experimentally

determined this distance to be 230 pm (bulk water: 275 pm). If we use one water layer (7 water molecules) on top of the surface we get an average distance of 166 pm, which is much to short. Introducing a second layer of water (18 water molecules) brings the average distance to 248 pm which is much closer to the experimental result. Thus we were able to establish the importance of using more than one layer of water for an accurate description of the interface water/corundum. Another interesting result is that we find different water species adjacent to the surface. Some water molecules gave only one OH bond pointing towards the surface, some two OH bonds (see Fig. 4).

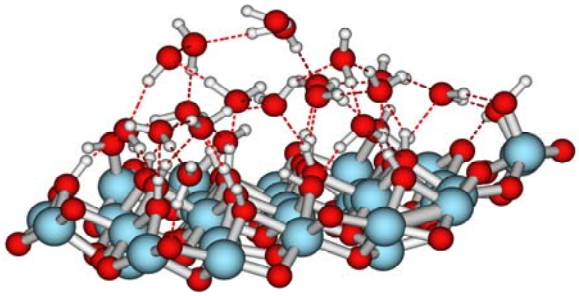

Fig. 4: *$Al_{31}O_{60}H_{21}$ cluster in contact with water to study the interaction of the water with the corundum surface*

Interaction of lanthanides and actinide ions with the corundum (0001) surface: In this study we determined the arrangement of hydrated La^{3+}, Eu^{3+} and Cm^{3+} on the corundum surface. This is of main relevance for the research on nuclear waste disposals. Information of the interaction of the radionuclides with the surface provide theoretical insight whether these ions are adsorbed on the surface or remain in the bulk water. For this task we covered the cluster with 12 water molecules and added one ion. In bulk water the ions are nine fold coordinated, thus surrounded by nine water molecules. As shown in Fig. 5, upon adsorption on the surface the number of neighbouring water molecules is reduced to six.

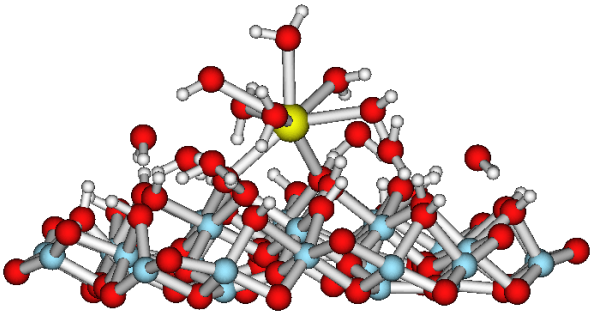

Fig. 5: *$Al_{31}O_{60}H_{21}$ cluster in contact with water and Ln^{3+} to study the interaction with the corundum surface in aqueous solution*

Interaction of organic substances with the corundum (0001) surface: We studied the interaction of simple aliphatic alcohols with the corundum surface. For this task we used the largest cluster ($Al_{31}O_{60}H_{21}$) and added methanol, ethanol, propanol and butanol on top of this cluster. In this way gain a systematic overview of the bonding of these alcohols with the surface. As shown for butanol in Fig. 6, the derived equilibrium structure shows the expected structure with the OH group of the alcohols pointing towards the surface. This determines the slope of the whole C-H chain towards the surface. The slope angle of butanol determined in our calculations agrees excellently with the experiment. In a further step we placed up to 2 butanol molecules on the surface, hence, providing a realistic model for the interaction of the butanol with the surface.

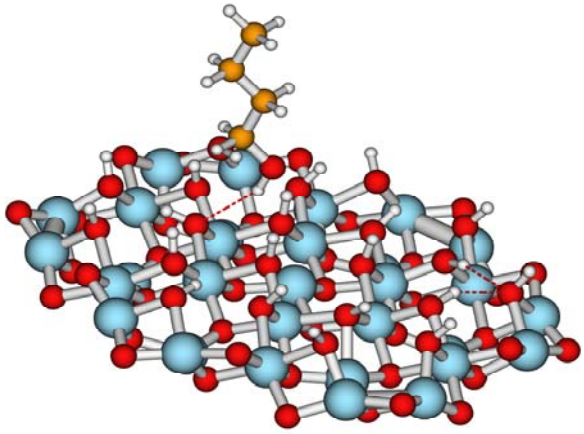

Fig. 6: *$Al_{31}O_{60}H_{21}$ cluster in contact with butanol to study the interaction with the corundum surface in aqueous solution*

Complexation and Spectroscopy of An(IV) ions in aqueous solution

The coordination and structure of actinide(IV) ions in the aqueous face, sometimes as polynuclear species, is still a challenge for computational chemistry. We were investigating possible conformations of Th(IV)-oxo-hydroxo species in solution together with EXAFS studies by J. Rothe [4] and mass-spectrometry by C. Walther [5]. The combined experimental data gives clear indication of a pentamer species, with Th-Th bond distances of approx. 390 pm, however, no immediate structure model could be deduced from the data. An extensive literature study as well as an initial guess of a tetramer ring of a structural element suggested a pyramidal structure as a likely candidate, however, DFT calculations at BP86 DFT-level, using a small-core pseudo-potential on Th and basis sets with triple-zeta plus polarization

quality (TZVP) employing the TURBOMOLE software package, revealed Th-Th distances of typically 360-365 pm, which were far to short compared to experimental data. Even taking various error sources into account, e.g., insufficient treatment of solvent effects, deficiencies of the employed functional, such a pyramidal structure could be ruled out. Other potential structures are under investigation.

A second study is ongoing with C. Marquardt (INE) and V. Vallet (Lille / France) on the coordination and fluorescence spectroscopy of Pa(IV) in aqueous solution and changes on complexation with hydroxide or fluoride ions. This system is especially interesting for a theoretical study as, with just one unpaired electron it allows to apply a wide selection of accurate methods for investigating excited states. An initial DFT study using B3LYP, basis sets of TZVP quality, and a small-core PP on Pa in combination with a dielectric continuum approach to describe solvent effects (COSMO), revealed Pa(IV) to be coordinated to nine water molecules with the eight-coordinated structure energetically close-by. Upon replacing water with fluoride or hydroxide, the much shorter bonds to these ligands, lead to a lack of space in the first coordination sphere and by increasing the number of non-water ligands, the complexes show a strong tendency to push water into the second coordination sphere. Our joint study revealed the coordination number to be reduced to seven or even six, when three hydroxides or fluorides were attached to the metal center. Using the structures obtained in the DFT-study, investigations are ongoing to describe and rationalise the effects of changed coordination on the character and position of the excited states including spin-orbit effects. Preliminary results reveal strong ligand-field effects on the 6d-manifold and the 7s-like excited state and even low-lying charge-transfer states have been observed in this theoretical study. Despite the still preliminary character of the results, the current state of the project indicates a surprisingly rich and unexpected interaction of effects such as ligand-field splitting and spin-orbit coupling in such a comparably simple system.

Actinide(III)-aquo-triflates

P. Lindqvist-Reis and co-workers determined recently XRD-structures of An(III)$(H_2O)_9$ triflate crystals (An = Pu, Am and Cm) [6]. Looking at the possibility to describe these complexes by a cluster model, it turned out that comparably large clusters such as $(M(III)_3(H_2O)_9)_3(triflate)_9$ are necessary to describe the central unit and the H-bridge bonding between triflates adequately. This local minimum structure of the cluster, shown in Fig. 7, reproduces the experimental structure with sufficient accuracy to deduce vibrational frequencies of the first hydration shell. Especially for Cm(III), where totally 21 unpaired electrons need to be treated, we found a compromise between accuracy and computer time by replacing the two outer metal centers with La(III), for which a computational less demanding approximation can be used. This project is still ongoing and we will elucidate the errors of approximation the An(III) ions using f-in-core pseudo potentials [7]. Despite the technical uncertainties discussed above, a cluster ansatz for these crystals looks promising for investigations using quantum chemical methods.

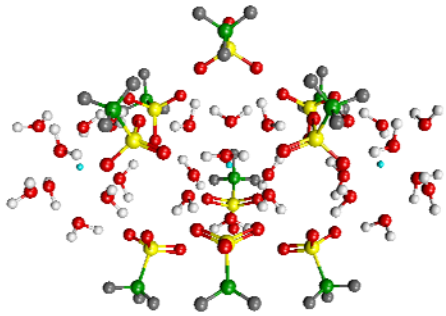

Fig. 7: *DFT-optimised structure of a Cm(III) $(H_2O)_9$ triflate model with three triflate bridged Cm-aquo units.*

The Theoretical Userlab (ThUL) in the NoE ACTINET

INE coordinates the Theoretical Userlab (ThUL) in the European Network of Excellence ACTINET and supports there the interaction between theory and experiment and gives specific emphasis to training and education of students from theory and experiment in state-of-the-art computational tools in actinide sciences. The activities in 2007 comprised support and presentation of the ThUL at the REHE 2007 conference, co-organising and supporting the ACTINET workshop “How can we improve coupling theoretical chemistry with X-ray absorption spectroscopy?” in Avignon, one school dedicated to solid states in Cadarache and supporting the international Helsinki Winter School in Finland with the leading experts in experimental and theoretical actinide sciences. At all these events the ThUL promoted its activities and those of ACTINET in general.

References

[1] Plaschke, M., Rothe, J., Altmaier, M., Denecke, M.A., Fanghänel, Th., J. Electron Spectrosc. Relat. Phenom. 135 (2004) 53.

[2] Baldea, I., Schimmelpfennig, B., Plaschke, M., Rothe, J., Schirmer, J., Trofimov, A.B., Fanghänel, Th., J. Electron Spectrosc. Relat. Phenom. 154 (2007) 109.

[3] Polly, R., Flörsheimer, M., Kruse, K., Abdelmonem, A., Schimmelpfennig, B., Klenze, R., Fanghänel, Th., 11th Internat. Conf. on the Chemistry and Migration Behaviour of Actinides and Fission Products in the Geosphere, Migration´07, Book of Abstracts A5-6, p 267

[4] Brendebach, B., Altmaier, M., Rothe, J., Neck, V., Denecke, M.A., 11th Internat. Conf. on the Chemistry and Migration Behaviour of Actinides and Fission Products in the Geosphere, Migration´07, Book of Abstracts, PA3-23, p 193

[5] Walther, C., Fuss, M., Rothe, J., Büchner S., Geckeis, H., 11th Internat. Conf. on the Chemistry and Migration Behaviour of Actinides and Fission Products in the Geosphere, Migration´07, Book of Abstracts, A7-3, p 158

[6] Lindqvist-Reis, P., Apostolidis, C., Rebizant, J., Morgenstern, A., Klenze, R., Walter, O., Fanghänel, Th., Haire, R.G., Angew. Chem. Int. Ed. 46, 919-922 (2007).

[7] Wiebke, J., Moritz, A., Cao, X., Dolg, M., Phys. Chem. Chem. Phys. 9, 459–465 (2007)

7. Separation of long-lived Minor Actinides

A. Geist, P.J. Panak, S. Trumm, U. Müllich

Introduction

The separation of plutonium and the minor actinides (neptunium, Np; americium, Am; curium, Cm) from spent nuclear fuels and their subsequent transmutation by nuclear fission in advanced reactors could significantly reduce the long-term radiotoxicity of the highly active waste to be stored in a final repository [1]. This is the so-called Partitioning & Transmutation strategy [2]. The required chemical separations can be achieved by hydrometallurgical or pyrometallurgical processing [3, 4].

We study two hydrometallurgical (i.e., based on liquid-liquid extraction) separations processes, in the frame of the EC Integrated Project, EUROPART [5], and a joint FZK-INE/Université de Liège ACTINET project [6]:

1. The DIAMEX process, which is the co-extraction of Am(III), Cm(III), and the lanthanides (LnIII) from the PUREX raffinate solution.

2. The SANEX process, involving separation of Am(III) and Cm(III) from the chemically similar lanthanides, from the DIAMEX product solution.

Whereas the DIAMEX process is considered mature, the SANEX process is still under development. This is primarily to the fact that SANEX extracting agents developed so far all have their shortcomings with respect to stability, solubility, and kinetics. Thus, there is a need for improved extracting agents. To move ahead from the usual “cook and look” strategy, a fundamental understanding of the chemistry governing the selectivity of nitrogen (N)-donor extracting agents is required.

However, the separation chemistry involved in the SANEX process is not understood from a fundamental point of view: Why do N-donor extracting agents preferentially extract Am(III) and Cm(III) over the lanthanides, in spite of their chemical similarity? Finding answers to this question covers a large part of our R&D effort. To this, we study the complex formation of trivalent actinides (An(III)) and lanthanides with N-donor ligands such as bis-triazinyl-pyridines (BTP, Fig. 1) and bis-triazinyl-bipyridyls (BTBP, Fig. 2). Furthermore we work on the synthesis of improved N-donor ligands, and studies related to DIAMEX and SANEX process development.

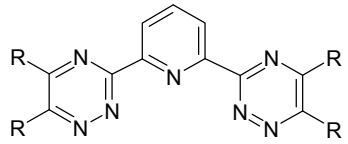

***Fig. 1:**. Bis-triazinyl-pyridines (BTP).*

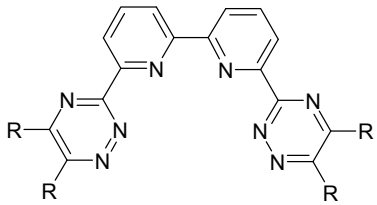

***Fig. 2:** Bis-triazinyl-bipyridyls (BTBP).*

BTP: An(III) and Ln(III) Distribution Data

For the interpretation of EXAFS and TRLFS results on An(III) and Ln(III) complexation with *n*-Pr-BTP (Fig. 1, R = *n*-C_3H_7) [7, 8], a correlation with liquid-liquid distribution data is desirable. Thus, the extraction of Am(III), Cm(III), and Ln(III) (Ln = Y, La – Lu except Pm) from nitric acid into *n*-Pr-BTP dissolved in kerosene/1-octanol mixture was studied.

Fig. 3 shows the distribution ratios for An(III) and Ln(III) at given experimental conditions. First of all, the large selectivity for An(III) over Ln(III) is evident, with the smallest separation factor, $SF_{Am(III)/Ho(III)}$ = 9, and the largest, $SF_{Cm(III)/La(III)} > 10^5$.

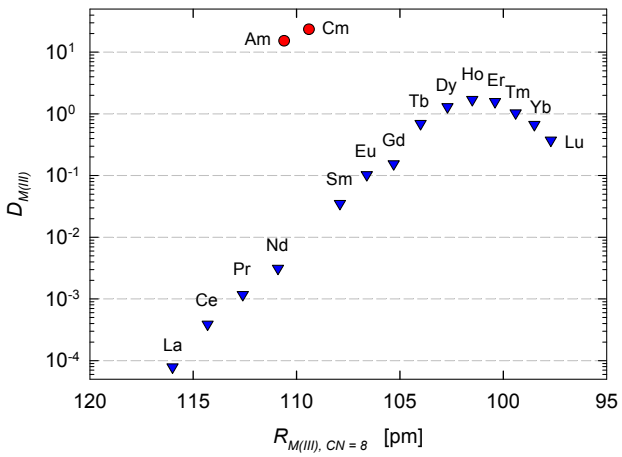

***Fig. 3.** Distribution ratios as function of the ionic radii for the extraction of An(III) and Ln(III) from 1 M HNO_3 into 40 mM n-Pr-BTP in kerosene/1-octanol.*

The extractability of Ln(III) increases steeply with atomic number up to Ho(III), followed by a slight decrease up to Lu(III). This decrease may be due to a misfit between the size of the N-donor cavity and the ionic radii of the heaviest Ln(III). This assumption is supported by EXAFS results [8]: the difference between M(III)–N bond length and ionic radius is larger with Lu(III) (namely 1.67 Å) than with Am(III), Cm(III), Eu(III), and Gd(III) (1.61 – 1.62 Å).

It is interesting to compare the behaviour of Am(III) and Eu(III) with that of Cm(III) and Gd(III): In both cases, the selectivity is $SF_{An(III)/Ln(III)}$ = 150. We need to find out whether or not this "parallel" behaviour also holds for other An(III)/Ln(III) pairs. Thus, this investigation is currently expanded to include further An(III).

BTBP: TRLFS Studies

Objective of the project is to investigate the selectivity of N-donor ligands such as BTP and BTBP for the extraction of trivalent actinides over lanthanides. Previous studies from our group indicate that the structural differences (as from different M(III)–N bond lengths) found between $[U(BTP)_3]^{3+}$ and $[Ce(BTP)_3]^{3+}$ do not apply to the respective Am(III), Cm(III), Eu(III), and Gd(III) complexes. Whereas the shortened bond lengths in the $[U(BTP)_3]^{3+}$ complex are ascribed to a higher degree of covalence in the U(III)–N bond, more subtle differences seem to be causal for e.g., BTP's Am(III)/Eu(III) selectivity. Work is performed comparing selected BTBPs' complex formation and extracting behaviour towards trivalent actinides and lanthanides. The EXAFS studies are complemented by liquid-liquid extraction (cf. above) and TRLFS studies. The following TRLFS investigations were made:

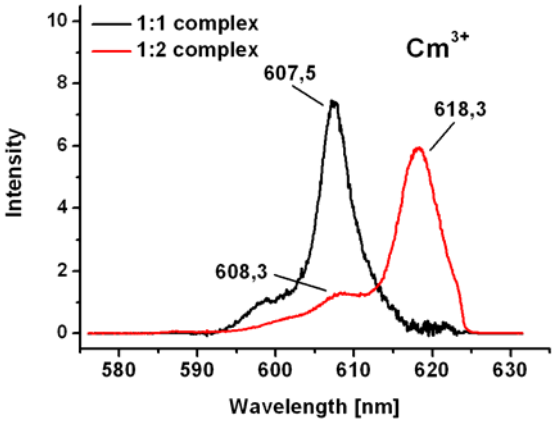

Fig. 4: *Fluorescence emission spectra of the 1:1 and 1:2 Cm(III)-BTBP complexes.*

The complex formation of five different BTBPs with Cm(III) and Eu(III) in 1-octanol was studied by TRLFS. Fig. 4 shows the fluorescence emission spectra of the 1:1 and 1:2 Cm(III) complexes, $[Cm(BTBP)]^{3+}$ and $[Cm(BTBP)_2]^{3+}$. In any case, a higher BTBP concentration is required to form the Eu(III) 1:2 complexes than to form the corresponding Cm(III) 1:2 complexes (the 1:2 complexes are the ones relevant under conditions applying to liquid-liquid extraction).

There is a pronounced anion effect; going from nitrate to perchlorate results in a stabilisation of the 1:2 complexes. This effect is also observed in the complex formation kinetics: with perchlorate as counter-ion; formation of the 1:2 complexes shows much higher rate constants, probably due to a destabilisation of the 1:1 complexes. This is remarkable as the anion concentrations present in the organic solutions are very low (< 10^{-4} M).

Data is currently being completed to determine complex formation constants and enthalpy and entropy data.

BTBP: Equilibrium and Kinetic Studies

$CyMe_4$-BTBP (6,6'-bis(5,5,8,8-tetramethyl-5,6,7,8-tetrahydrobenzo[1,2,4]triazin-3-yl)-[2,2']-bi-pyridine, Fig. 5) is the current European reference molecule for SANEX (i.e., An(IIII)/Ln(III) separation) process development [9].

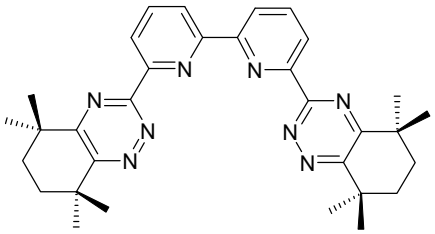

Fig. 5 *$CyMe_4$-BTBP.*

To support flow-sheet and process development, an equilibrium model was developed to calculate the extraction of An(III) and Ln(III) from nitric acid into $CyMe_4$-BTBP. It takes into account the extraction of metal nitrates and nitric acid by $CyMe_4$-BTBP, and the extraction of nitric acid by the diluent, 1-octanol:

$$M^{3+} + 3\ NO_3^- + 2\ BTBP_{org} = M(NO_3)_3(BTBP)_{2,org}$$

$$H^+ + NO_3^- + BTBP_{org} = HNO_3 \cdot BTBP_{org}$$

$$H^+ + NO_3^- + octanol = HNO_3 \cdot octanol_{org}$$

In the aqueous phase, activities calculated with SIT [10] are used, whereas concentrations are used in the organic phase.

As shown in Fig. 6, the calculations describe well the influence of both nitric acid and BTBP concentrations on the Am(III) distribution ratio, as well as the effect of loading with Eu(III).

The kinetics for the extraction of An(III) and Ln(III) from nitric acid into solutions of $CyMe_4$-BTBP is rather slow. To speed up kinetics, a second extracting agent (an alkylated malonamide) is added [9], presumably acting as a phase transfer catalyst.

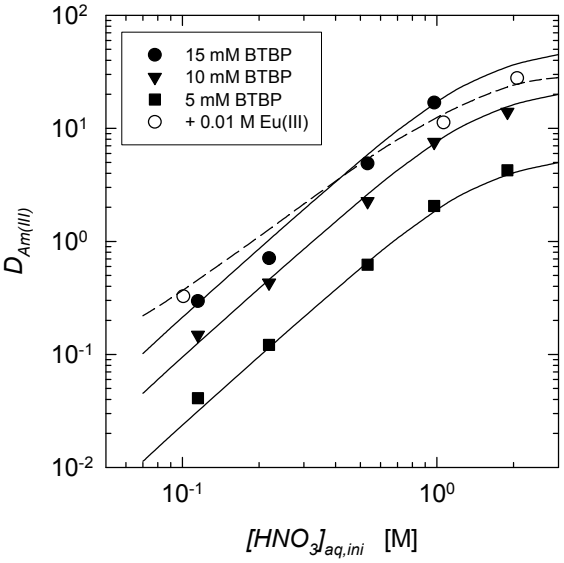

Fig. 6. *Extraction of Am(III) from HNO_3 into $CyMe_4$-BTBP in 1-octanol. Symbols, experiment. Lines, calculated.*

Besides the expected effect (i.e., increasing the rate of the chemical reaction), the phase transfer catalyst also causes the formation of smaller droplets in a shaking tube. To study the kinetic effect in the absence of such a hydrodynamic effect, Am(III) was extracted from nitric acid into solutions of $CyMe_4$-BTBP with or without a phase transfer catalyst, using a miniature hollow fibre module [11, 12] as phase contacting device. Thus, a known and constant specific interfacial area and well-described hydrodynamics are employed, and the rate of the chemical reaction is accessible.

The forward reaction rate constant is adjusted to fit the calculated Am(III) effluent concentrations to experimental data. Indeed, the rate constant was larger by a factor of three with the phase transfer catalyst as compared to without it. A more detailed kinetic study will follow.

New N-Donor Ligands

A series of new N-donor ligands similar to BTPs were synthesised and tested for their ability to selectively extract An(III) from nitric acid. Indeed, some of the compounds are able to extract Am(III) with favourable distribution ratio and with good selectivity over Ln(III) from up to 0.5 M nitric acid. The compounds exhibit rapid extraction kinetics and good stability versus nitric acid, thus showing improved behaviour over BTPs or BTBPs (depending on the alkyl moieties *R*, cf. Fig. 1 and Fig. 2, these are either chemically instable or have very slow kinetics). Structures of the compounds and details will be presented in a forthcoming publication.

References

[1] Magill, J., Berthou, V., Haas, D., Galy, J., Schenkel, R., Wiese, H.-W., Heusener, G., Thommasi, J., Youinou, G., Nucl. Energy 42 (2003) 263-277.

[2] Actinide and fission product partitioning and transmutation, status and assessment report. OECD-NEA (1999).

[3] Madic, C., Boullis, B., Baron, P., Testard, F., Hudson, M.J., Liljenzin, J.-O., Christiansen, B., Ferrando, M., Facchini, F., Geist, A., Modolo, G., Espartero, A.G., De Mendoza, J., J. Alloys Comp. 2007, 444-445, 23-27.

[4] Geist, A., Malmbeck, R., Separation of actinides in the partitioning & transmutation context. Proc. Eighth International Topical Meeting on Nuclear Applications and Utilization of Accelerators (AccApp'07), Pocatello, Idaho, U.S.A., July 30 – August 2, 2007, American Nuclear Society, LaGrange Park, Illinois 60526, USA.

[5] EUROpean research programme for the PARTitioning of minor actinides from high active wastes issuing the reprocessing of spent nuclear fuels (contract no. FI6W-CT-2003-508854).

[6] ACTINET JP 06-14, Investigations of the coordination and electronic structure of An(III)/ Ln(III) complexed with N-donor ligands.

[7] Denecke, M.A., Rossberg, A., Panak, P.J., Weigl, M., Schimmelpfennig, B., Geist, A., Inorg. Chem. 44 (2005) 8418-8425.

[8] Denecke, M.A., Panak, P.J., Burdet, F., Weigl, M., Geist, A., Klenze, R., Mazzanti, M., Gompper, K., C. R. Chimie 10 (2007) 872-882.

[9] Geist, A., Hill, C., Modolo, G., Foreman, M.R.S., Weigl, M., Gompper, K., Hudson, M.J., Madic, C., Solvent Extr. Ion Exch. 2006, 24 (4), 463-483.

[10] Ciavatta, L., Ann. Chim. 70 (Rome) (1980) 551.

[11] Geist, A., Weigl, M., Gompper, K., Radiochim. Acta 93 (2005) 197-202.

[12] Geist, A., Gompper, K., Radiochim. Acta 2008, 96, 211-218.

8. Vitrification of High-Level Radioactive Liquid Waste

W. Grünewald, J. Knobloch, W. Tobie, G. Roth, A. Salimi, K.H. Weiß, H. Braun, S. Weisenburger, M. Nesovic

Introduction

Vitrification is applied world wide as an appropriate technology for the solidification of high-level liquid waste for a subsequent final disposal. The special melter design developed at INE for liquid waste rich in noble metals and the related technology has been realized in the Karlsruhe Vitrification Plant (VEK) at the campus of the former Karlsruhe Pilot Reprocessing Plant (WAK). Hot operation is foreseen to start within the next months. In addition, research activities focus on waste glass development with enhanced sulfur incorporation capacity. They are performed within the envisaged Vitrification Project China (VPC). Finally, activities within the framework of an engineering assistance agreement between FZK and the Japanese Company IHI/Yokohama on the further development of vitrification technology are reported.

VEK Project

In 2007 the HLLW vitrification plant VEK has passed the cold commissioning procedure which has been finalized by performance of a long-term (3 months) integral plant operation (cold test). The cold test has been required to accomplish the goals laid down in the first partial operation license. During this test about 17 m^3 of HLLW simulate were processed and the produced simulated waste glass poured into 32 stainless steel canisters. The positive results of the test form the basis of granting the license for hot operation.

Goals, boundary conditions and performance of the cold test

Precondition of the start of the cold test operation was the completion of all function tests for single components (e.g. glass melter) and systems (e.g. wet off-gas cleaning). This requirement did not only comprehend process-related installations but also other areas like process control system or remote handling equipment.

In the focus of the cold test were:

- Long-term demonstration of the vitrification operation in accordance with the established regulations
- Verification of the operational manuals
- Proving of the procedure of sampling and chemical analysis
- Demonstration of canister transfer, treatment and handling procedure to meet product requirements
- Education and training of operational staff

Overall purpose of the cold test was the demonstration of the vitrification operation under conditions close to that of the hot operation. Control of the whole plant operation had to be carried out by means of the central process control system, consisting of a conventional and a safety system. The requirements included the conduction and control of the process according to the operational manuals which had been approved by the regulatory body. All routine remote operations as well as possibly occurring maintenance or intervention actions had to be exclusively carried out by the installed remote handling equipment. Manual operations are routinely necessary to carry out all steps of glass canister handling and treatment. Performance of the cold test included to focus on sustaining stable process conditions and operational safety. Another main goal was the verification of the control strategy to produce a specified glass product according to the quality assurance program. The control sequence from sampling the HLLW until determination and control of the material stream of HLLW simulate and glass frit had to be checked.

HLLW simulate

The simulated waste solution used for the test had been composed according to the available reference composition data of the genuine HLLW (see Table 1). The radioactive constituents which do not exist in a stable isotope form (e.g. Tc, actinides) were replaced by suitable elements on an oxide mass by mass basis. The noble metals elements (Ru, Rh, and Pd) were omitted and also substituted. The suitability of the melter design with respect to processing noble metals bearing HLLW simulate had been demonstrated before in extensive long-term testing in INE's 1:1 scale prototype facility [1].

Results of the cold test operation

Cold test operation was carried out from April 3 to July 12. The operational period was divided into three phases (see Table 2). The intermediate idling phases were intentionally induced

and not caused by any occurring problems. The stops served for software modification of the process control system. During the idling phases the glass pool in the melter was kept at temperature of about 950 °C.

Production data

During the cold test totally 17 m^3 of HLLW simulate were processed to 12.7 t of glass product. The glass melt was filled into 32 canisters. The complete duration of the processing period was 77 d. During processing of simulate in all three operation phases no forced interruption of melter feeding was necessary.

Table 1: *Chemical composition of the HLLW simulate used for cold test operation in comparison with that of the genuine waste solution (in terms of oxide residue at 900°C)*

Oxide	Concentration (g/dm^3)	
	HLLW	Simulate
SeO2	0,13	0,13
Rb2O	0,46	0,46
SrO	1,32	1,32
Y2O3	1,04	1,04
ZrO2	5,42	5,42
MoO3	6,57	6,57
TcO3	1,65	–
RuO2	5,03	–
Rh2O3	1,09	–
PdO	2,30	–
Ag2O	0,21	0,21
CdO	0,14	0,14
SnO2	0,12	0,12
Sb2O3	0,02	0,02
TeO2	1,00	1,00
Cs2O	3,79	3,79
BaO	3,81	3,81
La2O3	2,72	13,93
CeO2	5,38	5,38
Pr2O3	2,38	2,38
Nd2O3	8,44	8,44
Pm2O3	0,01	0,00
Sm2O3	1,83	1,83
Eu2O3	0,23	0,23
Gd2O3	0,70	0,70
U3O8	9,69	–
Np2O3	0,60	–
PuO2	0,29	–
Am2O3	0,61	–
Cm2O3	0,03	–
Cr2O3	2,96	2,96
MnO2	0,50	7,18
Fe2O3	10,91	10,91
CoO	–	1,09
NiO	2,02	4,32
CuO	0,04	0,04
ZnO	0,03	0,03
PbO	0,01	0,01
Na2O	32,46	32,46
MgO	0,98	0,98
Al2O3	0,16	0,16
K2O	0,38	0,38
CaO	0,71	0,71
F	0,07	0,07
Cl	0,05	–
P2O5	2,63	2,63
Total	**120,92**	**120,85**

Table 2*: Main production data from long-term cold test operation*

Production parameters	Part 1	Part 2	Part 3	Total
Operation period (2007)	3.4. - 13.5.	29.5. - 28.6.	30.6. - 12.7.	3.4. - 12.7.
Simulate feeding time (d)	39	28,3	9,8	77
Average feed rate (dm^3/h)	10,1	9,9	9,8	10
Vitrified simulate (m^3)	8,67	6,15	2,11	16,93
Mass of glass frit (t)	5,4	3,9	1,4	10,7
Mass of glass product (t)	6,4	4,7	1,6	12,7
Number of glass pourings	64	47	16	127
Number of filled canisters	16	11,75	4	31,75
Average waste glass loading (wt.-%)	16,0	16,0	16,1	16,0

S:\Jahresb\Jahresbericht07\Tab7-1a.xls

Throughout the whole operation period, the melter feed rate met precisely the design feed rate of 10 dm^3/h. The feeding rate vs. operation time is shown in Fig. 1.

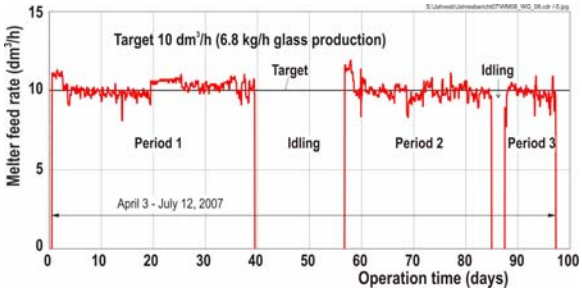

Fig. 1: *Melter feed rate determined during the cold test operation plotted versus operation time*

Process behaviour

Processing of the HLLW simulate proved to be in accordance with the experience gained in the long-term inactive testing. Control of the melter feeding, of the process zone on top of the glass pool (cold cap), of glass pool heating as well as the glass pouring operation was reliable and did never exceed tolerable proc ess conditions. One essential outcome of the test was the extension of the melter underpressure range from 2 to 7 mbar. It was necessary because of the tightness of the melter structure leading to a low inflow rate of leak age air combined with routine and intended gas flow changes in off gas line.

The sophisticated glass pouring system is an essential part of the noble metals-compatible design of the melter. Main requirements for the bottom drain are:safe and reliable function, efficient controllability, noble metals removal and melter emptying. During 127 glass discharges the control of the bottom drain system turned out to be very reliable and the characteristics of the pourings were excellently reproducible. Fig. 2 shows a typical example of a pouring diagram containing the induction power for heating of the metallic glass outlet channel, the cumulative mass of glass in the canister and the glass flow rate deduced form the mass curve by differentiation as function of

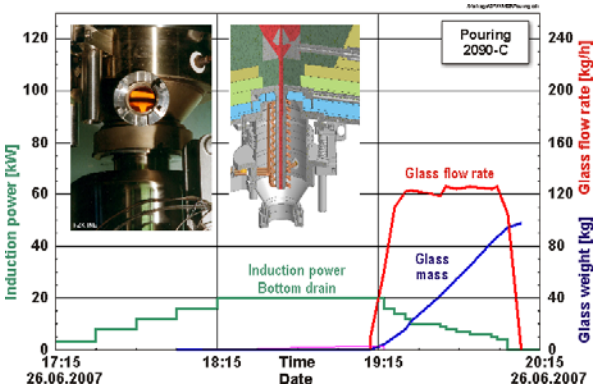

Fig. 2: *Typical glass pouring diagram. Induction power for heating the glass discharge channel, glass pouring rate and weight of glass in the canister as function of time*

time. The diagram shows that the target glass flow rate of 120 kg/h could be maintained accurately.

The retention of noxious materials in the melter and the subsequent off-gas treatment proved to be effective. As design values for cesium a value of 30 had been established, for Strontium a design value of 60 had been specified. Due to the high retention efficiency of the melter, various elements could not be measured in the scrub solution down-stream of the jet scrubber by wet-chemical methods as the values were below the detection limit.

Glass product quality

Application of the control steps to produce a glass within specified ranges showed to be very effective. Basis of the proper glass composition generated in the melter is the control of the material streams introduced into the melter. The mass flow rate of the glass frit is adapted to the mass flow rate (waste oxide residue) of the HLLW simulate. Therefore it is necessary to determine the oxide residue resulting from the waste solution in every batch overtaken from the storage tanks prior to release for vitrification. Fig. 3 shows the results of the oxide residue obtained from samples of the receipt tank. It reveals that in the average the measured values met the target, but a few single measurements showed deviations up to ±10 %.

Fig. 4 shows the results of the waste oxides loading of the glass product. The values are derived from accumulation of the mass of glass frit and HLLW simulate oxides fed into the melter within a feeding cycle period. It covers 10 feeding vessel cycles (9 HLLW batches + 1 batch recycled from the dust scrubber scrub solution). One period is typically about 22 h. It can be seen that the glass loading coincides good with the target value of 16 wt%. The ranges for a tolerable glass were 13 - 19 wt%.

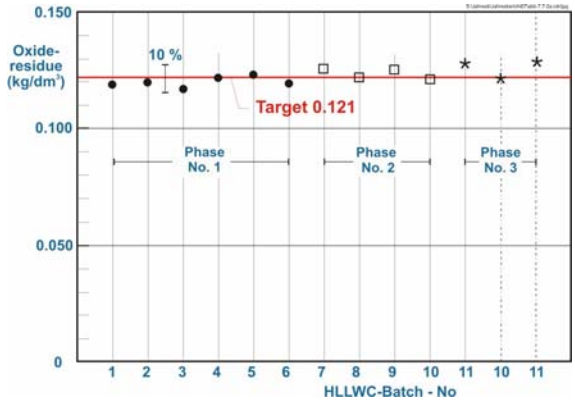

Fig. 3: *Results of oxide residues (900°C/1h) measured from samples taken from the receipt tanks after refillings with HLLW simulate*

Canister treatment

During the cold test operation all filled canisters were transferred into the canister handling cell where they had to undergo the steps of cooling (3-5 days) inside a heat-insulated cooling station, subsequent lid-welding, decontamination by an ultrasonic acidic pool and final water rinsing. Fig. 5 shows the lid-welding of a canister. During this qualified procedure the welding parameters are recorded and compared to the reference data. An additional visual check completes the examination of the welding. After the treatment steps the canisters were stored inside the internal VEK buffer store (capacity 36 canisters). The loading of the canisters from the buffer store into the transport cask had already been demonstrated in a separate program. According to the requirements for acceptance of the glass canisters in the intermediate and later final storage facilities all the treatment steps are documented in the canister life sheet which serves for identification and characterization of each glass canister. This sheet will also contain information about concentration of

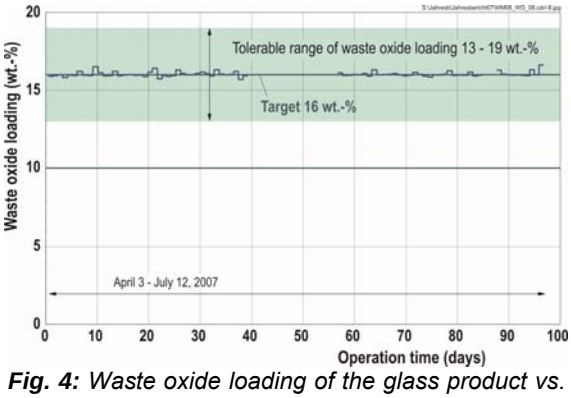

Fig. 4: *Waste oxide loading of the glass product vs. operation time. Values calculated from melter feed streams of HLLW oxides and glass frit*

selected waste constituents, the radioactivity inventory and production features.

Fig. 5: *Lid-welding of glass canister*

Summary and outlook

The performance and results of the long-term cold test operation proved evidence of the suitability of INE's vitrification technology used by VEK to immobilize the HLLW of WAK in glass. Within the core process area no operational, safety or hardware problem arose. The vitrification process proved to be well controllable, the process parameters never showed the tendency to move out of the normal operation status. The glass product composition could be precisely kept at the waste oxide loading target by applying the quality assurance control steps to the melter feed material streams.

The positive results of the cold test operation form the basis for granting the second partial operation license which allows the start of radioactive activities and operation in the VEK plant. After granting the license, preparation for hot operation of the plant connection to the HLLW storage area will be performed. In a first step a short hot test of approximately 1 week duration using diluted HLLW will be carried out to check the radiometric measurement devices and to get information of the radiological status of the hot cells and the plant in general. The test will then immediately be followed by start-up of hot production operation scheduled to last about 1.5 years.

VPC Project

Waste glass development with enhanced sulfur incorporation capacity

According to requirements of the envisaged Vitrification Project China (VPC) the waste glass must be able to incorporate at least 0.9 wt% of sulfate without accumulation of a molten yellow phase on top of the molten glass pool (mainly composed of Na_2SO_4, melting point 884°C). The lab-scale work has been started early 2006 and finished in late 2007 [2]. A glass matrix is now available which has the capacity to incorporate at least 1 wt% of sulfate. The glass matrix contains, in compare-son with former typical chemical compositions, significant amounts of CaO, MgO and BaO, as well as additives of Sb_2O_5 and V_2O_5 on the expense of portions of SiO_2, B_2O_3 and TiO_2. The function of the oxides CaO, MgO and BaO includes the required increase of the glass basicity as a precondition for enhancement of sulfur incorporation into the glass. The additive Sb_2O_5 is used to release additional oxygen during processing during which it is converted to Sb_2O_3 in order to shift the equilibrium in the glass between the sulfate SO_4^{2-} and gaseous SO_3 to the sulfate side. The additive V_2O_5 is used to accelerate the kinetic of dissolution of the sulfate into the glass. As to understand the latter mechanism in detail further work is underway.

The specified quality parameters of the waste glass with 16 wt% waste oxide loading could be achieved including those from Soxhlet test and Product Consistency Test (PCT).

The overall results of the work allow to order the glass frit and VPC simulate and to make the required technical glass formulation test within the basic design period of the VPC project. INE's inactive PVA facility will be used for this purpose with vitrifying approximately 6 m^3 of VPC HLLW simulate.

R+D contract with IHI

Engineering assistance agreement with IHI

An engineering assistance agreement between FZK and the Japanese Company IHI/Yokoha-ma has been established in 2007 dealing with the further development of large-scale LFCM-technology with particular emphasis for pro-cesssing high noble metals bearing HLLW. Two work packages have been carried out in 2007. One covered an evaluation of the cold crucible technology and comparison with the ceramic-lined liquid fed melter technique (LFCM). The other involved the basic and engineering design of a glass level detection device for a large-scale waste glass melter of IHI.

The evaluation of the cold crucible technique has shown that this system is well suitable as long as the liquid waste stream is calcined and the resulting dry powder fed to melter. In

contrast, liquid feeding is less advantageous because of physical constraints. They limit the diameter of the crucible and thus the glass melt surface area. This in turn limits the throughput capacity when liquid feeding is applied. Overcoming of the problem is reported to be underway by an advanced cold crucible design. But it requires induction heating beneath the water-cooled melter bottom which must additionnally be designed for transparency for a high frequency electro-magnetic field. This new technique is not yet fully demonstrated for use in a hot cell environment. The LFCM technique has been favoured in the evaluation. Despite the associated bigger hot cell and the later signify-cantly higher dismantling volume of the melter it provides a substantial number of advantages compared to the cold crucible technique. Nevertheless, each type of LFCM needs care-ful design considerations in respect to process-sing HLLW with high content of noble metals.

The engineering design of a melt level detection device for a large-scale IHI melter has been carried out and based on INE's development and PVA test results obtained in the year 2003. The method is also used in the melter of VEK and has been tested in 2007 during the cold test operation of VEK facility. The engineering work for IHI had to be focused on the adoption of the design to the large-scale melter operated by IHI in the Japanese industrial reprocessing and waste vitrification plant at Rokkasho.

References

[1] W. Grunewald, G. Roth, W. Tobie, K.H. Weiß, Cold demonstration of the vitrification technology in full-scale mock-up facility. Waste Management Symp., (WM00), Tucson, Ariz., Febr. 27–March 2, (2000)

[2] Weisenburger, S., Roth, G., Grünewald, W., Tobie, W., Weiß, K.H., Salimi, A., Hilpp, S., Nesovic, M., „Results of the Waste Glass Development for Vitrification of High-Sulfur, High-Sodium bearing HLLW", Internal Report INE (March 2008) p. 1-35

9. List of Publications

Papers in Books and Peer Reviewed Journals

BAIK, M.H.; YUN, J.I.; BOUBY, M.; HAHN, P.S.; KIM, J.I.
Characterization of aquatic groundwater colloids by a laser-induced breakdown detection and ICP-MS combined with an asymmetric flow field-flow fractionation.
Korean Journal of Chemical Engineering 24 (2007) 723–29

BALDEA, I.; SCHIMMELPFENNIG, B.; PLASCHKE, M.; ROTHE, J.; SCHIRMER, J.; TROFIMOV, A.B.; FANGHÄNEL, T.
C 1s near edge X-ray absorption fine structure (NEXAFS) of substituted benzoic acids. A theoretical and experimental study.
Journal of Electron Spectrosocpy and Related Phenomena 154 (2007) 109–18

BARBOT, C.; BOULOUSSA, O.; SZYMCZAK, W.; PLASCHKE, M.; BUCKAU, G.; DURAND, J.P.; PIERI, J.; KIM, J.I.; GOUDARD, F.
Self-assembled monolayers of aminosilanes chemically bonded onto silicon wafers for immobilization of purified humic acids.
Colloids and Surfaces A 297 (2007) 221–39

BRANDT, H.; BOSBACH, D.; PANAK, P.J.; FANGHÄNEL, T.
Structural incorporation of Cm(III) in trioctahedral smectite hectorite: A time-resolved laser fluorescence spectroscopy (TRLFS) study.
Geochimica et Cosmochimica Acta 71 (2007) 145–54

BRENDEBACH, B.; DARDENNE, K.; DENECKE, M.A.; ROTHE, J.; VITOVA, T.
New developments at the INE-Beamline for actinide research at ANKA.
Nuclear Instr. Methods Phys. Research A 582 (2007) 80–81

BRENDEBACH, B.; ALTMAIER, M.; ROTHE, J.; NECK, V.; DENECKE, M.A.
EXAFS study of aqueous Zr^{IV} and Th^{IV} complexes in alkaline $CaCl_2$ solutions: $Ca_3[Zr(OH)_6]^{4+}$ and $Ca_4[Th(OH)_8]^{4+}$.
Inorganic Chemistry 46 (2007) 6804–810

BRENDEBACH, B.; DENECKE, M.A.; ROTHE, J.; DARDENNE, K.; RÖMER, J.
The INE-Beamline for Actinide Research at ANKA.
in "X-Ray Absorption Fine Structure (XAFS13)", B. Hedman, P. Pianetta (Eds.) Proc. of the 13th Intern. Conf., Stanford (Calif.), July 9–14, 2007, AIP Conference Proceedings Vol. 882, (2007) p. 875–77

BRUNO, J., BOSBACH,D., KULIK, D., NAVROTSKY, A.
CHEMICAL THERMODYNAMICS Vol. 10, Chemical thermodynamics of solid solutions of interest in radioactive waste management: A state-of-the-art report. 266 pages
OECD NEA (F. Mompean, M. Illemassene, J. Perone, Eds.) OECD Publishing, Paris (2007)

DEGUELDRE, C.; KASTORYANO, M.; DARDENNE, K.
Variable incident angle X-ray absorption spectroscopy for the study of zircaloy corrosion layers.
Journal of Nuclear Materials 362 (2007) 316–26

DENECKE, M. A., PANAK, P. J., BURDET, F., WEIGL, M., GEIST, A., KLENZE, R., MAZZANTI, M., GOMPPER, K.
A comparative spectroscopic study of U(III)/Am(III) and Ln(III) complexed with N-donor ligands.
Special Issue "Nuclear Energy and Radiochemistry", Comptes Rendus Chimie 10 (2007) 872–882

DENECKE, M.A.; SOMOGYI, A. ; JANSSENS, K.; SIMON, R. ; DARDENNE, K.; NOSECK, U.
Microanalysis (μ-XRF, μ-XANES and μ-XRD) of a tertiary sediment using synchrotron radiation.
Microscopy Microanal. 13 (2007) 165–72

DENECKE, M.A.; JANSSENS, K.; BRENDEBACH, B.; DE NOLF, W.; FALKENBERG, G.; ROTHE, J.; SIMON, R.; SOMOGYI, A.; VEKEMANS, B.; NOSECK, U.
Confocal μ-XRF, μ-XAFS, and μ-XRD studies of sediment from a nuclear waste disposal natural analogue site and fractured granite following a radiotracer migration experiment.
in "X-Ray Absorption Fine Structure (XAFS13)", B. Hedman, P. Pianetta (Eds.) Proc. of the 13th Intern. Conf., Stanford (Calif.), July 9–14, 2007, AIP Conference Proceedings Vol. 882, (2007) p. 187–89

EINSIEDL, F.; SCHÄFER, T.; NORTHRUP, P.
Combined sulfur K-edge XANES spectroscopy and stable isotope analyses of fulvic acids and groundwater sulfate identify sulfur cycling in a karstic catchment area.
Chemical Geology 238 (2007) 268–76

HOU Z.; WOLTERS R; ROKAHR R.; ZAPF D.; SALZER K. GÜNTHER R.; MINKLEY W.; PUDEWILLS A.; HEEMANN U.; SCHULZE, O.; ZETSCHE F.; HAMPEL A.
Comparison of advanced constitutive models for the mechanical behavior of rock salt-results from a joint research project- II. Numerical modeling of two in situ case studies and comparison,
Proc. of the 6th Conference on Mechanical Behavior of Salt, Hannover, Germany 22–25 May 2007, in "Mechanical Behavior of Salt – Understanding the THMC Processes in Rock Salt"
M. Wallner, K.-H.Lux, W. Minkley, H.R. Hardy, H.R. Hardy, Jr. (Eds.), Taylor & Francis Group, London (2007), p. 89–98

JUNG, E.C.; YUN, J.I.; KIM, J.I.; BOUBY, M.; GECKEIS, H.; PARK, Y.J.; PARK, K.K.; FANGHÄNEL, T.; KIM, W.H.
Measurement of bimodal size distribution of nanoparticles by using the spatial distribution of laser-induced plasma.
Applied Physics B 87 (2007) 497–502

KHELASHVILI, G.; BEHRENS, S.; HINSCH, A.; HABICHT, W.; SCHILD, D.; EICHHÖFER, A. ; SASTRAWAN, R.; SKUPIEN, K.; DINJUS, E.; BÖNNEMANN, H.
Preparation and characterisation of low platinum loaded Pt: SnO_2 electrocatalytic films for screen printed cell counter electrode.
Thin Solid Films 515 (2007) 4074–79

KIENZLER,B., METZ,V., LÜTZENKIERCHEN, J., KORTHAUS, E., FANGHÄNEL, T.
Geochemically Based Safety Assessments.
Journal of Nuclear Science and Technology 44 (2007) 470–76

KIENZLER,B., BUCKAU, G.
IP FUNMIG: The European Far-Field Project
Atomwirtschaft 52 (2007) 408–11

KIM, J. I. and WALTHER, C.
Laser-induced breakdown detection.
in J. Lead and K. Wilkinson: "Environmental colloids and particles: Behaviour, separation and characterisation", John Wiley & Sons Ltd, 2007, p. 555–612

KIM, M.A.; PANAK, P.J.; BREBAN, D.C.; PRIEMYSHEV, A.; YUN, J.I.; MANSEL, A.; KIM, J.I.
Interaction of actinides(III) with aluminosilicate colloids, Part IV.: Influence of humic acid.
Colloids and Surfaces A 296 (2007) 206–15

KOLOKASSIDOU, C.; PASHALIDIS, I.; COSTA, C.N.; EFSTATHIOU, A.M.; BUCKAU, G.
Thermal stability of solid and aqueous solutions of humic acid.
Thermochimica Acta 454 (2007) 78–83

KUNZE, S.
Entwicklung von Dekontaminationsmitteln bis zum jetzigen Stand.
Atomwirtschaft 52 (2007) 429–31

LINDQVIST-REIS, P.; APOSTOLIDIS, C.; REBIZANT, J.; MORGENSTERN, A.; KLENZE, R.; WALTER, O.; FANGHÄNEL, T.; HAIRE, R. G.
The structures and optical spectra of hydrated transplutonium ions in the solid state and in solution.
Angew. Chem. Int. Ed. 46 (2007) 919–22, Angew. Chem. 119 (2007) 937–940

LOIDA, A.; KIENZLER, B.; AND METZ, V.
Alteration behavior of high burnup spent fuel in salt brine under hydrogen overpressure and in presence of bromide.
Scientific Basis for Nuclear Waste Management XXX ,Mat. Res. Soc. Symp. Proc. 985, (2007) 15–20

LÜTZENKIRCHEN, J.
Influence of impurities on acid-base data for oxide minerals – Analysis of "observable" surface charge and proton affinity distributions and model calculations for single crystal samples.
Croatica Chemica Acta 80 (2007) 333–343

LÜTZENKIRCHEN, J.; HUBER, F.
Heterogeneities in adsorption from aqueous solution – an example for the effect of surface coverage.
Adsorption, Science and Technology 25 (2007) 503–516

MADIC, C.; BOULLIS, B.; BARON, P.; TESTARD, F.; HUDSON, M.J.; LILJENZIN, J.-O.; CHRISTIANSEN, B.; FERRANDO, M.; FACCHINI, A.; GEIST, A.; MODOLO, G.; ESPARTERO, A.G.; DE MENDOZA, J.

Futuristic back-end of the nuclear fuel cycle with the partitioning of minor actinides.
J. Alloys Compounds 444–445 (2007) 23–27

METZ V.; BOHNERT E.; KELM M.; SCHILD D.; REINHARDT J.; KIENZLER B.; BUCHMEISER M. R.
Gamma-radiolysis of NaCl brine in the presence of UO_2(s): Effects of hydrogen and bromide.
Scientific Basis for Nuclear Waste Management XXX, Mat. Res. Soc. Symp. Proc. 985, (2007) 33–40

MONTAVON, G.; MARKAI, S.; RIBET, S.; RABUNG, T.; GECKEIS, H.; GRAMBOW, B.
Modeling the complexation properties of mineral-bound organic polyelectrolyte: An attempt at comprehension using the model system alumina/polyacrylic acid/M (M = Eu, Cm, Gd).
Journal of Colloid and Interface Science 305 (2007) 32–39

NECK, V., ALTMAIER, M., FANGHÄNEL, TH.:
Solubility of plutonium hydroxides / hydrous oxides under reducing conditions and in the presence of oxygen.
Special Issue "Nuclear Energy and Radiochemistry", Comptes Rendus Chimie 10 (2007) 959–977

NECK, V., ALTMAIER, M., FANGHÄNEL, TH.:
Thermodynamic data for hydrous and anhydrous PuO_{2+x}(s).
Journal of Alloys and Compounds 444 – 445 (2007) 464–469

NECK, V.; ALTMAIER, M.; SEIBERT, A.; YUN, J.I.; MARQUARDT, C.M.; FANGHÄNEL, T.
Solubility and redox reactions of Pu(IV) hydrous oxide: Evidence for the formation of PuO_{2+x}(s, hyd).
Radiochimica Acta 95 (2007) 193–207

PASHALIDIS I., BUCKAU G
“U(VI) Mono-Hydroxo Humate Complexation“,.
Journal of Radioanalytical and Nuclear Chemistry. 273/2 (2007) 315–22

PUDEWILLS, A.
Modeling of hydro-mechanical behavior of rock salt in the near field of repository excavations.
Proc. of the 6th Conference on Mechanical Behavior of Salt, Hannover, Germany 22–25 May 2007, in “Mechanical Behavior of Salt – Understanding the THMC Processes in Rock Salt”
M. Wallner, K.-H.Lux, W. Minkley, H.R. Hardy, H.R. Hardy, Jr. (Eds.), Taylor & Francis Group, London (2007), p. 195–200

ROTHE, J.; PLASCHKE, M.; DENECKE, M. A.
Understanding humic Acid / Zr(IV) interaction – a spectromicroscopy approach.
in “X-Ray Absorption Fine Structure (XAFS13)”, B. Hedman, P. Pianetta (Eds.) Proc. of the 13th Intern. Conf., Stanford (Calif.), July 9–14, 2007, AIP Conference Proceedings Vol. 882, (2007) p. 193–95

SCHÄFER, T., CHANUDET, V., CLARET, F. AND FILELLA, M.
Spectromicroscopy mapping of colloidal/particulate organic matter in Lake Brienz, Switzerland.
Environmental Science & Technology, 41 (2007) 7864–69

SCHULZE,O.; HEEMANN U.; ZETSCHE F.; HAMPEL A.; GÜNTHER R.; MINKLEY W.; SALZER K.; PUDEWILLS A.; ZAPF D.; HOU Z.; WOLTERS R; DÜSTERLOH U.
Comparison of advanced constitutive models for the mechanical behavior of rock salt-results from a joint research project- I. Modeling of deformation processes and benchmark calculations.
Proc. of the 6th Conference on Mechanical Behavior of Salt, Hannover, Germany 22–25 May 2007, in “Mechanical Behavior of Salt – Understanding the THMC Processes in Rock Salt”
M. Wallner, K.-H.Lux, W. Minkley, H.R. Hardy, H.R. Hardy, Jr. (Eds.), Taylor & Francis Group, London (2007), p. 77–88

SOLOMON, D.; LEHMANN, J.; KINYANGI, J.; AMELUNG, W.; LOBE, I.; PELL, A.; RIHA, S.; NGOZE, S.; VERCHOT, L.; MBUGUA, D.; SKJEMSTA, J.; SCHÄFER, T.
Long-term impacts of anthropogenic perturbations on dynamics and speciation of organic carbon in tropical forest and subtropical grassland ecosystems.
Global Change Biology 13 (2007) 511–30

SOLOMON, D.; LEHMANN, J.; THIES, J.; SCHÄFER, T.; LIANG, B.; KINYANGI, J.; NEVES, E.; PETERSEN, J.; LUIZAO, F.; SKJEMSTAD, J.
Molecular signature and sources of biochemical recalcitrance of organic C in Amazonian Dark Earths.
Geochimica Et Cosmochimica Acta 71 (2007) 2285–98

STUMPF, S.; BILLARD, I.; PANAK, P.J.; MEKKI, S.
Differences of Eu(III) and Cm(III) chemistry in ionic liquids: investigations by TRLFS.
Dalton Transactions (2007) 240–48

STUMPF, S.; BILLARD, I.; PANAK, P. J.
Solution chemistry of Cm(III) and Eu(III) in ionic liquids.
In: “Ionic Liquids IV, Not just solvents anymore”, J.F. Brennecke, R.D. Rogers, K.R. Seddon, (Eds.) ACS Symposium Series 975, ACS, Washington, DC, (2007) p. 247–256

STUMPF, T.; CURTIUS, H.; WALTHER, C.; DARDENNE, K.; UFER, K.; FANGHÄNEL, T.
Incorporation of Eu(III) into hydrotalcite: A TRLFS and EXAFS study.
Environmental Science and Technology 417 (2007) 3186–91

SZABO, G.; GUCZI, J.; REILLER, P.; GECKEIS, H.; BULMAN, R.A.
Investigation of complexation of thorium by humic acid using chemically immobilized humic acid on silica gel.
Radiochimica Acta 94 (2007) 553–57

WALTER, M.; NÄSTREN, C.; SOMERS, J.; JARDIN, R.; DENECKE, M.A.; BRENDEBACH, B.
Local atomic structure of a zirconia-based americium transmutation fuel.
J. Solid State Chem. 180 (2007) 3130–35

WALTER, M; SOMERS, J; FERNANDEZ, A.; SPECHT, E. D.; HUNN, J. D.; BOULET, P.; DENECKE, M.A.; GÖBEL, C.
Structure of yttria stabilized zirconia beads produced by gel supported precipitation.
J. Mater. Sci. 42 (2007) 4650–58

WALTER, M.; SOMERS, J.; FERNANDEZ, A.; HAAS, D.; DARDENNE, K.; DENECKE, M.A.
Structural investigation on an aged americium transmutation fuel.
Journal of Nuclear Materials 362, (2007) 343–49

WALTHER, C.; CHO, H.R.; MARQUARDT, C.M.; NECK, V.; SEIBERT, A.; YUN, J.I.; FANGHÄNEL, T.
Hydrolysis of plutonium(IV) in acidic solutions: no effect of hydrolysis on absorption-spectra of mononuclear hydroxide complexes.
Radiochimica Acta 95 (2007) 7–16

WALTHER,C., ROTHE, R., FUSS, M., BÜCHNER, B., KOLTSOV, S., BERGMANN,T.
Investigation of polynuclear Zr-hydroxide complexes by nano-electrospray mass-spectrometry combined with XAFS.
Anal. Bioanal. Chem. 388 (2007) 409–31

YUN, J.I.; CHO, H.R.; NECK, V.; ALTMAIER, M.; SEIBERT, A.; MARQUARDT, C.; WALTHER, C.; FANGHÄNEL, T.
Investigation of the hydrolysis of plutonium(IV) by a combination of spectroscopy and redox potential measurements.
Radiochimica Acta 95 (2007) 89–95

Proceedings of Workshops and Conferences

ALTMAIER, M.; NECK, V.; BRENDEBACH, B.; ROTHE, J., FANGHÄNEL, TH.
Solubility of Zr(IV), Th(IV) and Pu(IV) hydrous oxides and the formation of ternary $Ca_x[M(OH)_n]^{4-n+2x}$ complexes in alkaline $CaCl_2$ solution.
11th Internat. Conf. on the Chemistry and Migration Behaviour of Actinides and Fission Products in the Geosphere (Migration '07), Munich (D), Aug. 26–31, 2007, Book of Abstracts p. 285

BANIK, N.L.; MARQUARDT, C.M.
Speciation of Np(IV) in fulvic acid solution.
11th Internat. Conf. on the Chemistry and Migration Behaviour of Actinides and Fission Products in the Geosphere (Migration ‘07), Munich (D), Aug. 26–31, 2007, Book of Abstracts p. 150

BATUK, O. N.; DENECKE, M. A.; SZABÓ, D.V.; KALMYKOV, ST.N.
XAFS investigation of thorium and uranium oxide nanoparticles incorporated into mesoporous silica.
11th Internat. Conf. on the Chemistry and Migration Behaviour of Actinides and Fission Products in the Geosphere (Migration ‘07), Munich (D), Aug. 26–31, 2007, Book of Abstracts p. 160

BATUK, O.N.; DENECKE, M.A.
Synthesis and XANES investigation of thorium and uranium oxide nanoparticles.
ANKA Annual Report (2007) p. 139–141

BATUK, O. N. ; SEIBERT, A. ; DARDENNE, K. ; DENECKE, M. A.
EXAFS investigation of UO_{2+x} thin films synthesized at various conditions: effect of substrate, oxygen

pressure and temperature.
ANKA Annual Report (2007) p. 142–144

BAUER, A.; FIEHN, B.; MARQUARDT, C.; RÖMER, J.; GÖRTZEN, A.; KIENZLER, B.
Results on Pu Diffusion Experiments in the Opalinus Clay.
11th Internat. Conf. on the Chemistry and Migration Behaviour of Actinides and Fission Products in the Geosphere (Migration '07), Munich (D), Aug. 26–31, 2007, Book of Abstracts p. 129

BAUER, A.; FIEHN, B.; MARQUARDT, CH.; KLEIN, M.; RÖMER, J.; SCHÄFER, TH.; GÖRTZEN, A.; KIENZLER, B.
Results on the Pu diffusion in the opalinus clay.
2nd Annual Workshop Proc.of the Integrated Project 'Fundamental Processes of Radionuclide Migration', 6th EC FP IP FUNMIG, Stockholm (S) Nov. 21–23, 2006, Svensk Kärnbränslehantering, Technical SKB Report TR-07-05 (June 2007) p. 231–38

BAUER, A., FIEHN, B., MARQUARDT, C., RÖMER, J., GÖRTZEN, A., KIENZLER, B.
Results on Pu Diffusion Experiments in the Opalinus Clay.
Proceedings of the International ANDRA meeting on Clay in natural and engineered barriers for radioactive waste confinement, 2007, Sept. 17–20, Lille (F), p. 473–474.

BOSBACH, D.; HECK, S.; RÖMER, J.; DARDENNE, K.; STANJEK, H.
Structural incorporation of trivalent f-elements in powellite.
11th Internat. Conf. on the Chemistry and Migration Behaviour of Actinides and Fission Products in the Geosphere (Migration '07), Munich (D), Aug. 26–31, 2007, Book of Abstracts p. 170

BOUBY, M.; GECKEIS, H
On the dynamics of tetravalent actinide(Th/Pu^{IV})-humic acid interaction.
11th Internat. Conf. on the Chemistry and Migration Behaviour of Actinides and Fission Products in the Geosphere (Migration '07), Munich (D), Aug. 26–31, 2007, Book of Abstracts p. 192

BOUBY, M.; GECKEIS, H.; SCHÄFER, T.; LÜTZENKIRCHEN, J.; SEHER, H.; BAUER, A.; PLASCHKE, M.; HAUSER, W.; KIENZLER, B.
Laboratory study on colloid stability and radionuclide-colloid interaction under Äspö groundwater conditions.
11th Internat. Conf. on the Chemistry and Migration Behaviour of Actinides and Fission Products in the Geosphere (Migration '07), Munich (D), Aug. 26–31, 2007, Book of Abstracts p. 135

BOVENKAMP, G.L.; BRENDEBACH, B.; GÖTTLICHER, J.; HORMES, J.; VITOVA, T.
XAFS investigation of the arsenic uptake of watercress.
ANKA Annual Report (2007) p. 187–189

BREBAN, D.C.; PANAK, P. J.; KIM, M. A.; ROTHE, J.; DARDENNE, K.; DENECKE, M. A.; KIM, J. I.; FANGHÄNEL, TH.
Interaction of Actinides(III, IV, V, VI) with Hydroxyaluminosilicate and -Polysilicate Colloids studied by TRLFS and EXAFS.
11th Internat. Conf. on the Chemistry and Migration Behaviour of Actinides and Fission Products in the Geosphere (Migration '07), Munich (D), August 26–31, 2007, Book of Abstracts p. 104

BREBAN, D.; PANAK, P.J.; ROTHE, J.; DENECKE, M. A.; KIM, M. A.; KIM, J. I.; FANGHÄNEL, TH.
Interaction of Th(IV) with aluminosilicates 'in statu nascendi'.
ANKA Annual Report (2007) p. 171–173

BRENDEBACH, B.; ALTMAIER, M.; ROTHE, J.; NECK, V.; DENECKE, M.A.
An EXAFS study of aqueous Zr(IV) and Th(IV) complexes in alkaline $CaCl_2$ solutions: $Ca_3[Zr(OH)_6]^{4+}$ and $Ca_4[Th(OH)_8]^{4+}$.
11th Internat. Conf. on the Chemistry and Migration Behaviour of Actinides and Fission Products in the Geosphere (Migration '07), Munich (D), Aug. 26–31, 2007, Book of Abstracts p. 193

BRENDEBACH, B.; ALTMAIER, M.; ROTHE, J.; NECK, V.; DENECKE, M.A.
EXAFS characterization of a new type of ternary Ca-Th(IV)-OH complex.
ANKA Annual Report (2007) 135–137

BRENDEBACH B.; ALTMAIER, M.; ROTHE J.; NECK, V.; DENECKE M. A.
Structural Study of Thorium Complexes in Chloride Solution.
Selected Highlight for ANKA Annual Report (2007)

BRENDEBACH, B.; BOULET, P.; DARDENNE, K.; DENECKE, M.A.; RÖMER, J.; ROTHE, J.; MEXNER, W.; CERFF, C.
The INE-Beamline for actinide research at ANKA – a status report.

4th Workshop on Speciation, Techniques, and Facilities for Radioactive Materials at Synchrotron Light Sources (Actinide-XAS-2006), Karlsruhe (D), 2007, OECD–NEA Proceedings No. 6288, p.135–40

BRENDEBACH, B.; DARDENNE, K.; DENECKE, M.A.; ROTHE, J.; VITOVA, T.
New developments at the INE-beamline for actinide research at ANKA.
Nuclear Instruments and Methods in Physics Research A 582 (2007) 80–81

BRENDEBACH, B.; DARDENNE, K.; DENECKE, M.A.; GÖTTLICHER, J.; MANGOLD, S.; ROTHE, J.; STEININGER, R.; SIMON, R.
X-ray Spectroscopy Beamlines.
ANKA Annual Report (2007) 279–282

BRENDEBACH, B.; DENECKE, M.A.; DARDENNE, K.; ROTHE, J.; LUCKSCHEITER, B.; WEISENBURGER, S.; ROTH, G.; NESOVIC, M.; MANGOLD, S.
XAFS investigation of high level waste glasses.
4th Workshop on Speciation, Techniques, and Facilities for Radioactive Materials at Synchrotron Light Sources (Actinide-XAS-2006), Karlsruhe (D), 2007, OECD–NEA Proceedings No. 6288, p.183–191

BRENDEBACH, B.; WEISENBURGER, S.; ROTH, G.; DENECKE, M.A.
XANES fingerprinting investigation of sulfur in high level waste glasses.
ANKA Annual Report (2007) 147–149

BUCKAU, G.
A simple approach to the An(III) and An(VI) humate complexation.
11th Internat. Conf. on the Chemistry and Migration Behaviour of Actinides and Fission Products in the Geosphere (Migration '07), Munich (D), Aug. 26–31, 2007, Book of Abstracts p. 192

BÜCHNER, S.; FUSS, M.; ROTHE, J.; WALTHER, C.
Direct observation of polynuclear Zr(IV) hydroxide complexes in solution by nano-electrospray MS and Zr K-XAFS.
ANKA Annual Report (2007) 183–185

CHARDON, E.S.; BOSBACH, D.; LIVENS, F.R.; LYON, I.C.; MARQUARDT, C.; RÖMER, J.; SCHILD, D.; WINCOTT, P.L.; WOGELIUS, R.A.; VAUGHAN, D.J.
Surface analytical studies of feldspar surface reaction with U(VI).
17th Annual V.M. Goldschmidt Conference, Cologne (D), 19–24 Aug. 2007,
Geochimica et Cosmochimica Acta, 71 (2007) Suppl. S., p. A160

CHRISTIANSEN, B.C.; SKOVBJERG, L.L.; GECKEIS, H.; MARQUARDT, C.M.; SCHILD, D.; PLASCHKE, M.; STIPP, S.L.S.
Green rust interaction with neptunyl (NpO_2^+) and selenate (SeO_4^{2-}).
11th Internat. Conf. on the Chemistry and Migration Behaviour of Actinides and Fission Products in the Geosphere (Migration '07), Munich (D), Aug. 26–31, 2007, Book of Abstracts p. 165

CLARET, F.; SCHÄFER, T.; REILLER, P.
Natural organic matter fractionation on mineral surfaces: a spectroscopic approach.
Proceedings of the International ANDRA meeting on Clay in natural and engineered barriers for radioactive waste confinement, 2007, Sept. 17–20, Lille (F), p. 385–386.

CLARET, F.; SCHÄFER, T.; REILLER, P.
Sorption induced fractionation of fulvic acids.
2nd Annual Workshop Proc.of the Integrated Project 'Fundamental Processes of Radionuclide Migration', 6th EC FP IP FUNMIG, Stockholm (S) Nov. 21–23, 2006,
Svensk Kärnbränslehantering, Technical SKB Report TR-07-05 (June 2007) p. 253–60

DARDENNE, K.; BOSBACH, D.; DENECKE, M. A.; BRENDEBACH, B
Local structure EXAFS investigation of the $NaLn(MoO_4)_2$ - $Ca_2(MoO_4)_2$ solid solution series.
4th Workshop on Speciation, Techniques, and Facilities for Radioactive Materials at Synchrotron Light Sources (Actinide-XAS-2006), Karlsruhe (D), 2007, OECD–NEA Proceedings No. 6288, p.193–201

DARDENNE, K.; BOSBACH, D. ; DENECKE, M. A. ; BRENDEBACH, B.
EXAFS Investigation of the $NaLn(MoO_4)_2$ - $Ca_2(MoO_4)_2$ solid solution series local structure.
11th Internat. Conf. on the Chemistry and Migration Behaviour of Actinides and Fission Products in the Geosphere (Migration '07), Munich (D), Aug. 26–31, 2007, Book of Abstracts p. 173

DARDENNE, K.; DENECKE, M. A.; CALIEBE, W.
High resolution X-ray fluorescence investigation of Eu(III) sorbed onto 2-line -ferrihydrite (2LFh) and its transformation products.
HASYLAB Annual Report (2007) p. 1587–88

DELOS, A.; SCHÄFER, T.; CARRERA, J.; GUIMERA, J.; WALTHER, C.; SANCHEZ-VILA, X.; GECKEIS, H.
Reversibility of actinide binding on montmorillonite colloids.
11th Internat. Conf. on Chemistry and Migration Behaviour of Actinides and Fission Products in the Geosphere (Migration '07), Munich (D), Aug. 26–31, 2007, Book of Abstracts p. 220

DENECKE, M.A.; JANSSENS, K.; FALKENBERG, G.; BRENDEBACH, B.; RÖMER, J.
Confocal µ-XRF and µ-XAFS studies of fractured granite following a radiotracer migration experiment.
11th Internat. Conf. on the Chemistry and Migration Behaviour of Actinides and Fission Products in the Geosphere (Migration '07), Munich (D), Aug. 26–31, 2007, Book of Abstracts p. 156

DENECKE, M.A.; HUBER, F.; RICKERS, K.; BRENDEBACH, B.; MICHEL, P.; SCHÄFER, T.
µ-XRF and µ-XAFS investigation of a uranium-rich clay from a natural analogue site.
HASYLAB Annual Report (2007) p. 1293–94

DENECKE, M.A.; BRENDEBACH, B.; DARDENNE, K.; ROTHE, J.; GOMPPER, K.
Actinide-XAS-2006-Workshop hosted by Forschungszentrum Karlsruhe, Germany
Synchrotron Radiation News, 20 (2007) No.2, p. 21–22

DENECKE, M.A.; HAVLOVA, V.
Elemental correlations observed in Ruprechtov tertiary sediment: micro-focus fluorescence mapping and sequential extraction.
2nd Annual Workshop Proc.of the Integrated Project 'Fundamental Processes of Radionuclide Migration', 6th EC FP IP FUNMIG, Stockholm (S) Nov. 21–23, 2006,
Svensk Kärnbränslehantering, Technical SKB Report TR-07-05 (June 2007) p. 315–20

DENECKE, M.A.; JANSSENS, K.; BRENDEBACH, B.; FALKENBERG, G.; SIMON, R.; VEKEMANS, B.
Confocal µ-XRF and µ-XAFS studies of fractured granite following a radiotracer migration experiment.
4th Workshop on Speciation, Techniques, and Facilities for Radioactive Materials at Synchrotron Light Sources (Actinide-XAS-2006), Karlsruhe (D), 2007, OECD–NEA Proceedings No. 6288, p.203–210

EIDNER, S.; FREYER, M.; STUMPF, TH.; WALTHER, C.; KUMKE, M.U.
New insights in the complexation of actinide ions by humic acids.
11th Internat. Conf. on Chemistry and Migration Behaviour of Actinides and Fission Products in the Geosphere (Migration '07), Munich (D), Aug. 26–31, 2007, Book of Abstracts p. 190

EINSIEDL, F.; SCHÄFER, T.; WOLF, M.
Hydrogeological conditions and biogeochemical processes governing metal transport in groundwater systems.
International Conference on WAter POllution in natural Porous media at different scales. Assessment of fate, impact and indicators. WAPO2, Barcelona (E) 2007, April 11–13, p. 1–6

FILBY, A.; PLASCHKE, M.; GECKEIS, H.; BOSBACH, D.:
Interaction of carboxylated latex colloids with mineral surfaces.
11th Internat. Conf. on Chemistry and Migration Behaviour of Actinides and Fission Products in the Geosphere (Migration '07), Munich (D), Aug. 26–31, 2007, Book of Abstracts p. 139

FINCK. N.; DARDENNE, K.; SCHLEGEL, M.L.; BOSBACH, D.
Structural incorporation of trivalent f elements into the trioctahedral clay mineral hectorite.
17th Annual V.M. Goldschmidt Conference, Cologne (D), 19 – 24 Aug. 2007,
Geochimica et Cosmochimica Acta, 71 (2007) Suppl. S., p. A279

FINCK. N.; DARDENNE, K.; SCHLEGEL, M.L.; BOSBACH, D.
Structural incorporation of trivalent f elements into the trioctahedral clay mineral hectorite.
11th Internat. Conf. on the Chemistry and Migration Behaviour of Actinides and Fission Products in the Geosphere (Migration '07), Munich (D), Aug. 26–31, 2007, Book of Abstracts p. 93

FINCK. N.; DARDENNE, K.; SCHLEGEL, M.L.; BOSBACH, D.
Structural incorporation of trivalent f elements into the trioctahedral clay mineral hectorite.
Proceedings of the International ANDRA meeting on Clay in natural and engineered barriers for radioactive waste confinement, 2007, Sept. 17–20, Lille (F), p. 357–358

FINCK, N.; SCHLEGEL, M.L.; BOSBACH, D.
Eu(III)/Lu(III) coprecipitation with trioctahedral smectite hectorite.
ANKA Annual Report (2007) 154–156

FLEISCH, J.; WEISHAUPT, M.; GRÜNEWALD, W.; ROTH, G.; TOBIE, W.
Inbetriebsetzung und Kaltbetrieb der Verglasungsanlage VEK

Annual Meeting on Nuclear Technology / Jahrestagung Kerntechnik, Karlsruhe, May 22–24, 2007, Book of Abstracts, section 4, CD-ROM Conference Proceedings, p. 406–409

FLEISCH, J.; WEISHAUPT, M.; GRÜNEWALD, W.; ROTH, G.; TOBIE, W.; WEISENBURGER, S.
Commissioning and cold test operationof the German HLLW vitrification plant VEK.
WM07 Conference, Tucson, AZ, USA, Febr. 25–March 1, 2007, CD-ROM Conference Proceedings

FLÖRSHEIMER, M.; KRUSE, K.; POLLY, R.; ABDELMONEM, A.; SCHIMMELPFENNIG, B.; KLENZE, R.; FANGHÄNEL, T.
The functional species of a mineral surface and their interaction with the adjacent water molecules determined by nonlinear optics and quantum chemistry.
17th Annual V.M. Goldschmidt Conference, Cologne (D), 19–24 Aug. 2007
Geochimica et Cosmochimica Acta, 71(2007) Suppl. S., p. A286

FLÖRSHEIMER, M.; KRUSE, K.; POLLY , R.; ABDELMONEM, A.; SCHIMMELPFENNIG, B.; KLENZE, R.; FANGHÄNEL, T.
Understanding Mineral/Water Interaction at the Molecular Level by Means of Nonlinear Optics and Quantum Chemistry.
11th Internat. Conf. on the Chemistry and Migration Behaviour of Actinides and Fission Products in the Geosphere (Migration ‘07), Munich (D), Aug. 26–31, 2007, Book of Abstracts p. 93

GAILLARD, C.; STUMPF, S.; DENECKE, M.A.
Am(III) solvation in Room Temperature Ionic Liquids.
ANKA Annual Report (2007) 156–157

GECKEIS, H.
Actinide geochemistry: From the molecular level to the real system.
17th Annual V.M. Goldschmidt Conference, Cologne (D), 19–24 Aug. 2007
Geochimica et Cosmochimica Acta, 71 (2007) Suppl.S., p. A313

GOMPPER, K.; BOSBACH, D.; DENECKE, M.A.; GECKEIS, H.; KIENZLER, B.; KLENZE, R.
Research on long term safety of nuclear waste disposal at the research center Karlsruhe, Germany.
Global 2007: Advanced Nuclear Fuel Cycles and Systems, Boise, Idaho, U.S.A., Sept. 9–13, 2007, Proceed. by American Nuclear Society, ANS Order #: 700331 on CD-Rom, p. 486–495

GUCZI, J.; REILLER, P.; BULMAN, R.A.; GECKEIS, H.; SZABO, G.
Preliminary results for complexation of Pu with humic acid.
2nd Annual Workshop Proc.of the Integrated Project 'Fundamental Processes of Radionuclide Migration', 6th EC FP IP FUNMIG, Stockholm (S) Nov. 21–23, 2006,
Svensk Kärnbränslehantering, Technical SKB Report TR-07-05 (June 2007) p. 353–60

HARTMANN, E.; GECKEIS, H.; RABUNG, TH.; FANGHÄNEL, Th.; BOSBACH, D.
Sorption of radionuclides onto natural clays.
11th Internat. Conf. on the Chemistry and Migration Behaviour of Actinides and Fission Products in the Geosphere (Migration ‘07), Munich (D), Aug. 26–31, 2007, Book of Abstracts p. 94

HAVLOVA, V.; CERVINKA, R.; DENECKE, M.A.; NOSECK, U.; BRASSER, T.; SUKSI, J.
Uranium forms and the role of organic matter on Ruprechtov natural analogue site: Multimethod approach.
11th Internat. Conf. on the Chemistry and Migration Behaviour of Actinides and Fission Products in the Geosphere (Migration ‘07), Munich (D), Aug. 26–31, 2007, Book of Abstracts p. 234

HAUSER, W.; GÖTZ; R.; SKERENCAK, A.; PANAK, P.J.; RABUNG, T.; GECKEIS, H.; FANGHÄNEL, TH.
A new fibre connected optical detection cell for time-resolved laser-fluorescence spectroscopy at elevated temperature.
11th Internat. Conf. on the Chemistry and Migration Behaviour of Actinides and Fission Products in the Geosphere (Migration ‘07), Munich (D), Aug. 26–31, 2007, Book of Abstracts p. 108

HAUSER, W.; GECKEIS, H.; GÖTZ, R.; NOSECK, U.; LACIOK, A.
Colloid detection in natural ground water from Ruprechtov by laser-induced breakdown detection.
2nd Annual Workshop Proc.of the Integrated Project 'Fundamental Processes of Radionuclide Migration', 6th EC FP IP FUNMIG, Stockholm (S) Nov. 21–23, 2006,
Svensk Kärnbränslehantering, Technical SKB Report TR-07-05 (June 2007) p. 367–74

HEBERLING, F.; DENECKE, M.A.; BOSBACH, D.
Np(V) co-precipitation with calcite.

2nd Annual Workshop Proc.of the Integrated Project 'Fundamental Processes of Radionuclide Migration', 6th EC FP IP FUNMIG, Stockholm (S) Nov. 21–23, 2006, Svensk Kärnbränslehantering, Technical SKB Report TR-07-05 (June 2007) p.301–06

HEBERLING, F.; DENECKE M. A.;BOSBACH, D.
Np(V) co-precipitation with calcite.
17th Annual V.M. Goldschmidt Conference, Cologne (D), 19–24 Aug. 2007
Geochimica et Cosmochimica Acta, 71(2007) Suppl. S., p. A388

HEBERLING, F.; BOSBACH, D.
U(VI) co-precipitation with calcite.
ANKA Annual Report (2007) 162–164

HEBERLING, F.; DENECKE M. A.;BOSBACH, D.
Structural incorporation of Np(V) into calcite.
11th Internat. Conf. on the Chemistry and Migration Behaviour of Actinides and Fission Products in the Geosphere (Migration '07), Munich (D), Aug. 26–31, 2007, Book of Abstracts p. 170

HEBERLING, F.; DENECKE, M.A.; BOSBACH, D.
Np(V) co-precipitation with calcite.
4th Workshop on Speciation, Techniques, and Facilities for Radioactive Materials at Synchrotron Light Sources (Actinide-XAS-2006), Karlsruhe (D), 2007, OECD–NEA Proceedings No. 6288, p.213–18

HUITTINEN, N.; RABUNG, TH.; LÜTZENKIRCHEN, J.; GECKEIS, H.; LEHTO, J.
Gd/Cm(III) sorption onto aluminium oxides/hydroxides.
11th Internat. Conf. on the Chemistry and Migration Behaviour of Actinides and Fission Products in the Geosphere (Migration '07), Munich (D), Aug. 26–31, 2007, Book of Abstracts p. 95

KIENZLER, B.; GMAL, B.
Critical safe disposal of spent fuel: behavior of neutron poisons.
Global 2007: Advanced Nuclear Fuel Cycles and Systems, Boise, Idaho, U.S.A., Sept. 9–13, 2007, Proceed. by American Nuclear Society, ANS Order #: 700331 on CD-Rom, ISBN: 0-89448-055-3, p. 1453–1460

KIENZLER, B.; GECKEIS, H.; GOMPPER, K.; KLENZE, R.
Radioactive waste disposal in Germany: no site decision-keeping competence.
Proc.of the 11th Internat.Conf.on Environmental Remediation and Radioactive Waste Management (ICEM2007), Bruges, B, September 2–6, 2007
New York, N.Y. : ASME, 2007 CD-ROM Paper ICEM07-7222

LAAKSOHARJU, M.; SMELLIE, J.; TULLBORG, E.L.; MOLINERO, J.; GIMENO, M.; BUCKAU, G.
Results from the groundwater hydrogeochemical investigation programme in Sweden.
2nd Annual Workshop Proc.of the Integrated Project 'Fundamental Processes of Radionuclide Migration', 6th EC FP IP FUNMIG, Stockholm (S) Nov. 21–23, 2006, Svensk Kärnbränslehantering, Technical SKB Report TR-07-05 (June 2007) p. 123–30

LINDQVIST-REIS, P.; WALTHER, C; KLENZE, R.; FANGHÄNEL, T.
Influence of "chemical pressure" on the structure and crystal-field energy levels of $[Cm(H_2O)_9]^{3+}$ in $[M(H_2O)_9](CF_3SO_3)_3$ (M = La, Lu, Y).
11th Internat. Conf. on the Chemistry and Migration Behaviour of Actinides and Fission Products in the Geosphere (Migration '07), Munich (D), Aug. 26–31, 2007, Book of Abstracts p. 195

LOIDA, A.; KELM, M.; MÜLLER, N.; METZ, V.; BOHNERT, E.; KIENZLER, B.
Experimental approach to distinguish between alpha- and beta-, gamma-radiolysis effects on spent fuel matrix dissolution.
31th International MRS Symposium on the Scientific Basis for Nuclear Waste Management, Sept. 16–21, 2007, Sheffield (UK), Book of Abstracts p. 33

LOIDA, A.; KIENZLER, B.; METZ,V.
High level waste forms for repositories in rock salt and argillaceous rocks: concepts for future investigations.
Annual Meeting on Nuclear Technology / Jahrestagung Kerntechnik, Karlsruhe, May 22–24, 2007, Book of Abstracts, section 4, CD-ROM Conference Proceedings, p. 387–390

MARKAI, S.; MONTAVON, G.; GRAMBOW, B.; RABUNG, TH.; BOUBY, M.; GECKEIS, H.; AMEKRATZ, B.; MOULIN, C.
Interaction of Eu(III) with polyacrylic acids: Effect of pH.

11th Internat. Conf. on the Chemistry and Migration Behaviour of Actinides and Fission Products in the Geosphere (Migration '07), Munich (D), Aug. 26–31, 2007, Book of Abstracts p. 272

MARQUARDT, C.M.; SEIBERT, A.
Redox behaviour of plutonium in presence of hydroquinone or fulvic acid under anaerobic conditions.
11th Internat. Conf. on the Chemistry and Migration Behaviour of Actinides and Fission Products in the Geosphere (Migration '07), Munich (D), Aug. 26–31, 2007, Book of Abstracts p. 210

MARQUARDT, C.M.; SEIBERT, A.
The reduction of plutonium: comparison between hydroquinone and fulvic acid as reducing compound.
2nd Annual Workshop Proc.of the Integrated Project 'Fundamental Processes of Radionuclide Migration', 6th EC FP IP FUNMIG, Stockholm (S) Nov. 21–23, 2006, Svensk Kärnbränslehantering, Technical SKB Report TR-07-05 (June 2007) p. 389–96

MARQUES-FERNANDES, M.; RABUNG, TH.; DÄHN, R.; BAEYENS, B.; BRADBURY, M.H.
A time resolved laser fluorescence and X-ray absorption spectroscopy study of lanthanide/actinide sorption on clay minerals: Influence of carbonate complexation.
Proceedings of the International ANDRA meeting on Clay in natural and engineered barriers for radioactive waste confinement, Sept. 17–20, Lille (France), p. 317–318.

MBUDI, C.; BRENDEBACH, B.; MERKEL, B.; BEHRA, P.
Speciation of Uranium and Arsenic Sorbed onto Scrap Metallic Iron and Shewanella Putrefaciens Surfaces: A XANES Fingerprinting Investigation.
58. Berg- und Hüttenmännischer Tag: Behandlungstechnologien für bergbaubeeinflusste Wässer / GIS – Geowissenschaftliche Anwendungen und Entwicklungen, B. Merkel, H. Schaeben, Ch. Wolkersdorfer, A. Hasche-Berger, (Eds.),
Wissenschaftliche Mitteilungen 35, Freiberg, 2007, p. 35–42

MBUDI, C.; BRENDEBACH, B.; MERKEL, B.J.; BEHRA, P.
Speciation of Uranium and Arsenic Sorbed onto Scrap Metallic Iron and Shewanella Putrefaciens Surfaces.
ANKA Annual Report (2007) 166–168

METZ, V.; LOIDA, A.; BOHNERT, E.; SCHILD, D.; RÖMER, J.; DARDENNE, K.
Effects of hydrogen and bromide on radiation induced UO_2(s) corrosion in NaCl brine.
11th Internat. Conf. on the Chemistry and Migration Behaviour of Actinides and Fission Products in the Geosphere (Migration '07), Munich (D), August 26–31, 2007, Book of Abstracts p. 280

METZ, V.; BOHNERT, E.; DARDENNE, K.; BRENDEBACH, B.; ROTHE, J.; DENECKE, M. A.; NAZMOV, V.
GI-XAFS investigation on gamma-irradiated UO_2 pellets.
ANKA Annual Report (2007) 168–170

MICHEL, P.; SCHÄFER, T.; CLARET, F.; ELIE, M.
Examination of clay mineral organic matter interactions at submicron-scale during confined pyrolysis of a simplified system Volclay bentonite – type II kerogen.
Proceedings of the International ANDRA meeting on Clay in natural and engineered barriers for radioactive waste confinement, 2007, Sept. 17–20, Lille (F), p. 387–388.

NECK, V.; ALTMAIER, M.; LÜTZENKIRCHEN, J.; KORTHAUS, E.; FANGHÄNEL, TH.
A comprehensive thermodynamic model for the solubility and hydrolysis of Nd(III) and Am(III) in dilute to concentrated NaCl, $MgCl_2$ and $CaCl_2$ solutions.
11th Internat. Conf. on the Chemistry and Migration Behaviour of Actinides and Fission Products in the Geosphere (Migration '07), Munich (D), Aug. 26–31, 2007, Book of Abstracts p. 60

NOSECK, U.; BRASSER, T.; SUKSI, J.; HAVLOVA, V.; DENECKE, M.A.
Identification of uranium enrichment scenarios by multimethod characterisation of immobile uranium phases.
11th Internat. Conf. on the Chemistry and Migration Behaviour of Actinides and Fission Products in the Geosphere (Migration '07), Munich (D), Aug. 26–31, 2007, Book of Abstracts p. 46

NOSECK, U.; BRASSER, T.; LACIOK, A.; HERCIK, M.; HAVLOVA, V.; BUCKAU, G.; ROZANSKI, K.; DULINSKI, M.
Evaluation of isotope data from Ruprechtov site.
2nd Annual Workshop Proc.of the Integrated Project 'Fundamental Processes of

Radionuclide Migration', 6th EC FP IP FUNMIG, Stockholm (S) Nov. 21–23, 2006,
Svensk Kärnbränslehantering, Technical SKB Report TR-07-05 (June 2007) p. 155–62

NOSECK, U.; BRASSER, TH.; HAVLOVA, V.; DENECKE; M.A.; HAUSER, W.; BUCKAU, G.; SUKSI, J.
IP FUNMIG RTDC 5: Processes and transport studies relevant for salt rock disposal concepts.
11th Internat. Conf. on the Chemistry and Migration Behaviour of Actinides and Fission Products in the Geosphere (Migration '07), Munich (D), Aug. 26–31, 2007, Book of Abstracts p. 264

NOSECK, U.; KEESMANN, S.; GECKEIS, H.; SCHÄFER, T.; KUNZE, P.; SEHER, H.
Impact of kinetic effects on colloid facilitated radionuclide transport at Grimsel.
11th Internat. Conf. on Chemistry and Migration Behaviour of Actinides and Fission Products in the Geosphere (Migration '07), Munich (D), Aug. 26–31, 2007, Book of Abstracts p. 133

PANAK, J.P.; DENECKE, M.A.; WEIGL, M.; GEIST, A.; SCHIMMELPFENNIG, B.
Combined TRLFS, EXAFS and theoretical investigations on actinide/lanthanide complexed with portioning relevant ligands.
4th Workshop on Speciation, Techniques, and Facilities for Radioactive Materials at Synchrotron Light Sources (Actinide-XAS-2006), Karlsruhe (D), 2007, OECD–NEA Proceedings No. 6288, p. 21

PETROVA (KHASANOVA), A.B.; KALMYKOV, ST.N.; PERMINOVA, I.V.; SHCHERBINA, N.S.; SCHÄFER, T.; CLARET, F.
Redox behaviour and sorption of Pu(V) and Np(V) by goethite in the presence of different humic acids.
11th Internat. Conf. on Chemistry and Migration Behaviour of Actinides and Fission Products in the Geosphere (Migration '07), Munich (D), Aug. 26–31, 2007, Book of Abstracts p. 90

POLLY, R.; FLÖRSHEIMER, M.; KRUSE, K.; ABDELMONEM, A.; SCHIMMELPFENNIG, B.; KLENZE, R.; FANGHÄNEL, T.
Quantum Chemical Description of the Sapphire(001)/Water Interface Using Cluster Models and Comparison with Results from Nonlinear Optical Spectroscopy.
11th Internat. Conf. on the Chemistry and Migration Behaviour of Actinides and Fission Products in the Geosphere (Migration '07), Munich (D), Aug. 26–31, 2007, Book of Abstracts p. 267

PRIEMYSHEV, A.; KIM, M.A.; KIM, J.I.
Binding affinity of humic colloids to actinides and what's behind.
2nd Annual Workshop Proc.of the Integrated Project 'Fundamental Processes of Radionuclide Migration', 6th EC FP IP FUNMIG, Stockholm (S) Nov. 21–23, 2006,
Svensk Kärnbränslehantering, Technical SKB Report TR-07-05 (June 2007) p. 267–72

RABUNG, TH.; ALTMAIER, M.; NECK, V.; FANGHÄNEL, TH.
A TRLFS study of Cm(III) hydroxide complexes in alkaline $CaCl_2$ solution.
11th Internat. Conf. on the Chemistry and Migration Behaviour of Actinides and Fission Products in the Geosphere (Migration '07), Munich (D), Aug. 26–31, 2007, Book of Abstracts p. 60

REGENSPURG, S.; SCHÄFER, T.; DARDENNE, K.; SCHILD, D., MALMSTRÖM, M.E.
Uranyl uptake on granitic minerals in presence of carbonate.
2nd Annual Workshop Proc.of the Integrated Project 'Fundamental Processes of Radionuclide Migration', 6th EC FP IP FUNMIG, Stockholm (S) Nov. 21–23, 2006,
Svensk Kärnbränslehantering, Technical SKB Report TR-07-05 (June 2007) p. 381–387

REGENSPURG, S.; SCHÄFER, T.; DARDENNE, K.; MALMSTRÖM, M.
U(VI) interaction with Fe(II) containing minerals.
ANKA Annual Report (2007) 174–176

REGENSPURG, S.; SCHÄFER, T.; SCHILD, D., MALMSTRÖM, M.E.
Uranium(VI) sorption and reduction by granitic minerals in bicarbonate solutions.
11th Internat. Conf. on the Chemistry and Migration Behaviour of Actinides and Fission Products in the Geosphere (Migration '07), Munich (D), Aug. 26–31, 2007, Book of Abstracts p. 196

RÖMER, J.; KIENZLER, B.; SCHILD, D.
Sorption of redox sensitive actinides onto granite and altered material from Äspö HRL.
2nd Annual Workshop Proc.of the Integrated Project 'Fundamental Processes of Radionuclide Migration', 6th EC FP IP FUNMIG, Stockholm (S) Nov. 21–23, 2006,
Svensk Kärnbränslehantering, Technical SKB Report TR-07-05 (June 2007) p.247–252

ROTHE, J.; PLASCHKE, M.; SCHIMMELPFENNIG, B.; DENECKE, M. A.
X-ray Absorption Fine Structure Spectroscopy of Eu(III) and UO_2^{2+} Complexation with Polyacrylic Acid.

4th Workshop on Speciation, Techniques, and Facilities for Radioactive Materials at Synchrotron Light Sources (Actinide-XAS-2006), Karlsruhe (D), 2007, OECD–NEA Proceedings No. 6288, p.193–201

ROTHE, J.; WALTHER, C.; NECK, V.; ALTMAIER, M.; BÜCHNER S.; YUN, J.I.
A combined XAFS and LIBD study on the formation of polynuclear Pu complexes and colloids in acidic solution.
11th Internat. Conf. on the Chemistry and Migration Behaviour of Actinides and Fission Products in the Geosphere (Migration '07), Munich (D), Aug. 26–31, 2007, Book of Abstracts p. 61

SCHÄFER, T.
Studies on "less well established processes" as colloids, influence of organics, redox- and microbial-processes within the IP "FUNMIG".
11th Internat. Conf. on Chemistry and Migration Behaviour of Actinides and Fission Products in the Geosphere (Migration '07), Munich (D), Aug. 26–31, 2007, Book of Abstracts p. 261

SCHÄFER, T.; ENZMANN, F.; KERSTEN, M.; BOUBY, M.; KIENZLER, B.; GECKEIS, H.
Radionuclide transport in a granite fracture from Äspö (Sweden): Insights from migration experiments and computed X-Ray tomography (XCT).
11th Internat. Conf. on Chemistry and Migration Behaviour of Actinides and Fission Products in the Geosphere (Migration '07), Munich (D), Aug. 26–31, 2007, Book of Abstracts p. 222

SCHÄFER, T.; MICHEL, P.; CLARET, F.; BUCKAU, G.; ELIE, M.
Transformation of organic matter in the presence of smectite: Fate of lanthanides during polymerization reactions.
Proceedings of the International ANDRA meeting on Clay in natural and engineered barriers for radioactive waste confinement, 2007, Sept. 17–20, Lille (F), p. 379–380.

SCHMIDT, M.; MARQUES-FERNANDES, M.; STUMPF, T.; WALTHER, C.; KLENZE, R.; FANGHÄNEL, T.
Site-selective TRLFS investigations on Eu(III) doped calcite.
11th Internat. Conf. on the Chemistry and Migration Behaviour of Actinides and Fission Products in the Geosphere (Migration '07), Munich (D), Aug. 26–31, 2007, Book of Abstracts p. 42

SEHER, H.; SCHÄFER, T.; GECKEIS, H.; FANGHÄNEL, T.
Febex bentonite colloid stability in ground water.
2nd Annual Workshop Proc.of the Integrated Project 'Fundamental Processes of Radionuclide Migration', 6th EC FP IP FUNMIG, Stockholm (S) Nov. 21–23, 2006,
Svensk Kärnbränslehantering, Technical SKB Report TR-07-05 (June 2007) p. 397–402

SEHER, H.; SCHÄFER, T.; KUNZE, P.; BOUBY, M.; HAUSER, W.; PANAK, P.J.; GECKEIS, H.; FANGHÄNEL, TH.
FEBEX bentonite colloid stability and radionuclide speciation in the groundwater/porewater mixing zone.
11th Internat. Conf. on the Chemistry and Migration Behaviour of Actinides and Fission Products in the Geosphere (Migration '07), Munich (D), Aug. 26–31, 2007, Book of Abstracts p. 103

SKERENCAK; A.; PANAK, P.J.; HAUSER, W.; NECK, V.; LINDQVIST-REIS, P.; KLENZE, R.; FANGHÄNEL, TH.
Complexation of Eu(III) and Cm(III) with nitrate in the temperature range of 20-200°C by time-resolved laser fluorescence spectroscopy.
11th Internat. Conf. on the Chemistry and Migration Behaviour of Actinides and Fission Products in the Geosphere (Migration '07), Munich (D), Aug. 26–31, 2007, Book of Abstracts p. 193

STUMPF, T.; MARQUES-FERNANDES, M.; WALTHER, C.; SCHMIDT, M.; DARDENNE, K.; BOSBACH, D.; FANGHÄNEL, T.
Incorporation of An(III) and Ln(III) into calcite: Process understanding on a molecular level.
11th Internat. Conf. on the Chemistry and Migration Behaviour of Actinides and Fission Products in the Geosphere (Migration '07), Munich (D), Aug. 26–31, 2007, Book of Abstracts p. 172

STUMPF, T.; MARQUES-FERNANDES, M.; WALTHER, C.; SCHMIDT, M.; DARDENNE, K.; BOSBACH, D.; FANGHÄNEL, T.
Structural incorporation of Eu(III) into calcite: Process understanding on a molecular level.
17th Annual V.M. Goldschmidt Conference, Cologne (D), 19–24 Aug. 2007
Geochimica et Cosmochimica Acta, 71(2007) Suppl. S., p. A982

STUMPF, S.; STUMPF, T.; LÜTZENKIRCHEN, J.; WALTHER, C.; FANGHÄNEL, TH.
Immobilization of trivalent actinides by sorption onto quartz and incorporation into a siliceous gel:

investigations by TRLFS.
11th Internat. Conf. on the Chemistry and Migration Behaviour of Actinides and Fission Products in the Geosphere (Migration '07), Munich (D), Aug. 26–31, 2007, Book of Abstracts p. 97.

SZABO, G.; GUCZI, J.; MIYAJIMA, T.; GECKEIS, H.; REILLER, P.; BULMAN, R.A.
Determination of conditional stability constants for metals ions with humic acid using chemically immobilised humic acid on silica gel.
2nd Annual Workshop Proc.of the Integrated Project 'Fundamental Processes of Radionuclide Migration', 6th EC FP IP FUNMIG, Stockholm (S) Nov. 21–23, 2006, Svensk Kärnbränslehantering, Technical SKB Report TR-07-05 (June 2007) p. 171–78

SZABO, G.; GUCZI, J.; GECKEIS, H.; REILLER, P.; BULMAN, R.A.
Interaction of Th with humic acid over a wide pH region.
2nd Annual Workshop Proc.of the Integrated Project 'Fundamental Processes of Radionuclide Migration', 6th EC FP IP FUNMIG, Stockholm (S) Nov. 21–23, 2006, Svensk Kärnbränslehantering, Technical SKB Report TR-07-05 (June 2007) p. 239–46

VALLET, V.; SCHIMMELPFENNIG, B.; MARQUARDT, C.M.; PANAK, P.J.; KLENZE, R.
Theoretical study of the spectroscopy of protactinium(IV) in aqueous solution.
11th Internat. Conf. on the Chemistry and Migration Behaviour of Actinides and Fission Products in the Geosphere (Migration '07), Munich (D), Aug. 26–31, 2007, Book of Abstracts p. 34

WALTHER, C.; FUSS M.; ROTHE, J.; BÜCHNER S.; GECKEIS, H.
Mass Spectrometry of Actinide Oligomers by ESI TOF
11th Internat. Conf. on the Chemistry and Migration Behaviour of Actinides and Fission Products in the Geosphere (Migration '07), Munich (D), Aug. 26–31, 2007, Book of Abstracts p. 158

Reports

BOUBY, M.; GECKEIS, H.; SCHÄFER, T.; LÜTZENKIRCHEN, J.; SEHER, H.; BAUER, A.; PLASCHKE, M.: HAUSER, W.; KIENZLER, B.
Laboratory study on colloid stability and radionuclide-colloid interaction under Äspö groundwater conditions.
INE Project Report for the COLLOID DIPOLE Project, (SKB order 20002160), Mars, 2007

BUCKAU, G., KIENZLER,B., DURO, L., MONTOYA, V. (Eds.)
Proceedings of the 2nd Annual Workshop of the 6th EC FP Integrated Project: 'Fundamental Processes of Radionuclide Migration' (FUNMIG), Stockholm (S) Nov. 21–23, 2006,
Svensk Kärnbränslehantering, Technical SKB Report TR-07-05 (June 2007)

GECKEIS, H.; KLENZE, R.; [HRSG.]
Institute for Nuclear Waste Disposal. Annual report 2006.
Wissenschaftliche Berichte, FZKA-7360 (Oktober 2007)

HAUSER, W.; GÖTZ, R.; SCHÄFER, T.; GECKEIS, H.
Quantification of colloids in natural groundwater from Forsmark boreholes KFM11A, section (447.5-454.64 m) and KFM08D, sections (828.4-835.54 m) and (669.7-676.84 m)
INE Project Report, (SKB order 16987), Oct. 2007

HAUSER, W.; GÖTZ, R.; SCHÄFER, T.; BOUBY, M.; GECKEIS, H.
Quantification of colloids in natural groundwater from Laxemar boreholes KLX13A, section (432–439.2 m) and KLX17A, sections (642–701 m) and (416–437.5 m)
INE Project Report, (SKB order 15664, 16237), June 2007

HAUSER, W.; GÖTZ, R.; SCHÄFER, T.; GECKEIS, H.
Quantification of colloids in natural groundwater from Laxemar borehole KLX15A, section (623–634.5 m)
INE Project Report, (SKB order 17065), June 2007

JEGOU, C.; LOIDA, A.; METZ, V.; WEGEN, D.; COBOS, J.; JONSSON, M.; MENNECART, T.; SPAHIU, K.; EKEROTH, E.; GRAMBOW, B.; DE PABLO, J.; CLARENS, F.; CASAS, I.
MICADO, Model uncertainty for the mechanism of dissolution of spent fuel in nuclear waste repository. Selection of a common experimental database. European Commission project, deliverable 7.4, pp. 14.

LOIDA, A.; BOHNERT, E.; DARDENNE, K.; KIENZLER, B.; METZ, V.; AND SCHILD, D.
Spent fuel key processes: Final activity report for FZK-INE. (2007)
EU project NF-PRO deliverable 1.5.19.

PUDEWILLS, A.
BMBF-Verbundvorhaben Modellierung des mechanischen Verhaltens von Steinsalz:
Vergleich aktueller Stoffgesetze und Vorgehensweisen.
Wissenschaftliche Berichte, FZKA-7314 (Juni 2007)

PUDEWILLS, A.
Numerical modelling of the long-term evolution of EDZ,
EU project NF-PRO, Contract Number: F16W-CT-2003-02389, RTDC 4 - Deliverable 4.4.15,
Final Report (Dec. 2007)
http://inf-pro.sckcen.be/workspace/rtdc4/deliverables

SCHÄFER, T. IIJIMA, K.
CFM Phase I – Status report of the laboratory programme,
NAGRA Arbeitsbericht NAB 07-41, Wettingen (CH) (2007), 97pages.

Invited oral presentations

ALTMAIER, M.:
Solubility and Complex Formation of Actinides: Recent Studies at FZK-INE.
International Workshop on Aquatic Chemistry of Actinides.
Korea Advanced Institute of Science and Technology (KAIST), Daejon, Korea, Nov. 13, 2007

ALTMAIER, M.:
Löslichkeit und Speziation von drei- und vierwertigen Metallionen in alkalischen $CaCl_2$-Lösungen.
Institut für Kernchemie, Johannes Gutenberg Universität Mainz (D), Dec. 10, 2007

BAUER, A.
Actinidendiffusion im Opalinuston.
Paul Scherrer Institut, Villigen (CH), March 20, 2007

BOSBACH, D.
RadioGeochemie der Actiniden: Mischkristallbildung in aquatischen Systemen.
Institut für Geowissenschaften, Universität Kiel, (D), May, 2007

BOSBACH, D.
Solid solution – aqueous solution systems: Radionuclide co-precipitation with secondary phases.
International Conf. “Migration of Radionuclides in the Geosphere”, Munich (D), Aug. 26–31, 2007

BUCKAU,G.
European Commissions RD+D Program on Nuclear Waste Disposal.
International Conf. “Migration of Radionuclides in the Geosphere”, Munich (D), Aug. 26–31, 2007

BUCKAU, G.
Integrated Project Fundamental Processes of Radionuclide Migration (IP FUNMIG).
PAMINA Annual Workshop, Prague, Czech Republic, Sept. 26, 2007

BUCKAU, G.
NoE ACTINET: View from European research project implementation.
ACTINET Stake-holder Meeting, Brussels (B), Oct. 24, 2007

BUCKAU, G.
Metal Ion Complexation with Humic Acid.
International Workshop on Aquatic Chemistry of Actinides.
Korea Advanced Institute of Science and Technology (KAIST), Nov. 13, 2007

BUCKAU, G.
The EURATOM program on Nuclear Waste Disposal.
Korea Atomic Energy Research Institute (KAERI), Nov. 14, 2007

DENECKE, M.A.
Spatially resolved μ-XRF, μ -XAFS, and μ -XRD studies of related to nuclear waste disposal safety issues.
19th International Congress on X-ray optics and Microanalysis (ICXOM2007),
Kyoto (Japan), Sept. 17–21, 2007

DENECKE, M.A.
Confocal μ-XRF, μ-XAFS, and μ-XRD Studies of Sediment from a Nuclear Waste Disposal Natural

Analog Site Ruprechtov.
Forschungszentrum Karlsruhe – ISS (D), May 14, 2007

DENECKE, M.A.
Spatially resolved, three dimensional µ-XRF and µ-XAFS speciation studies of Np in Äspö fractured granite following a radiotracer migration experiment.
HASYLAB Annual Users Meeting, Jan. 25–26, 2007

FLÖRSHEIMER, M.
Chemical Analytical Study of Mineral/Electrolyte Interfaces in Environmental Geochemistry by Means of Nonlinear Optics.
Quantum Electronic Division, Physical Department, Moscow State University, and International Laser Centre (ILC), Moscow State University, Moscow, June 6, 2007

FLÖRSHEIMER, M.
Chemical Analytical Study of Mineral/Electrolyte Interfaces in Environmental Geochemistry by Means of Nonlinear Optics and Quantum Chemistry
Institute of Spectroscopy, Russian Academy of Sciences, Troitsk, June 8, 2007

GECKEIS, H.
Actinide geochemistry: from the molecular level to the real system.
17th Annual V.M. Goldschmidt Conference, Cologne (D), Aug. 19–24, 2007

GECKEIS, H.
Nuclear Waste Disposal: Facts and Perspectives.
ACTINET Summer School 2007, Karlsruhe (D), June 12–15, 2007

GECKEIS, H.,
Nuclear waste disposal: Facts and perspectives.
The 2007 Frederic Joliot&Otto Hahn Summer School on Nuclear Reactors,
Karlsruhe (D), Aug. 29–Sept. 07, 2007

GECKEIS, H.,
Sichere Endlagerung hochradioaktiver Abfälle.
Verein Deutscher Ingenieure, BV Karlsruhe, AK Energie- und Umwelttechnik,
Karlsruhe, March 06, 2007

GECKEIS, H.,
Geochemical aspects of nuclear waste disposal.
Universität Karlsruhe, Fakultät für Physik: Physikalische Kolloquien, June 29, 2007

GECKEIS, H.
Actinide geochemistry: from the molecular level to the real system.
Jahresseminar Graduiertenkolleg 826 (Johannes Gutenberg Universität, Mainz): "SPURENANALYTIK VON ELEMENTSPEZIES: METHODENENTWICKLUNG UND ANWENDUNGEN“
Bad Münster an der Nahe (D), Oct. 21–23, 2007

GEIST, A.; MALMBECK, R.
Separation of minor actinides in the partitioning & transmutation context.
The 8th Intern. Topical Meeting on Nuclear Applications and Utilization of Accelerators (AccApp’07),
Pocatello, Idaho, U.S.A., July 30–August 2, 2007

KIENZLER, B.
Safety Research for Nuclear Waste Disposal - Keeping Competence in Germany.
Idaho State University, Institute of Nuclear Science and Engineering,
1776 Science Center Dr, Idaho Falls, ID 83402, Sept. 14, 2007

KIENZLER, B.
Minor Actinides and Long-Lived Fission Products in Geologic Disposal.
International Workshop on recommondations and final results of the EU Project "Impact of Participation, Transmutation and Waste Reduction on the Final Nuclear Waste Disposal (RED-IMPACT)", Forschungszentrum Jülich, Sept. 19–20, 2007

LÜTZENKIRCHEN, J.
Acid-base reactions of gibbsite. Problems of solubility and phase transformations.
University of Zagreb (Croatia), April 30, 2007

LÜTZENKIRCHEN, J.
1-pK model–Why and how, Réunion CTDP.
Groupe « Sorption », Ecole des Mines de Paris (F), July 19, 2007

METZ, V.
Wechselwirkung Gasbildung - geochemisches Milieu im Endlager.
PTKA-WTE Workshop "Gase im Endlager", Berlin (D), April 17, 2007

METZ, V.
MACKSIMA-CHEMIST calculations: SFS case study salt environment.
Workshop on Model uncertainty for the mechanism of dissolution of spent fuel in a nuclear waste repository.
MICADO, Madrid (E), Febr. 16, 2007

NECK, V.:
Aquatic chemistry and thermodynamics of actinides.
ACTINET, 4th Summer School on Actinide Science and Applications.
Institute for Transuranium Elements (ITU), Karlsruhe (D) June 12–15, 2007

PANAK, P.J.; KIM, M.A.; BREBAN, D.C.; PRIEMYSHEV, A.; YUN, J.I.; KIM, J.I.
Wechselwirkung von Actiniden mit Alumosilikatkolloiden in “statu nascendi”.
Institut für Radiochemie, TU München, Garching (D), Jan. 30, 2007

PANAK, P.J.
Combined TRLFS, EXAFS and theoretical investigations on actininde/lanthanide complexed with partioning relevant N-Donor ligands.
Helsinki Winterschool in Computational Chemistry (Finnland), Dec. 10–14, 2007

POLLY, R.
Joint theoretical and experimental investigation of the water/corundum interface:
An application to the safety assessment of nuclear waste disposal.
OpusIB Workshop, Forschungszentrum Karlsruhe (D) IWR, Dec. 3, 2007

PUDEWILLS, A.
Benchmark -Teil 2, Modellberechnungen zur Untertagestruktur EU1-Sondershausen: Darstellung und Vergleich der Ergebnisse und deren Diskussion, BMBF-Verbundvorhaben "Die Modellierung des mechanischen Verhaltens von Steinsalz: Vergleich aktueller Stoffgesetze und Vorgehensweisen" (STOFFGESETZVERGLEICH), Abschlussveranstaltung, Hannover (D), Nov. 8, 2006

RABUNG, TH.
Metal ion speciation onto mineral surfaces by time resolved laser fluorescence spectroscopy (TRLFS).
International Workshop on Aquatic Chemistry of Actinides,
Korea Advanced Institute of Science and Technology (KAIST), Daejon, Korea, Nov. 13, 2007

ROTHE, J.
Actinidenforschung an der INE-Beamline - warum macht ANKA ein Nukleares Endlager sicherer?
Vortrag zur „ANKA-Teatime“, Forschungszentrum Karlsruhe-ISS (D), April 4, 2007

SCHÄFER, T.
The problem of upscaling in the field of nuclear waste repository research.
Bio-Geo Colloquium, Friedrich-Schiller-University Jena (D), Jan. 16, 2007

SCHÄFER, T.
Clay-organic interactions in natural claystone formations: What have we learnt?
1st bilateral IRSN (Institut de Radioprotection et de Sûreté Nucléaire) –
FZK-INE meeting, Tournemire (F), May 2, 2007

SCHÄFER, T.
Nuclear waste repository research at the nanoscale.
DOE Workshop on STXM and X-ray Nanoprobe Capabilities and Needs for Geo-, Environmental, and Biological Sciences, Stanford Campus, Stanford California., July 9, 2007

SCHIMMELPFENNIG, B.
ACTINET: A Network of Actinide Sciences.
Relativistic Effects in Heavy Elements, REHE 2007, Ottrott (F), March 21–25, 2007

SCHIMMELPFENNIG, B.
ACTINET: A Network of Actinide Sciences
Helsinki Winterschool in Computational Chemistry (Finnland), Dec. 10–14, 2007

STUMPF, TH.
Mit dem Laser auf Spurensuche: Grundlagenforschung als wichtiger Beitrag zur Langzeitsicherheit nuklearer Endlager.
Vortragsreihe bei Forschungszentrum Karlsruhe/FTU „Junge Talente“, July 12, 2007

Presentations at Workshops and Conferences

ALTMAIER, M.; NECK, V.; RABUNG, TH.; BRENDEBACH, B.; ROTHE, J.; FANGHÄNEL, TH.
Löslichkeit und Speziation von drei- und vierwertigen Metallionen in alkalischen $CaCl_2$-Lösungen: Bildung ternärer Komplexe $Ca_x[M(OH)_n]^{z+}$ (M = Nd, Cm, Zr, Th, Pu).
Jahrestagung der GDCh-Fachgruppe Nuklearchemie, Ulm (D), Sept. 16–19, 2007, Abstractband 177

ARMBRUSTER, M. K.; PLASCHKE, M.; ROTHE, J.; SCHIMMELPFENNIG, B.; DENECKE, M.A.
Metal-Ion complexation effects in C-1s-NEXAFS spectra – evidence by quantum chemical calculations
ACTINET-Workshop, Avignon (F)), Oct. 11–12, 2007

ARMBRUSTER, M. K.; WEIGEND, F.; Klopper, W.
Efficient Two-component Hartree-Fock and Density Functional methods.
Helsinki Winterschool in Computational Chemistry (Finnland), Dec. 1014, 2007

BAUER, A.; BOUBY, M.; FILBY, A.; GECKEIS, H.; HAUSER, W.; KIENZLER, B.; LÜTZENKIRCHEN J.; PLASCHKE, M.; SCHÄFER, T.; SEHER, H.
Update of laboratory studies: colloids generation, characterization and migration.
3rd Annual Workshop Proc.of the Integrated Project 'Fundamental Processes of Radionuclide Migration' 6th EC FP IP FUNMIG, Edinburgh (GB), Nov. 26–29, 2007

BAUER, A.; FIEHN, B.; MARQUARDT, C.; RÖMER, J.; SCHÄFER, TH.; GÖRTZEN, A.; KIENZLER, B.
Results on Pu Diffusion Experiments in the Opalinus Clay.
International Conference on Radioactive Waste Disposal in Geological Formations (REPOSAFE)
Braunschweig (D), Nov. 6–9, 2007, Book of Abstracts

BELMECHERY, R.; VALLET, V.; FLAMENT, J.P.; SCHIMMELPFENNIG, B.; MARQUARDT, C.M.; PANAK, P.J.; KLENZE, R.
Theoretical study of the spectroscopy of protactinium(IV) in aqueous solution.
Helsinki Winterschool in Computational Chemistry (Finnland), Dec. 10–14, 2007

BOSBACH, D., KIENZLER, B., LUCKSCHEITER, B.,
Long-term Geochemical Evolution of HAW Glass under Repository Conditions:
Achievements and Perspectives
International Conference on Radioactive Waste Disposal in Geological Formations (REPOSAFE)
Braunschweig (D), Nov. 6–9, 2007, Book of Abstracts

BOUBY, M.; GECKEIS, H.; SCHÄFER, T.; LÜTZENKIRCHEN, J.; SEHER, H.; BAUER, A.; PLASCHKE, M.; HAUSER, W.; KIENZLER, B.
Laboratory study on colloid stability and radionuclide-colloid interaction under Äspö groundwater conditions.
SKB colloid workshop, Stockholm (S), Nov. 14–16, 2007

M. BOUBY, H. GECKEIS, T. SCHÄFER, J. LÜTZENKIRCHEN, H. SEHER, A. BAUER, M. PLASCHKE, W. HAUSER, B. KIENZLER,
Laboratory study on colloid stability and radionuclide-colloid interaction under Äspö groundwater conditions.
3rd Annual Workshop Proc.of the Integrated Project 'Fundamental Processes of Radionuclide Migration' 6th EC FP IP FUNMIG, Edinburgh (GB), Nov. 26–29, 2007

BRASSER, TH.; NOSECK, U., LACIOK, A.; HAVLOVA, V.; HERCIK, M.; DENECKE, M.A.; SUKSI, J.; DULINSKI, M.; ROZANSKI, K.; SCHÖNWIESE, D.
Uranium Deposits at the Ruprechtov Site (CZ) and Hesselbach Site as Natural Analogues for Radionuclide Transport and Retention in Lignitic Clay Formations
International Conference on Radioactive Waste Disposal in Geological Formations (REPOSAFE)
Braunschweig (D), Nov. 6–9, 2007, Book of Abstracts

BRENDEBACH, B.; DARDENNE, K.; DENECKE, M.A.; ROTHE, J.; VITOVA, T.
New developments at the INE-beamline for actinide research at ANKA.
14th Nat.Conf.on Synchrotron Radiation Instrumentation (SRI2007),
Baton Rouge, La., April 25–27, 2007

BUCKAU, G., WOLF, M., KIM, J.I.
The Gorleben Aquifer System: State of Isotope Geochemical Characterization and Implications for the Hydrological Modeling
International Conference on Radioactive Waste Disposal in Geological Formations (REPOSAFE)
Braunschweig (D), Nov. 6–9, 2007, Book of Abstracts

DARDENNE, K. ; BRENDEBACH, B. ; DENECKE, M. A. ; ROTHE, J.
The INE-Beamline for Actinide Research at ANKA
Jahrestagung der GDCh-Fachgruppe Nuklearchemie, Ulm (D), Sept. 16–19, 2007, Abstractband 151

FILBY, A., PLASCHKE, M., GECKEIS, H., BOSBACH, D.
Interaction of colloids with mineral surfaces.
Mineralogisch-geochemisches Seminar Universität Karlsruhe (D), June 19, 2007

FILBY, A., PLASCHKE, M., GECKEIS, H., BOSBACH, D.:
Interaction of latex colloids with Grimsel granodiorite and its component minerals
SKB colloid workshop, Stockholm (S), Nov. 14–16, 2007

FLÖRSHEIMER, M.; POLLY, R.; KRUSE, K.; ABDELMONEM, A.; SCHIMMELPFENNIG, B.; KLENZE, R.; FANGHÄNEL, T.
Chemical Analytical Study of Mineral/Electrolyte Interfaces by Means of Nonlinear Optics.
ACTINET Project Meeting, Forschungszentrum Karlsruhe, INE, June 21, 2007

GÖTTLICHER, J.; MANGOLD, S.; DENECKE, M.A.; SIMON, R.; STEININGER, R.
X-ray Spectroscopy with Synchrotron Radiation at the Forschungszentrum Karslruhe,
„PRORA“ – Prozessnahe Röntgenanalytik, Berlin (D), Nov. 14 –16, 2007

HARTMANN, E.; GECKEIS, H.; RABUNG, TH.; KIENZLER, B.; FANGHÄNEL, TH.; BOSBACH, D.
Sorption of Radionuclides onto Natural Clays.
Jahrestagung der GDCh-Fachgruppe Nuklearchemie, Ulm (D), Sept. 16–19, 2007, Abstractband 171

HAUSER, W., GECKEIS, H., GÖTZ, R., WOLD, S.
Investigations on the Stability of Background Colloids in Natural Groundwater by Laser-Induced Breakdown Detection.
International Conference on Radioactive Waste Disposal in Geological Formations
Braunschweig (D), Nov. 6–9, 2007, Book of Abstracts (REPOSAFE)

HAUSER, W.; GECKEIS, H.; SCHÄFER, T.; GÖTZ, R.
LIBD characterization of colloids in natural Ruprechtov groundwater – What could be learnt from in-situ colloid detection?
FUNMIG RTDC5 Meeting, September 26, 2007, Prague, Czech Republic

HUITTINEN, N.; RABUNG, TH.; LÜTZENKIRCHEN, J.
Cm(III) and Gd(III) sorption onto gibbsite.
ACTINET Project Meeting, Forschungszentrum Karlsruhe, INE, June 21, 2007

KALLAY, N.; LÜTZENKIRCHEN, J.; BRENDLER, V.; VAN DER LEE, J.
“Surface Reactions & Electrical Interfacial Layer, Experiments and Models: Towards a common basis”, Discussion Meeting/Workshop, Opatija (Croatia), Oct. 8–15, 2007

KIENZLER, B.; GECKEIS, H.; GOMPPER, K.; KLENZE, R.
Radioactive waste disposal in Germany: no site decision-keeping competence.
Proc. of the 11th Internat. Conf.on Environmental Remediation and Radioactive Waste Management (ICEM2007), Bruges (B), Sept. 2–6, 2007

LARTIGES, B.S. ;WALTHER, C. ;MICHOT, L.J. ;MONTARGÈS-PELLETIER, E. ;BRIOIS V.
Colloidal aggregation with hydrolyzing coagulants: nature and role of hydrolyzed species
PARTICLE SEPARATION IWA 2007.
Toulouse (F), July 9-11, 2007, Book of Abstracts p.17

LOIDA, A.; KELM, M.; MÜLLER, N.; METZ, V.; BOHNERT, E.; KIENZLER, B.
Spent fuel matrix dissolution behavior governed by α-, β-, γ- and α-radiolyisis effects: Experimental approach.
Internat.Spent Fuel Workshop, Böttstein (CH), Sept. 11–12, 2007

LOIDA, A.; KIENZLER, B.
Corrosion behavior of spent fuel in non saline solutions. Experimental studies at FZK/INE.
Internat.Conf.on Radioactive Waste Disposal in Geological Formations, (REPOSAFE)
Braunschweig, 6–9 November 2007, Book of Abstracts

LÜTZENKIRCHEN, J.; HUBER, F.
Testing a new nonelectrostatic surface complexation model.
3rd Annual Workshop Proc.of the Integrated Project 'Fundamental Processes of Radionuclide Migration' 6th EC FP IP FUNMIG, Edinburgh, November 26–29, 2007

LÜTZENKIRCHEN, J.; ZIMMERMANN, R.; RABUNG, T.; SCHILD, D.; GECKEIS, H.; WERNER, C.
Physical adsorption of hydroxide ions at oxide electrolyte interfaces?,
2nd Symposium on Electrosurface Phenomena in Advanced Materials Science,
Dresden (D), Sept. 23–24, 2007

METZ, V., LOIDA, A., BOHNERT, E., MÜLLER, N., KELM, M., KIENZLER, B.
Radiation Induced UO_2(s) Corrosion in Presence of H_2 and Br^- : Corrosion of Spent Fuel and Depleted UO_2(s) in NaCl-Brine.
International Conference on Radioactive Waste Disposal in Geological Formations (REPOSAFE)
Braunschweig (D), Nov.6–9, 2007, Book of Abstracts

NABER, A.; PLASCHKE, M.; ROTHE, J.; DENECKE, M.A.; SCHIMMELPFENNIG, B.; HOFMANN, H.; EISNER, V.; WISSLER J.; SCHIRMER, J.; BALDEA, I.
Nahfeld-mikroskopisches und -spektroskopisches Studium der Wechselwirkung von Actiniden und Lanthaniden mit Oberflächen und Huminstoffen.
Abschluß-Seminar des Virtuellen Instituts Funktionelle Eigenschaften aquatischer Grenzflächen,
Forschungszentrum Karlsruhe, INE, Sept. 24, 2007

PANAK, P.; KIM, M.A.; BREBAN, D.; YUN, Y.I.; KLENZE, R.; LIM, J.I.; FANGHÄNEL, T.
Interactions of Actinides with Hydroxyaluminosilicate Colloids in Statu Nascendi.
International Conference on Radioactive Waste Disposal in Geological Formations (REPOSAFE)
Braunschweig, November 6–9, 2007, Book of Abstracts

PANAK, P. J.; DENECKE, M. A.; WEIGL, M.; GEIST, A.; SCHIMMELPFENNIG, B.; TRUMM, S.; KLENZE, R.; FANGHÄNEL, TH.
Combined TRLFS, EXAFS and Theoretical Investigations on Actininde/ Lanthanide Complexed with Alkylated 2,6-di(1,2,4-triazin-3-yl)pyridines (BTPs)
Jahrestagung der GDCh-Fachgruppe Nuklearchemie, Ulm (D), Sept. 16–19, 2007, Abstractband 160

PLASCHKE, M.; ROTHE, J.; NABER, A.
Nahfeld-mikroskopisches und –spektroskopisches Studium der Wechselwirkung von Actiniden und Lanthaniden mit Oberflächen und Huminstoffen.
5. Statusseminar des Virtuellen Instituts Funktionelle Eigenschaften aquatischer Grenzflächen,
Forschungszentrum Karlsruhe, INE, Sept. 24, 2007

POLLY, R. ; SCHIMMELPFENNIG, B.; FLÖRSHEIMER M.; KRUSE K.; ABDELMONEM A.; KLENZE R.; FANGHÄNEL Th.
Joint theoretical and experimental study of the water/corundum (Al_2O_3) interface: An application to the safety assessment of nuclear waste disposal.
Symposium Theoretische Chemie, Saarbrücken (D), Sept. 17 –20, 2007

PUDEWILLS, A.
Numerical Investigation of the Long-term Evolution of the Excavation Disturbed Zone
International Conference on Radioactive Waste Disposal in Geological Formations (REPOSAFE)
Braunschweig (D), Nov. 6–9, 2007, Book of Abstracts

RABUNG, TH.; GECKEIS, H.; FANGHÄNEL, TH.
Influence of pH and Metal Ion Loading on the Cm(III) Humate Complexation. A Time Resolved Laser Fluorescence Spectroscopy Study.
Jahrestagung der GDCh-Fachgruppe Nuklearchemie, Ulm (D), Sept. 16–19, 2007, Abstractband 190

RABUNG, TH; LÜTZENKIRCHEN, J.; HUITTINEN, N.
Metal ion sorption onto aluminum oxides/hydroxides.
International workshop: electrical interfacial layer: Experiments and models towards a common basis
Opatija, Kroatien, Oct. 7–14, 2007

RABUNG, TH; LÜTZENKIRCHEN, J.; HUITTINEN; N.
Cm(III) sorption onto aluminum oxides/hydroxides.
5. Statusseminar des Virtuellen Instituts Funktionelle Eigenschaften aquatischer Grenzflächen,
Forschungszentrum Karlsruhe, INE, Sept. 24, 2007

RABUNG, TH; LÜTZENKIRCHEN, J.; HUITTINEN; N.
Cm(III) sorption onto aluminum oxides/hydroxides

Abschluß-Seminar des Virtuellen Instituts Funktionelle Eigenschaften aquatischer Grenzflächen, Forschungszentrum Karlsruhe, INE, Sept. 24, 2007

SCHÄFER, TH.; GECKEIS, H.; KIENZLER, B.; RÖMER, J.; SCHILD, D.
Colloid/Radionuclide Migration Studies in Fractured Rocks; Lessons learnt from the Grimsel and Äspö System.
International Conference on Radioactive Waste Disposal in Geological Formations (REPOSAFE) Braunschweig (D), Nov.6–9, 2007, Book of Abstracts

SCHIMMELPFENNIG, B.; PATZSCHKE, M.; GEIST, A.; PANAK, P.J.; DENECKE, M.A.; KLENZE, R.; GOMPPER, K.
Can natural population analysis help to understand the difference in binding of An(III) and Ln(III) ions to soft-donor ligands?
Symposium Theoretische Chemie, Saarbrücken (D), Sept. 17 –20, 2007

SCHIMMELPFENNIG, B.; KLENZE, R.; GOMPPER, K.
Joint theoretical and experimental research on actinide compounds.
Symposium Theoretische Chemie, Saarbrücken (D), Sept. 17 –20, 2007

SCHIMMELPFENNIG, B.; PATZSCHKE, M.; GEIST, A.; PANAK, P.J.; DENECKE, M.A.; KLENZE, R.; GOMPPER, K.
Can natural population analysis help to understand the difference in binding of An(III) and Ln(III) ions to soft-donor ligands?
Relativistic Effects in Heavy Elements, REHE 2007, Ottrott (F), March 21–25, 2007

SCHMIDT, M.; MARQUES-FERNANDES, M.; STUMPF, TH.; WALTHER, C.; KLENZE, R.; FANGHÄNEL, TH.
Site-selective TRLFS investigations on Eu(III) doped calcite.
Jahrestagung der GDCh-Fachgruppe Nuklearchemie, Ulm (D), Sept. 16–19, 2007, Abstractband 182

SIRIANGKHAWUT, W.; BOUBY, M.; GECKEIS, H.; JAKMUNEE, J.; GRUDPAN,K.
Flow-Based Analytical Methods to Study Kinetics of Metal-Humic Acid Complexes.
International Conference on flow Injection Analysis (ICFIA 2007), Berlin (D), Sept. 3–7, 2007

SKERENCAK, A.; PANAK, P.J.; HAUSER, W.; NECK, V.; LINDQVIST-REIS, P.; KLENZE, R.; FANGHÄNEL, T.
Spektroskopische und thermodynamische Untersuchungen des Komplexierungsverhaltens von Eu(III) und Cm(III) mit Nitrat bei erhöhten Temperaturen.
Jahrestagung der GDCh-Fachgruppe Nuklearchemie, Ulm (D), Sept. 16–19, 2007, Abstractband 169

STUMPF, S.; GAILLARD, C.; PANAK, P.
Spektroskopische Untersuchungen der Komplexierung von Eu(III), Cm(III) uns Am(III) in Ionic Liquids: Unterschiede und Ähnlichkeiten.
Jahrestagung der GDCh-Fachgruppe Nuklearchemie, Ulm (D), Sept. 16–19, 2007, Abstractband 189

STUMPF, T.; CURTIUS, H.; WALTER, C.; DARDENNE, K.; UFER, K.; FANGHÄNEL, T.
Incorporation of Eu(III) into hydrotalcite: A TRLFS and EXAFS study.
Jahrestagung der GDCh-Fachgruppe Nuklearchemie, Ulm (D), Sept. 16–19, 2007, Abstractband 178

TRUMM, S.; PANAK, P.J.; GEIST, A.; FOREMAN, M.R.S.; KLENZE, R.; FANGHÄNEL, TH.
Spektroskopische kinetische Untersuchungen zur Komplexierung von Eu(III) und Cm(III) mit BTBP-Liganden.
Jahrestagung der GDCh-Fachgruppe Nuklearchemie, Ulm (D), Sept. 16–19, 2007, Abstractband 192

WALTHER, C.; FUSS, M.; ROTHE, J.; BÜCHNER S.; GECKEIS, H.
Mass-spectrometry of actinide-oligomers by ESI TOF-MS.
Jahrestagung der GDCh-Fachgruppe Nuklearchemie, Ulm (D), Sept. 16–19, 2007, Abstractband 158

WEISENBURGER, S.
Prozesschemische Grundlagen und Technologie der Verglasung hochradioaktiver Abfalllösungen.
Jahrestagung der GDCh-Fachgruppe Nuklearchemie, Ulm (D), Sept. 16–19, 2007, Abstractband 166